

NDOT Research Report

Report No. 515-13-803

**LRFD Resistance Factor Calibration for Axially
Loaded Drilled Shafts in the Las Vegas Valley**

July, 2016

**Nevada Department of Transportation
1263 South Stewart Street
Carson City, NV 89712**



Technical Report Documentation Page

Report No. 515-13-803		2. Government Accession No.	3. Recipients Catalog No.
4. Title and Subtitle LRFD Resistance Factor Calibration for Axially Loaded Drilled Shafts in the Las Vegas Valley		5. Report Date July 19, 2016	
		6. Performing Organization Code	
7. Authors Ramin Motamed, Sherif Elfass, Kevin Stanton		8. Performing Organization Report No.	
9. Performing Organization Name and Address University of Nevada Reno 1664 N. Virginia St. Reno, NV 89557-0258		10. Work Unit No.	
		11. Contract or Grant No. P515-13-803	
15. Supplementary Notes			
16. Abstract Resistance factors for LRFD of axially loaded drilled shafts in the Las Vegas Valley are calibrated using data from 41 field load tests. In addition to the traditional implementation of Monte Carlo (MC) simulations for calibration, a more robust technique is investigated in which nested MC simulations are employed to capture the uncertainty associated with the interpretation of material properties from in-situ test data. Measures are also taken to improve design procedures regarding cemented sandy soils colloquially referred to as caliche. While caliche is common in Las Vegas, its potential contribution to resistance is difficult to predict using typical site investigation data and there is currently no consensus among local engineers regarding how it should be considered in design. Thus, an approach for treating caliche is proposed and compared to three other potentially viable methods. Overall it is found that the proposed design approach produces the most accurate nominal axial capacity predictions and the nested MC simulations yield lower resistance factors than traditional calibration procedures.			
17. Key Words Deep Foundations, Drilled Shafts, Reliability, LRFD		18. Distribution Statement	
19. Security Classif. (of this report)	20. Security Classif. (of this page)	21. No. of Pages 166	22. Price

Disclaimer

This work was sponsored by the Nevada Department of Transportation. The contents of this report reflect the views of the authors, who are responsible for the facts and the accuracy of the data presented herein. The contents do not necessarily reflect the official views or policies of the State of Nevada at the time of publication. This report does not constitute a standard, specification, or regulation.

LRFD Resistance Factor Calibration for Axially Loaded Drilled Shafts in the Las Vegas Valley

Prepared for

The Nevada Department of Transportation

Prepared by

Ramin Motamed (PI), Ph.D., P.E.

Assistant Professor

Email: motamed@unr.edu

Tel: 775-784-6960,

and

Sherif Elfass (Co-PI), Ph.D., P.E.

Research Associate Professor

Email: elfass@unr.edu,

and

Kevin Stanton

Graduate Research Assistant

Email: kevinstanton@nevada.unr.edu

Department of Civil and Environmental Engineering

University of Nevada

1664 N. Virginia St.

Reno, NV 89557-0258

July 19, 2016



University of Nevada, Reno

Contents

- Notation 5

- List of Figures 9

- List of Tables 13

- Abstract 14

- Acknowledgments 14

- Disclaimer 15

- 1 Introduction 15**
 - 1.1 Literature Review 16
 - 1.1.1 Other Resistance Factor Calibration Studies 16
 - 1.1.2 Principles of Resistance Factor Calibration 18
 - 1.1.3 Soil Conditions in the Las Vegas Valley 25
 - 1.1.4 Field Load Testing of Drilled Shafts 32

- 2 Measured Data 36**
 - 2.1 Database 36
 - 2.1.1 Sharing 41
 - 2.2 Interpretation of Bi-Directional Load Test Data 41
 - 2.3 Scoring System 45

- 3 Predicted Resistances 49**

- 4 Calibration Procedures 57**

- 5 Results 65**

6	Conclusions and Final Recommendations	69
6.1	Final Recommendations	71
6.2	Future Work	72
	References	73
	Appendices	76
A	NDFLTD	77
B	Collected Load Tests and GI Reports	78
C	Interpreted Stratigraphy and Geomaterial Properties	79
D	Equivalent Top-Down Load-Settlement Curves	138
E	Recommended Procedure for Analysis of Axially Loaded Drilled Shafts in Las Vegas	161
F	Example: Recommended LRFD Procedure for a Drilled Shaft in Las Vegas	163

Notation

The following symbols are used in this report:

- CDF = cumulative distribution function;
- COV = coefficient of variation;
- B = shaft diameter;
- g = margin of safety;
- L = shaft embedded length;
- L1 = level 1 approach for LRFD resistance factor calibration;
- L2 = level 2 approach for LRFD resistance factor calibration;
- N = number of iterations;
- N_{SPT} = Standard Penetration Test blow count (blows per foot);
- PDF = probability distribution function;
- q_u = unconfined compressive strength;
- Q = axial load at shaft head;
- R = random variable for axial resistance;
- Q = random variable for axial load;
- R_m = measured axial resistance;
- R_p = predicted nominal axial resistance;
- R_R = factored axial resistance;
- RQD = Rock Quality Designation;
- s_u = undrained shear strength;
- β = reliability index;
- ϕ' = effective friction angle;
- ϕ_{RT} = total LRFD resistance factor for the strength limit state;
- γ = total unit weight;
- λ = prediction bias (defined as R_m/R_p); and
- σ'_v = vertical effective stress.

List of Figures

1.1	(a) Interpreted measured and predicted drilled shaft resistances and (b) histogram of bias (R_m/R_p) from Abu-Farsakh et al. (2012)	17
1.2	Interpreted measured and predicted drilled shaft resistances from Garder et al. (2012)	18
1.3	Stages of a typical LRFD calibration for deep foundations after Paikowsky (2004)	20
1.4	Example of random variables of a limit state function, μ_R and μ_S , in standard normal space and the associated failure surface, $G(x) = 0$ ($G_L(x) = 0$ is the linearized version), after Paikowsky (2004) and Ayyub et al. (2000)	23
1.5	Example soil profiles and corrected standard penetration blow counts for the Vegas High Roller project (from Kluzniak et al., 2014)	28
1.6	V_s scatter for different soil unit in the Las Vegas Valley (Murvosh et al., 2013)	29
1.7	Characteristic V_s profiles for different soil unit in the Las Vegas Valley (Murvosh et al., 2013)	30
1.8	Using seismic methods to detect caliche: example case from the Las Vegas Springs Preserve (Luke et al., 2003)	30
1.9	Generalized cross-sections for the Las Vegas Valley showing the basin-fill deposits and components of the groundwater flow system under (A) pre-development conditions and (B) modern conditions (from Thiros et al., 2010)	31
1.10	Example of a traditional top-down static load test on a drilled shaft (Brown et al., 2010)	32
1.11	Example of a bi-directional (O-Cell) load test setup	33
1.12	Example of a statnamic loading apparatus (Brown et al., 2010): (a) piston and silencer assembly, (b) load cell and laser target, (c) laser for displacement measurement, (d) schematic diagram	33
1.13	Example dynamic load tests on drilled shafts using a drop weight (left) and pile hammer (right) (Brown et al., 2010)	34

2.1	Approximate locations of the test shafts included in the study	37
2.2	Distribution of select characteristics among the data employed for calibration	37
2.3	Object components and information mapping in the NDFLTD	38
2.4	Main search window in the NDFLTD	39
2.5	Example GI report in the NDFLTD	39
2.6	Example load test report in the NDFLTD	40
2.7	Determination of the rigid equivalent top-down load-settlement curve from bi-directional load test data where Q_{net_i} is the net load for movement increment i (modified from original figure provided by Loadtest Inc.)	42
2.8	Example patterns of developed side shear stress and corresponding parameters needed to estimate elastic compression above the load cell(s) in a bi-directional load test, after Loadtest Inc. (2000). Note that w' denotes the buoyant weight when below the water table	43
2.9	Analytical framework for a single shaft section in the $t-z$ method for correcting bi-directional load test data for elastic compression above the load cell, after Loadtest Inc. (2000)	44
2.10	Load test and GI quality scores for the data included in this study	45
3.1	Histogram of unconfined compressive strengths of caliche core samples in Las Vegas reported by Western Technologies Inc. (1994), Arup (2011), and Rinne et al. (1996)	52
3.2	Measured and predicted resistances computed with M1 and M1a (trend line and equation pertains only to M1)	54
3.3	Measured and predicted resistances computed with M2	54
3.4	Measured and predicted resistances computed with M3	55
3.5	Measured and predicted resistances computed with M4	55
3.6	Relationship between bias and relative amount of caliche along the embedded lengths of the test shafts	56
4.1	PDFs and CDFs of the bias developed with M1 for the L1 and L2 calibrations	59
4.2	PDFs and CDFs of the bias developed with M2 for the L1 and L2 calibrations	60
4.3	PDFs and CDFs of the bias developed with M3 for the L1 and L2 calibrations	61
4.4	PDFs and CDFs of the bias developed with M4 for the L1 and L2 calibrations	62
5.1	L1 and L2 calibration results for different data quality bins and design approaches (M1, M2, M3, and M4) based on AASHTO (2014)	66
5.2	Impact of data quality and calibration level on the computed resistance factors	68

D.1	Equivalent top-down load-settlement curve for data number 1	138
D.2	Equivalent top-down load-settlement curve for data number 2	139
D.3	Equivalent top-down load-settlement curve for data number 3	139
D.4	Equivalent top-down load-settlement curve for data number 4	140
D.5	Equivalent top-down load-settlement curve for data number 5	140
D.6	Equivalent top-down load-settlement curve for data number 6	141
D.7	Equivalent top-down load-settlement curve for data number 7	141
D.8	Equivalent top-down load-settlement curve for data number 8	142
D.9	Equivalent top-down load-settlement curve for data number 9	142
D.10	Equivalent top-down load-settlement curve for data number 10	143
D.11	Equivalent top-down load-settlement curve for data number 11	143
D.12	Equivalent top-down load-settlement curve for data number 12	144
D.13	Equivalent top-down load-settlement curve for data number 13	144
D.14	Equivalent top-down load-settlement curve for data number 14	145
D.15	Equivalent top-down load-settlement curve for data number 15	145
D.16	Equivalent top-down load-settlement curve for data number 16	146
D.17	Equivalent top-down load-settlement curve for data number 17	146
D.18	Equivalent top-down load-settlement curve for data number 18	147
D.19	Equivalent top-down load-settlement curve for data number 19	148
D.20	Equivalent top-down load-settlement curve for data number 20	148
D.21	Equivalent top-down load-settlement curve for data number 21	149
D.22	Equivalent top-down load-settlement curve for data number 22	149
D.23	Equivalent top-down load-settlement curve for data number 23	150
D.24	Equivalent top-down load-settlement curve for data number 24	150
D.25	Equivalent top-down load-settlement curve for data number 25	151
D.26	Equivalent top-down load-settlement curve for data number 26	151
D.27	Equivalent top-down load-settlement curve for data number 27	152
D.28	Equivalent top-down load-settlement curve for data number 28	152
D.29	Equivalent top-down load-settlement curve for data number 29	153
D.30	Equivalent top-down load-settlement curve for data number 30	153
D.31	Equivalent top-down load-settlement curve for data number 31	154
D.32	Equivalent top-down load-settlement curve for data number 32	154
D.33	Equivalent top-down load-settlement curve for data number 33	155
D.34	Equivalent top-down load-settlement curve for data number 34	155
D.35	Equivalent top-down load-settlement curve for data number 35	156
D.36	Equivalent top-down load-settlement curve for data number 36	156

D.37 Equivalent top-down load-settlement curve for data number 37	157
D.38 Equivalent top-down load-settlement curve for data number 38	157
D.39 Equivalent top-down load-settlement curve for data number 39	158
D.40 Equivalent top-down load-settlement curve for data number 40	158
D.41 Measured load-settlement curve for data number 41	159
D.42 Equivalent top-down load-settlement curve for data number 42	159
D.43 Equivalent top-down load-settlement curve for data number 43	160
D.44 Equivalent top-down load-settlement curve for data number 44	160

List of Tables

- 1.1 Probability of failure, p_f , for different reliability indices, β 22
- 1.2 Load statistics and factors employed in this study (Paikowsky, 2004). 25
- 1.3 Example classification and drilling/sampling characteristics of caliche in the Las Vegas Valley (Cibor, 1983). 27
- 2.1 Scoring criteria for load test and GI data quality. 46
- 2.2 Summary of test shaft and GI parameters. 47
- 3.1 Criteria for describing cementation (after ASTM (2000)). 49
- 3.2 Spearman’s ρ statistics to test for dependence between R_p and λ (assumed significance level of 0.05, null = independent). 51
- 4.1 Assumed COV values for design parameters in the L2 LRFD calibrations. 63
- 4.2 Comparable COV values for design parameters from literature. 63
- 4.3 Summary of statistical parameters used to describe the bias for the L1 and L2 calibrations. 64
- 5.1 Resistance factors computed with the MC simulations for the L1 and L2 calibration (using the global lognormal bias statistics). 67
- 5.2 Governing LRFD resistance factors for all design approaches and calibration levels 67
- C.1 Assumed stratigraphy and material properties for data number 1 (water table depth = 85 ft). 80
- C.2 Assumed stratigraphy and material properties for data number 2 (water table depth = 101 ft). 82
- C.3 Assumed stratigraphy and material properties for data number 3 (water table depth = 101 ft). 83
- C.4 Assumed stratigraphy and material properties for data number 4 (water table depth = 10 ft). 84

C.5 Assumed stratigraphy and material properties for data number 5 (water table depth = 7 ft).	85
C.6 Assumed stratigraphy and material properties for data number 6 (water table depth = 7 ft).	86
C.7 Assumed stratigraphy and material properties for data number 7 (water table depth = 12 ft).	87
C.8 Assumed stratigraphy and material properties for data number 8 (water table depth = 22 ft).	88
C.9 Assumed stratigraphy and material properties for data number 9 (water table depth = 20 ft).	90
C.10 Assumed stratigraphy and material properties for data number 10 (water table depth = 20 ft).	91
C.11 Assumed stratigraphy and material properties for data number 11 (water table depth = 24.5 ft).	92
C.12 Assumed stratigraphy and material properties for data number 12 (water table depth = 18 ft).	93
C.12 Assumed stratigraphy and material properties for data number 12 (water table depth = 18 ft). (continued)	94
C.13 Assumed stratigraphy and material properties for data number 13 (water table depth = 15.5 ft).	95
C.13 Assumed stratigraphy and material properties for data number 13 (water table depth = 15.5 ft). (continued)	96
C.14 Assumed stratigraphy and material properties for data number 14 (water table depth = 23 ft).	97
C.15 Assumed stratigraphy and material properties for data number 15 (water table depth = 24 ft).	99
C.16 Assumed stratigraphy and material properties for data number 16 (water table depth = 20 ft).	101
C.17 Assumed stratigraphy and material properties for data number 17 (water table depth = 20.5 ft).	102
C.18 Assumed stratigraphy and material properties for data number 18 (water table depth = 15 ft).	104
C.18 Assumed stratigraphy and material properties for data number 18 (water table depth = 15 ft). (continued)	105
C.19 Assumed stratigraphy and material properties for data number 19 (water table depth = 15 ft).	106

C.19 Assumed stratigraphy and material properties for data number 19 (water table depth = 15 ft). (continued)	107
C.20 Assumed stratigraphy and material properties for data number 20 (water table depth = 24 ft).	108
C.21 Assumed stratigraphy and material properties for data number 21 (water table depth = 20 ft).	109
C.22 Assumed stratigraphy and material properties for data number 22 (water table depth = 14 ft).	110
C.23 Assumed stratigraphy and material properties for data number 23 (water table depth = 14 ft).	112
C.24 Assumed stratigraphy and material properties for data number 24 (water table depth = 24 ft).	114
C.25 Assumed stratigraphy and material properties for data number 25 (water table depth = 30 ft).	115
C.26 Assumed stratigraphy and material properties for data number 26 (water table depth = 28 ft).	116
C.27 Assumed stratigraphy and material properties for data number 27 (water table depth = 62 ft).	117
C.28 Assumed stratigraphy and material properties for data number 28 (water table depth = 81.2 ft).	119
C.29 Assumed stratigraphy and material properties for data number 29 (water table depth = 18 ft).	121
C.30 Assumed stratigraphy and material properties for data number 30 (water table depth = 48.1 ft).	122
C.31 Assumed stratigraphy and material properties for data number 31 (water table depth = 5 ft).	124
C.32 Assumed stratigraphy and material properties for data number 32 (water table depth = 19 ft).	126
C.33 Assumed stratigraphy and material properties for data number 33 (water table depth = 20 ft).	128
C.34 Assumed stratigraphy and material properties for data number 34 (water table depth = 20 ft).	129
C.35 Assumed stratigraphy and material properties for data number 35 (water table depth = 15.5 ft).	130
C.36 Assumed stratigraphy and material properties for data number 36 (water table depth = 17.5 ft).	131

C.37 Assumed stratigraphy and material properties for data number 37 (water table depth = 20 ft).	132
C.38 Assumed stratigraphy and material properties for data number 38 (water table depth = 15 ft).	133
C.39 Assumed stratigraphy and material properties for data number 39 (water table depth = 80.5 ft).	134
C.40 Assumed stratigraphy and material properties for data number 40 (water table depth = 16 ft).	136
C.41 Assumed stratigraphy and material properties for data number 41 (water table depth = 16 ft).	137
F.1 Assumed stratigraphy and material properties for data number 26 (water table depth = 28 ft).	164

Abstract

Resistance factors for LRFD of axially loaded drilled shafts in the Las Vegas Valley are calibrated using data from 41 field load tests. In addition to the traditional implementation of Monte Carlo (MC) simulations for calibration, a more robust technique is investigated in which nested MC simulations are employed to capture the uncertainty associated with the interpretation of material properties from in-situ test data. Measures are also taken to improve design procedures regarding cemented sandy soils colloquially referred to as caliche. While caliche is common in Las Vegas, its potential contribution to resistance is difficult to predict using typical site investigation data and there is currently no consensus among local engineers regarding how it should be considered in design. Thus, an approach for treating caliche is proposed and compared to three other potentially viable methods. Overall it is found that the proposed design approach produces the most accurate nominal axial capacity predictions and the nested MC simulations yield lower resistance factors than traditional calibration procedures.

Acknowledgments

The authors would like to recognize the Nevada Department of Transportation for funding this project (award number P515-13-803) as well as Loadtest Inc. and Dr. Moses Karakuzian of UNLV for supplying much of the required data. We also extend our thanks to Abbas Bafghi and Brandon Kluzniak for their thoughtful insight and feedback.

Disclaimer

The opinions, findings, and conclusions expressed in this publication are those of the authors and not necessarily those of the Nevada Department of Transportation or University of Nevada, Reno. Alternative accessible formats of this document will be provided upon request. Persons with disabilities who need an alternative accessible format of this information, or who require some other reasonable accommodation to participate, should contact Dr. Ramin Motamed, Assistant Professor, Department of Civil and Environmental Engineering, University of Nevada, Reno. Tel: (775) 784-6960; Email: motamed@unr.edu.

Chapter 1

Introduction

The probabilistic framework which forms the basis of modern Load and Resistance Factor Design (LRFD) was introduced by [Melchers \(1987\)](#). After adopting probabilistic loads in the 1980s, the American Association of State Highway and Transportation Officials (AASHTO) formally adopted LRFD in 1994. At the same time, the American Institute of Steel Construction (AISC) also made the switch to LRFD and in 2002, the American Concrete Institute (ACI) did the same. Despite this steady progression into LRFD, however, deep foundation design still does not take full advantage of the probabilistic framework in many parts of the United States due to a lack of area-specific resistance factors derived using reliability theory-based calibrations. Instead, many regions rely on values given in [AASHTO \(2014\)](#) which were developed by fitting to Allowable State Design (ASD) safety factors. It is therefore necessary to develop new resistance factors in areas where sufficient full scale load test data is available. This report aims to contribute to this goal by calibrating resistance factors for LRFD of drilled shafts in the Las Vegas Valley of Southern Nevada.

There are a number of examples from past literature which highlight the advantages of properly calibrated resistance factors for LRFD of deep foundations (e.g. [Abu-Hejleh et al., 2015](#); [Paikowsky, 2004](#); [Allen et al., 2005](#)). Thus, area-specific calibrations have already been carried out for a number of state Departments of Transportation (DOTs). These include, but are not limited to, Oregon ([Smith et al., 2011](#)), Louisiana ([Abu-Farsakh et al., 2012](#)), Illinois ([Long et al., 2009](#)), Iowa ([Roling et al., 2011](#); [Garder et al., 2012](#)), North Carolina ([Rahman et al., 2002](#)), and Florida ([M. McVay et al., 2005](#)). While such studies represent improvements upon calibrations which fit to ASD, the interpretation of geomaterial properties from in-situ test data remains an unchecked source of epistemic uncertainty. In light of this, the reliability analyses in this study are performed using two approaches, both of which incorporate the Monte Carlo (MC) simulation technique and are validated with the First Order Reliability Method (FORM). The first approach is intended to represent

the current state-of-the-art calibration procedure and the second incorporates a proposed modification which allows uncertainty in estimating geomaterial properties from in-situ test data to be accounted for.

The design of drilled shafts in Las Vegas is complicated by the presence of cemented sandy soils, colloquially referred to as caliche. While these materials heavily influence axial response (Stone, 2009), it is difficult to predict their behavior with existing design procedures (Werle & Luke, 2007). Thus, a new practical approach for treating caliche in drilled shaft design is proposed in this report to improve overall predication accuracy. This is compared to design practice based on recommendations from the Nevada Department of Transportation (NDOT) as well as existing models intended for rock and cohesive Intermediate Geo-Material (IGM) described in Brown et al. (2010) and AASHTO (2014).

The impact of load test and Geotechnical Investigation (GI) data quality on the outcome of the reliability calibration is also investigated herein through the use of a scoring system modified from Motamed et al. (2016). A similar exercise was conducted by Smith et al. (2011) to calibrate resistance factors for driven piles in Oregon. Analyses are performed using three data subsets which are defined based on the average scores. This helps to ensure that poor data quality does not significantly skew the computed resistance factors in a non-conservative fashion.

1.1 Literature Review

1.1.1 Other Resistance Factor Calibration Studies

Past resistance factor calibration studies which pertain to drilled shafts include Liang and Li (2009), which does not apply to any specific region, as well as those carried out for Louisiana (Abu-Farsakh et al., 2012), Iowa (Roling et al., 2011; Garder et al., 2012), and Florida (M. C. McVay et al., 1998). All of these except for Liang and Li (2009) also incorporate calibrations for driven piles. Alternatively, studies performed for Oregon (Smith et al., 2011), Illinois/Wisconsin (Long et al., 2009), and North Carolina (Rahman et al., 2002) focus on driven piles exclusively.

Abu-Farsakh et al. (2012) utilized 26 drilled shaft load tests (22 of which were bi-directional) to calibrate resistance factors for Louisiana with the MC method and FORM. Figure 1.1 shows the distribution of measured and predicted resistances in the database. This indicates that drilled shaft design in the area typically underestimates nominal axial resistance by a small margin. Consequently, the study found that the local calibration justified an increase in resistance factors compared to the values recommended by AASHTO. They

also noted that the local calibration was particularly advantageous due to its applicability regarding local design procedures which are not covered in formal design manuals.

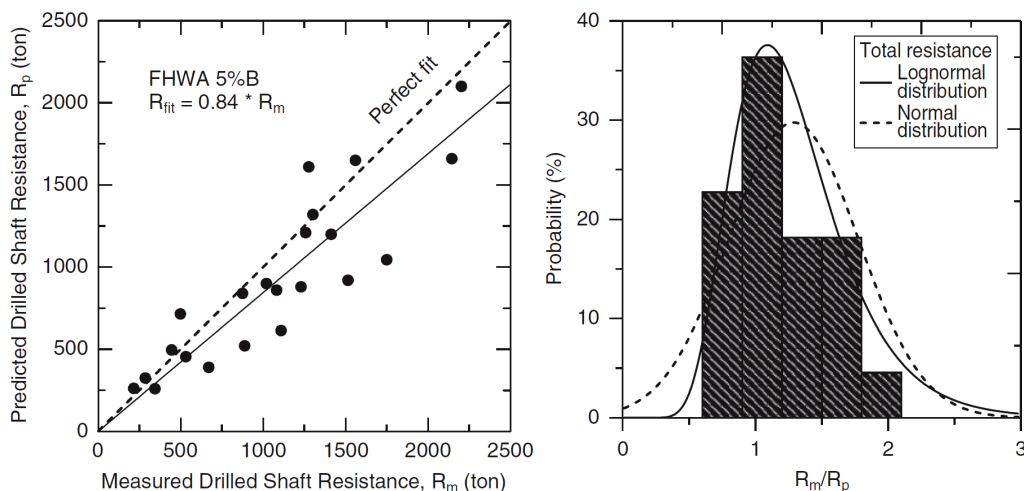


Figure 1.1: (a) Interpreted measured and predicted drilled shaft resistances and (b) histogram of bias (R_m/R_p) from Abu-Farsakh et al. (2012)

A relatively small data set consisting of 13 drilled shaft load tests was employed by Garder et al. (2012) as part of a preliminary study to calibrate resistance factors for Iowa. In this case, the predicted nominal axial resistances were slightly higher on average than the interpreted measured values (Figure 1.2). An estimate of the total resistance factor corresponding to a reliability index of 3 was obtained using the First Order Second Moment (FOSM) method. This suggested that 0.66 represented an appropriate value, which is greater than anything within the range recommended by AASHTO at the time (0.40 to 0.60).

Liang and Li (2009) compiled a data set of 65 drilled shaft load tests from the NCHRP Project 24-17 database and implemented the MC method to calibrate resistance factors. The data consisted entirely of traditional top-down load tests carried out to failure with soil conditions consisting of clay, sand, mixed soils, and weak rock. Unlike the other studies discussed in this section, the findings supported the suggested values from AASHTO. For additional information regarding deep foundation LRFD calibration analyses, refer to (Abu-Hejleh et al., 2015) which provides a summary of existing deep foundation load test databases and their uses in research.

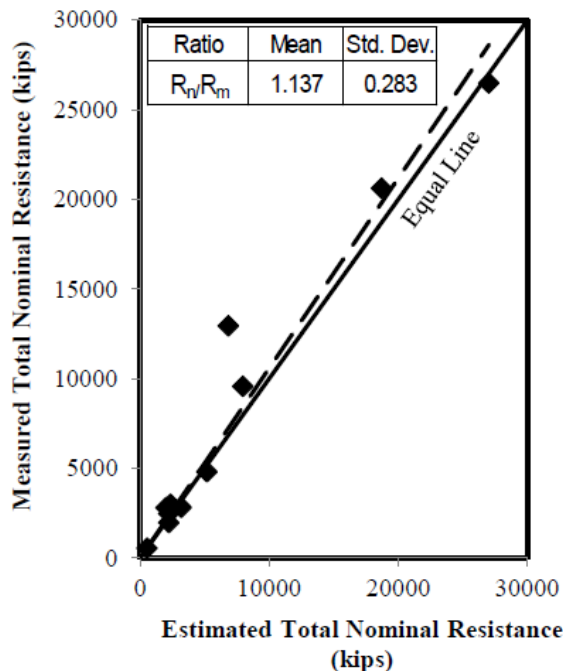


Figure 1.2: Interpreted measured and predicted drilled shaft resistances from [Garder et al. \(2012\)](#)

[M. C. McVay et al. \(1998\)](#) considered five different design methods to calibrate resistance factors for drilled shafts in Florida. Similar to the Las Vegas Valley, cemented soils are somewhat common in Florida. This led to complications/limitations which also pertain to this study. For example, [M. C. McVay et al. \(1998\)](#) did not separate side and tip resistance due to limitations in the load test data. Also, the size of the database employed for calibration purposes was kept relatively small so that only data which did not require extrapolation was considered. Alternatively, as is discussed later in this report, not enough data is available which did not require extrapolation in the Las Vegas Valley to allow for a similar approach to be carried out herein.

1.1.2 Principles of Resistance Factor Calibration

There are a number of methods available for conducting LRFD resistance factor calibrations. The simplest method is the Mean Value First Order Second Moment (MVFOSM), which relies on linearizing the limit state function at the mean values of random variables and estimating the mean and standard deviation of random variables using a Taylor series expansion in which only the first order terms are considered. However, such mathematical assumptions are potential sources of error in the MVFOSM and though they are slightly

improved in the FOSM method, a more advanced approach is preferred (Paikowsky, 2004). Hence, in this study resistance factors are calibrated using the MC simulation technique and are validated using a First Order Reliability Method (FORM) analysis. These methods consider the true mean, standard deviation, and distribution of the data to carry out the analysis.

Equation 1.1 is the design equation for LRFD when a total resistance factor is employed. This can be rearranged to serve as the limit state equation needed for calibration (Allen et al., 2005) as is shown in Equation 1.2.

$$\sum \eta_i \gamma_i Q_{ni} \leq \phi_{RT} R_n \quad (1.1)$$

where

$$\begin{aligned} \eta_i &= \text{factors to account for ductility } (\eta_D), \text{ redundancy } (\eta_R), \text{ and operational} \\ &\quad \text{importance } (\eta_I); \eta_i = \eta_D \eta_R \eta_I < 0.95 \\ \gamma_i &= \text{load factor applicable to a specific load component} \\ Q_{ni} &= \text{specific nominal load component} \\ \sum \gamma_i Q_{ni} &= \text{total factored load for the given limit state} \\ \phi_{RT} &= \text{total LRFD resistance factor} \\ R_n &= \text{total nominal resistance} \end{aligned}$$

$$g = g(X_1, X_2, \dots, X_n) = R - Q \quad (1.2)$$

where

$$\begin{aligned} g &= \text{random variable representing the safety margin} \\ R &= \text{random variable representing the factored resistance} \\ Q &= \text{random variable representing the factored load} \end{aligned}$$

The currently established procedure for performing an LRFD calibration for deep foundations is outlined in Allen (2005) and has been used in other studies including Barker et al. (1991) and Paikowsky (2004). This method, is described in general by a flowchart presented

in Paikowsky (2004) which is shown in Figure 1.3.

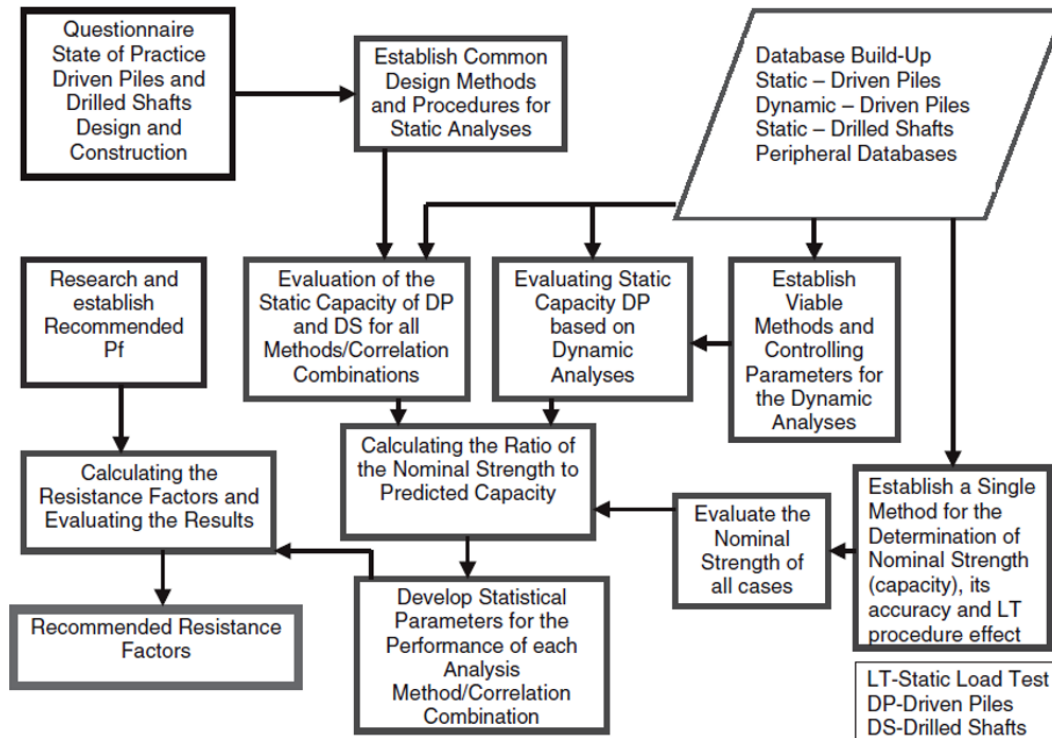


Figure 1.3: Stages of a typical LRFD calibration for deep foundations after Paikowsky (2004)

According to Figure 1.3, the first steps in a calibration for drilled shafts should include defining the state of practice, collecting a database, and determining the appropriate the reliability index, β . For the Las Vegas Valley, however, there is no well-established state of practice regarding cemented soils (this is discussed in greater detail hereafter in Section 1.1.3). The database compiled for this study is described in Section 2.1. The reliability index is used to quantify the level of reliability and is defined as the inverse of the Coefficient of Variation (COV) of g from Equation 1.2. For a normally distributed limit state function, β is related to the probability of failure, p_f , through the inverse of the normal Cumulative Distribution Function (CDF) as is shown in Equation 1.3. Alternatively, Equation 1.4 can be used to compute β if the distribution of bias ($\lambda = R_m/R_p$) is normal and Equation 1.5 can be used if the distribution is lognormal. Table 1.1 summarizes p_f corresponding to various values of β .

$$p_f = 1 - \Phi(\beta) \quad (1.3)$$

where

β = reliability index (normal distribution)

Φ = normal CDF

p_f = probability of failure

$$\beta = \frac{\mu - 1}{\sigma} \quad (1.4)$$

where

β = reliability index (normal distribution)

μ = mean of safety margin

σ = standard deviation of safety margin

$$\beta_{LN} = \frac{\ln \frac{\mu}{\sqrt{1+COV^2}}}{\sqrt{\ln 1 + COV^2}} \quad (1.5)$$

where

β_{LN} = reliability index (lognormal distribution)

μ = mean of safety margin

COV = coefficient of variation of safety margin

First Order Reliability Method

FORM is a technique developed by [Hasofer and Lind \(1974\)](#) which has the ability to assess the reliability of foundations for specific limit states (i.e. Equation 1.2). The methodology requires only first and second moment information concerning resistance and loads (i.e.

Table 1.1: Probability of failure, p_f , for different reliability indices, β .

β	p_f
2.0	2.2750E-2
2.5	6.2907E-3
3.0	1.3500E-3
3.5	2.3267E-4
4.0	3.1686E-5

means and variances) and an assumption of the distribution type. The calibration process using FORM is carried out in this research following the methods from [Ayyub et al. \(2000\)](#) which was also employed by [Paikowsky \(2004\)](#).

Figure 1.4, taken from [Paikowsky \(2004\)](#) which was adapted from [Ayyub et al. \(2000\)](#), illustrates a theoretical failure surface ($G(x) = 0$) and a space of basic random variables. In context, these are represented by Equation 1.2 and R and Q thereof. The reliability index is the distance between the origin of the space of basic random variables and the point on $G(x) = 0$ at which the joint Probability Distribution Function (PDF) of x is greatest. Hence, the latter, which is often referred to as the design point, is the most probable point on the failure surface. A FORM analysis iteratively solves for the design point and thereby enables the evaluation of reliability. Alternatively, if the target reliability index is known, the associated resistance factor(s) can be back-calculated using FORM.

In this study, Microsoft Excel Visual Basic for Applications (Excel VBA) was employed to perform FORM analyses to validate the results of the MCSs. The computational steps of this approach are based on the procedure described in [Ayyub et al. \(2000\)](#) and are adapted hereafter to evaluate the resistance factor for a given β .

1. In regular coordinates, assume a design point, x_i^* , and obtain its corresponding value in a reduced coordinate system, $x_i'^*$, using Equation 1.6. With the limit state defined by Equation 1.2, this translates to transforming R and Q into standard normal space (i.e. R' and Q'). The mean of the vector of basic random variables is commonly used as an initial guess for the design point.
2. If the distribution of basic random variables is non-normal, approximate the distribution with an equivalent normal distribution at the design point using Equations 1.7 and 1.8.
3. Set $x_i^* = \alpha_i^* \beta$, where α_i^* are direction cosines. These can be computed with Equation 1.9.

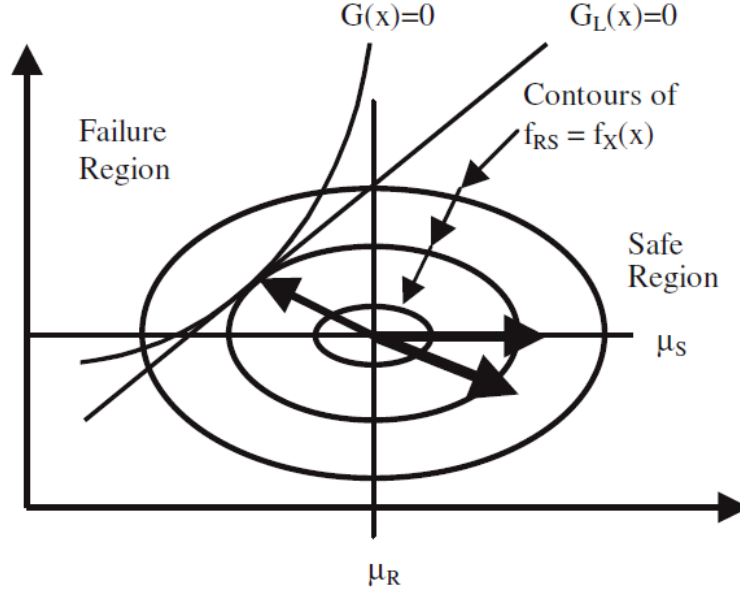


Figure 1.4: Example of random variables of a limit state function, μ_R and μ_S , in standard normal space and the associated failure surface, $G(x) = 0$ ($G_L(x) = 0$ is the linearized version), after Paikowsky (2004) and Ayyub et al. (2000)

4. Given a target β (3.0 in this study), solve Equation 1.10 for the mean resistance, μ_R^N .
5. Use Equation 1.11 to compute the resistance factor associated with the new mean resistance corresponding to the target β .

$$x_i^{*} = \frac{x_i^* - \mu_{x_i}}{\sigma_{x_i}} \quad (1.6)$$

where

μ_{x_i} = mean value of the basic random variable, X_i

σ_{x_i} = standard deviation of the basic random variable

$$\mu_x^N = x^* - \Phi^{-1}(F_x(x^*)) \sigma_x^N \quad (1.7)$$

$$\sigma_x^N = \frac{\phi(\Phi^{-1}(F_x(x^*)))}{f_x(x^*)} \quad (1.8)$$

where

μ_x^N = mean of the equivalent normal distribution

σ_x^N = standard deviation of the equivalent normal distribution

$F_x(x^*)$ = original CDF of X_i evaluated at the design point

$f_x(x^*)$ = original PDF of X_i evaluated at the design point

$\Phi()$ = CDF of the standard normal distribution

$\phi()$ = PDF of the standard normal distribution

$$\alpha_i^* = \frac{\left(\frac{\partial g}{\partial x_i'}\right)_*}{\sqrt{\sum_{i=1}^n \left(\frac{\partial g}{\partial x_i'}\right)_*^2}} \quad (1.9)$$

where

$$\left(\frac{\partial g}{\partial x_i'}\right)_* = \left(\frac{\partial g}{\partial x_i}\right)_* \sigma_{x_i}^N$$

$$g[(\mu_{x_i}^N - \alpha_{x_i}^* \sigma_{x_i}^N \beta), \dots, (\mu_{x_n}^N - \alpha_{x_n}^* \sigma_{x_n}^N \beta)] = 0 \quad (1.10)$$

$$\phi_{RT} = \frac{\sum_{i=1}^n \gamma_i \mu_{Li}}{\mu_R} \quad (1.11)$$

It should be noted that since the limit state equation is linear in this case, the selection of the initial design point does not impact the final result if closed form solutions are available to compute the equivalent normal means and standard deviations. Also, the assumed ratio of

dead to live load magnitude must be the same as assumed in the MC simulation for the results to be comparable. A ratio of 3 was selected for this research based on recommendations from Allen (2005) and Paikowsky (2004).

Monte Carlo Simulation Method

The MC method is a broad tool which has been used extensively in science and engineering since the mid 1940s (Lemieux, 2009) and now represents the state of the art in reliability calibrations for deep foundations (Paikowsky, 2004). With a MC simulation, repeated random sampling is used to obtain numerical results. Thus, for deep foundation resistance factor calibration, the LRFD limit state equation (Equation 1.2) is evaluated on each iteration by treating the load and resistances as random variables following specified probability distributions. While resistance statistics must be determined by analyzing field test data, it is appropriate to employ existing load statistics for superstructure analysis. In this report, the values recommended by Paikowsky (2004) are assumed to characterize the random variables for dead and live load. These are shown in Table 1.2.

Table 1.2: Load statistics and factors employed in this study (Paikowsky, 2004).

Load Type	Bias	COV	Load Factor
Dead load	$\lambda_{DL} = 1.05$	$COV_{DL} = 0.1$	$\gamma_{DL} = 1.25$
Live load	$\lambda_{LL} = 1.15$	$COV_{LL} = 0.2$	$\gamma_{LL} = 1.75$

1.1.3 Soil Conditions in the Las Vegas Valley

Typical soil conditions in the Las Vegas Valley are characterized by inter-bedded layers of silty clay and sand with seams of a hardened sedimentary deposit consisting of calcium carbonate cemented sandy soils, colloquially known as caliche. Caliche is found in arid regions around the world and represents a problematic geomaterial in terms of deep foundation design because of its general absence from design manuals and its uncommonly high strength. In Las Vegas, caliche is most prevalent in the western and central parts of the valley (Wyman et al., 1993). Recent research suggests that the presence of caliche layers at least one shaft width thick can reduce shaft settlement by more than 50% even if only a single such layer exists (Stone, 2009).

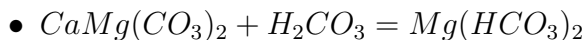
Caliche can be formed when carbonate basement rock exists beneath carbonate containing soil, the climate is arid to semi-arid, and there is significant capillary activity as well as

abundant CO_2 in the environment (Atabey et al., 1998). If these conditions exist, the process by which caliche may be formed is as follows:

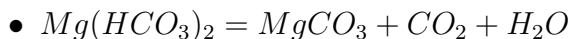
1. Carbonic acid (H_2CO_3) is formed when CO_2 reacts with water.



2. The newly formed carbonic acid dissolves calcium and magnesium bearing rocks resulting in a solution saturated with calcium and magnesium bicarbonate ($Ca(HCO_3)_2$ and $Mg(HCO_3)_2$).



3. The calcium and magnesium bicarbonate saturated water percolates down through loose soil and mudstone only to rise back towards the surface due to capillary effects and evaporates during dry seasons.
4. Evaporation removes the CO_2 and water from the calcium bicarbonate solution, leaving the $CaCO_3$ and $MgCO_3$ to cement the soil in which the solution previously resided.



Brown et al. (2010) provides a discussion concerning cemented soils and specifically refers to caliche in the western United States. Following this, Table 1.3 shows the recommended classification, drilling, and sampling characteristics of caliche in the Las Vegas Valley. It should be noted that some local practitioners in Las Vegas have called the information regarding drilling rates given in Table 1.3 into question.

Table 1.3: Example classification and drilling/sampling characteristics of caliche in the Las Vegas Valley (Cibor, 1983).

Nomenclature		Hardness Classifi- cation	Drilling Rates ¹ (min/ft)		Description of Material and Drill Cuttings
			Without Pull- down	With Pull- down	
Cemented Coarse- grained Deposits	Cemented Fine-grained Deposits				
Sand and gravel with scattered cementation	Decomposed caliche with silt and clay	Very dense to slightly hard	-	-	Variable matrix of unce- mented soil and cemented zones. Samples obtained with split-spoon or thick-walled sampler. Can be crumbled with fingers.
Partially cemented sand and gravel	Decomposed caliche	Moderately hard	≤5	≤3	Cemented to varying de- grees. Fine grained deposits sampled with thick walled sampler; coarse-grained samples cannot be obtained with thick-walled sampler. Drilling produces large, rounded cuttings. Cuttings can be broken with difficulty with hands or easily when hammered.
Cemented sand and gravel	Weathered caliche	Hard	6 to 30	3 to 6	Visible chemical alterations from fresh deposits. Com- pressive strength similar to fresh deposits. Slight sec- ondary porosity. Samples ob- tained by coring techniques. Drill cuttings less than 1/8 inch in diameter. Fragments can be broken with difficulty by hammering.
	Fresh caliche	Very hard	700	70	No visible signs of chemical alteration. Non-porous. Re- sembles metamorphic or sedi- mentary rock. Drill cuttings less than 1/8 inch in diam- eter. Samples obtained by coring techniques. Fragments cannot be broken by hammer- ing.

¹Using Mayhew 100 drill rig

A case study of the drilled shaft foundation system for the Vegas High Roller project was conducted by Kluzniak et al. (2014). They found that the nearly all of the load bearing for the drilled shafts was accommodated by a relatively shallow caliche layer and it was also determined that structural capacity of the shafts would likely govern the failure mode. The interpreted stratigraphy, which includes the aforementioned near-surface caliche layer, and corrected standard penetration blow counts for three example boreholes from this project are given in Figure 1.5.

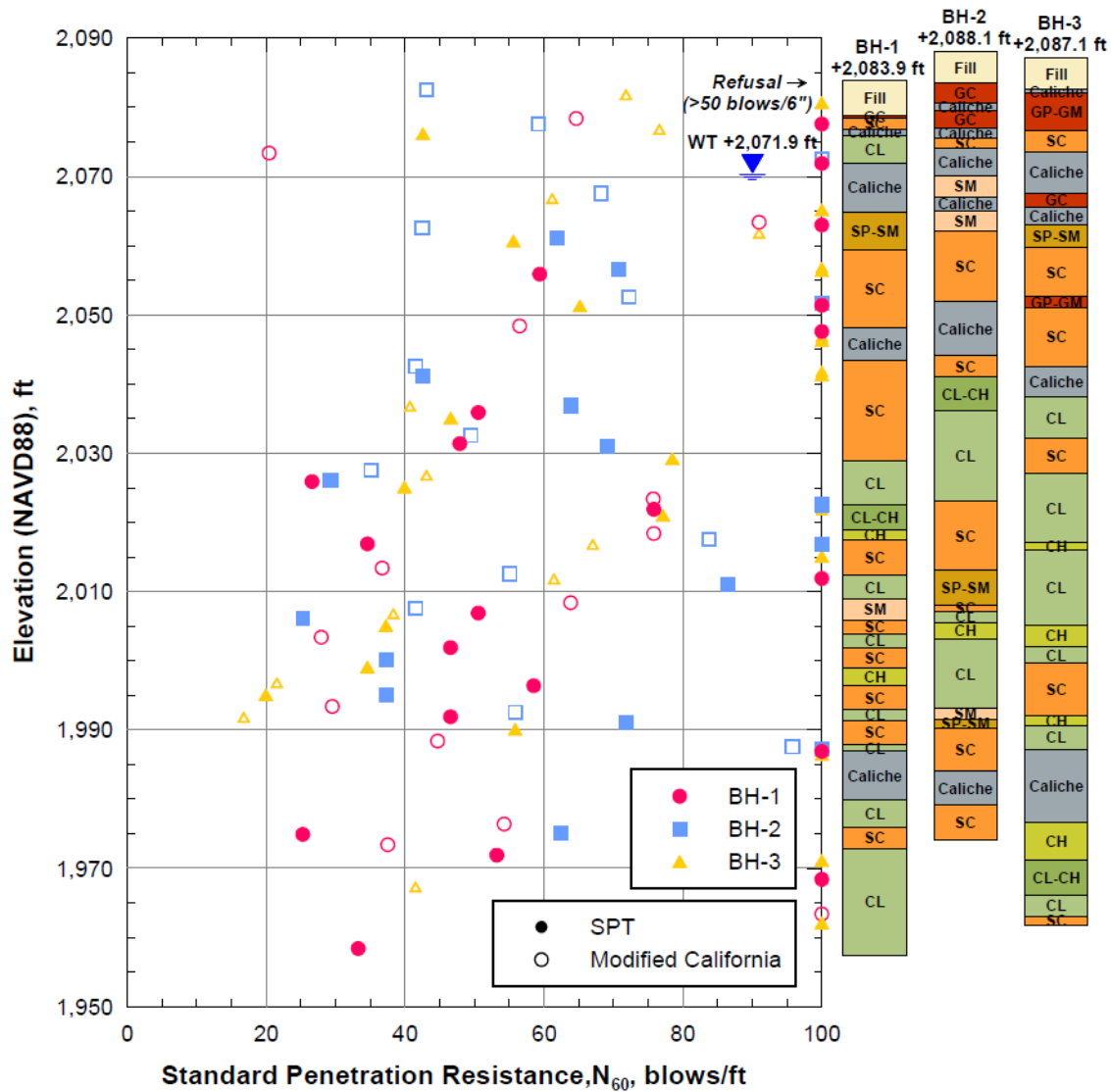


Figure 1.5: Example soil profiles and corrected standard penetration blow counts for the Vegas High Roller project (from Kluzniak et al., 2014)

Murvosh et al. (2013) employed data from 212 shear wave velocity (V_s) profiles and 1400 geologic well logs in Las Vegas to develop a three-dimensional model of the sediments in the

Las Vegas Valley. This involved building characteristic profiles for four main sediment units: sand, clay, gravel, and mixed. Figure 1.6 shows the scatter in V_s for each of these units with depth which was then used to develop the generalized characteristic profiles (Figure 1.7).

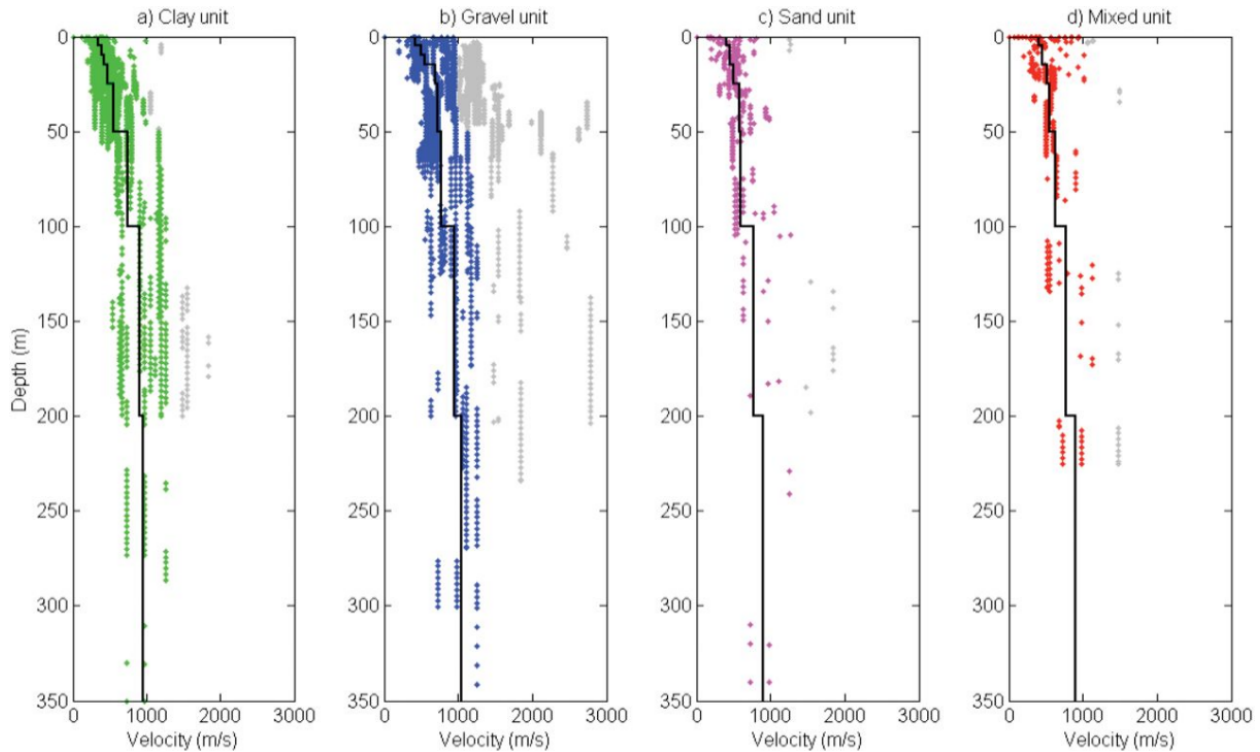


Figure 1.6: V_s scatter for different soil unit in the Las Vegas Valley (Murvosh et al., 2013)

Luke et al. (2003) provides evidence that the methodology for Spectral Analysis of Surface Waves (SASW) described by Stokoe et al. (1994) can be used to identify cemented material with reasonable accuracy. They compared profiles developed with SASW at the Las Vegas Springs Preserve to boring log information and independent seismic crosshole measurements made across three boreholes, nominally 3 m apart, located at the center of and in line with the SASW array. This is presented in Figure 1.8. While two relatively thin and deep caliche seams could not be resolved with the SASW method, two layers within the upper 10 m were correctly identified and there was a strong general agreement among the different data sets.

As noted earlier, groundwater conditions are a critical factor in the formation of cemented material. Thiros et al. (2010) provides a detailed discussion of the hydrological setting in the Las Vegas Valley and highlight the differences between pre-development and modern conditions. This is depicted in Figure 1.9 and suggests that development in the area has led to significant changes in the local hydrology. Thus, the pre-development hydrology is more pertinent to the formation of existing caliche in Las Vegas.

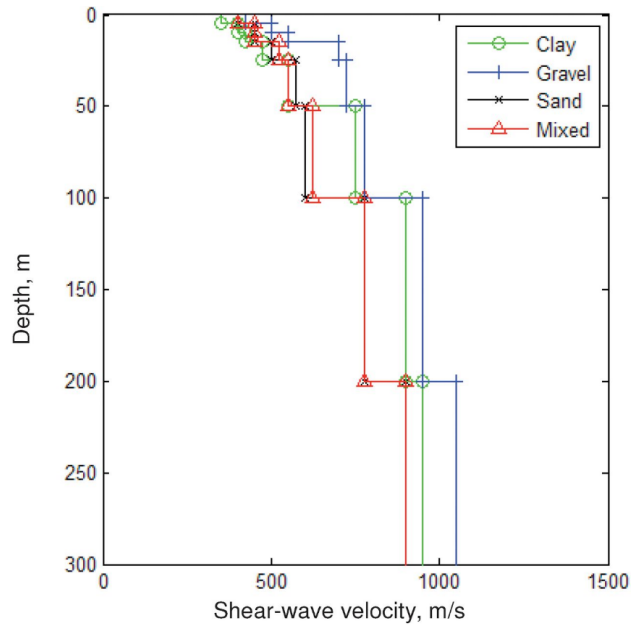


Figure 1.7: Characteristic V_s profiles for different soil unit in the Las Vegas Valley (Murvosh et al., 2013)

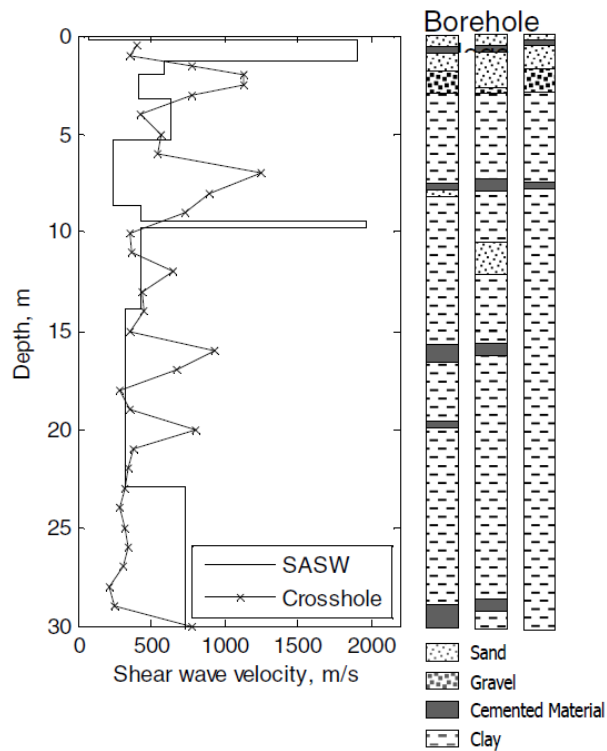


Figure 1.8: Using seismic methods to detect caliche: example case from the Las Vegas Springs Preserve (Luke et al., 2003)

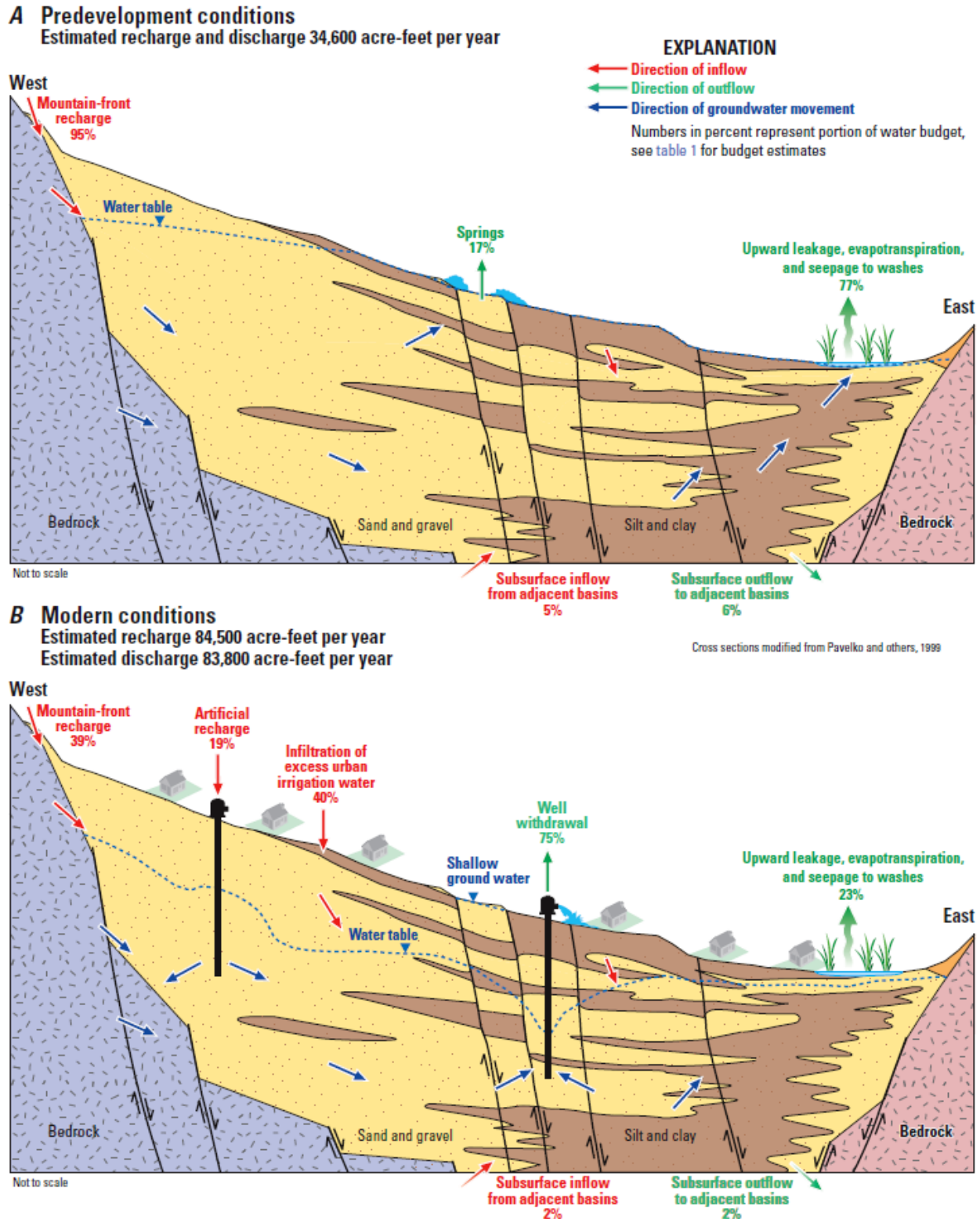


Figure 1.9: Generalized cross-sections for the Las Vegas Valley showing the basin-fill deposits and components of the groundwater flow system under (A) pre-development conditions and (B) modern conditions (from Thiros et al., 2010)

1.1.4 Field Load Testing of Drilled Shafts

A database of field load test is required to carry out a resistance factor calibration study for drilled shafts. However, full-scale load tests are typically performed to benefit individual projects for two general reasons (Brown et al., 2010): (1) to obtain information concerning load transfer is side and/or base resistance to allow for an improved design and (2) to prove that the constructed test shaft meets the required strength and/or serviceability criteria. Load tests performed with these goals are often referred to as design phase and proof tests, respectively. Another advantage of load testing is cost savings. For example, Vanderpool et al. (2011) performed a case-study on Utah Transit Authority's Airport Light Rail Trax project and found that load testing saved the owner in excess of \$800 thousand dollars.

There are many forms of field load tests for drilled shafts. Examples of the most prominent types are given in Figures 1.10 through 1.13. These include:

- top-down static load tests conducted with a hydraulic jack and above-ground reaction system,
- bi-direction load tests carried out with an embedded bi-directional load cell,
- top-down rapid testing using an accelerated reaction mass (i.e. statnamic), and
- dynamic testing with a drop weight impact system.

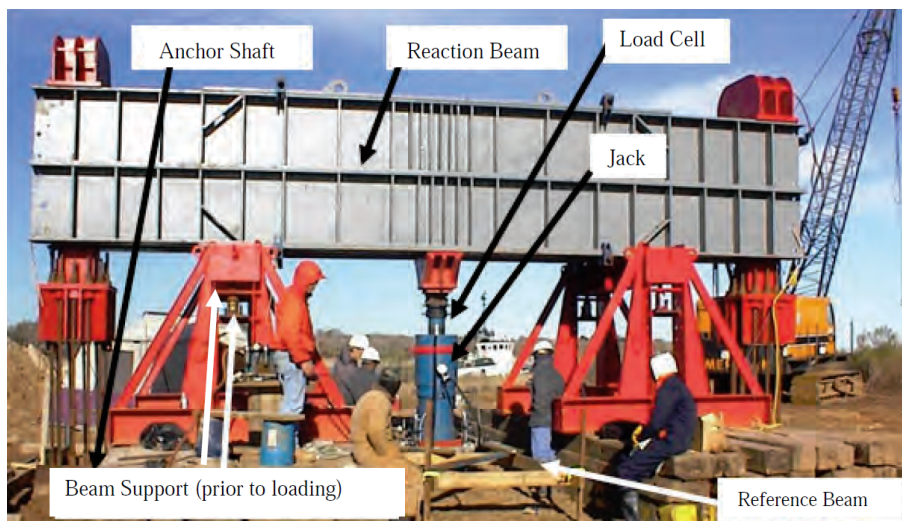


Figure 1.10: Example of a traditional top-down static load test on a drilled shaft (Brown et al., 2010)

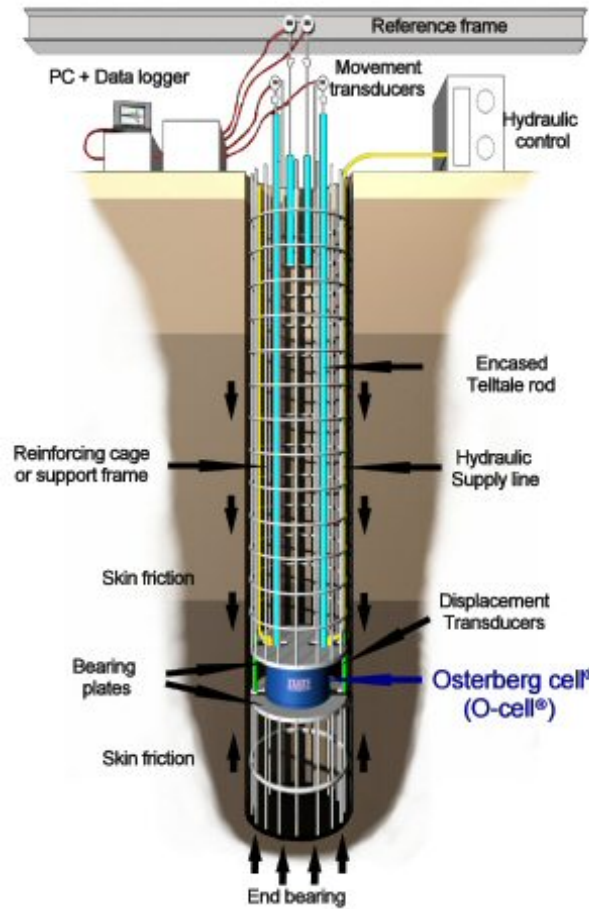


Figure 1.11: Example of a bi-directional (O-Cell) load test setup

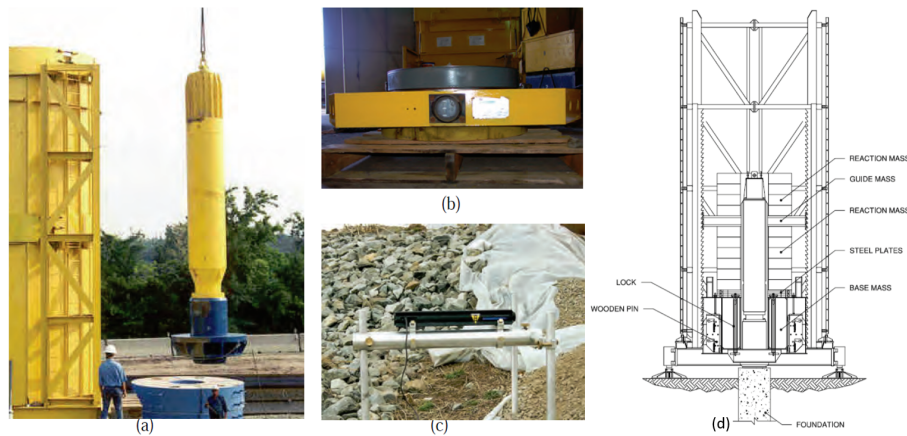


Figure 1.12: Example of a static loading apparatus (Brown et al., 2010): (a) piston and silencer assembly, (b) load cell and laser target, (c) laser for displacement measurement, (d) schematic diagram



Figure 1.13: Example dynamic load tests on drilled shafts using a drop weight (left) and pile hammer (right) (Brown et al., 2010)

Despite the inherent advantages of bi-directional load testing, such as relatively low cost and the ability to apply large loads, there are significant challenges associated with its use for resistance factor calibration studies. Mainly, the raw data is not in the form of a traditional top-down test so defining axial capacity according to common limit state criteria is not possible without some level of data processing. This is covered in greater detail in Chapter 2.

The most common type of bi-directional load test for drilled shafts was introduced by Dr. Jori Osterberg with development of the O-Cell, the first bi-directional load cell (Schmertmann & Hayes, 1997). While early forms of this technology have been in use since 1984 (Hannigan et al., 1997), alternatives from other sources have only recently entered the market. One example of this is the bi-directional load cell developed by Applied Foundation Testing, Inc. (AFT). The main advantages and disadvantages of using this type of load test for drilled shafts are summarized in Brown et al. (2010) and are reiterated in a general sense hereafter.

Advantages of bi-directional load testing:

- Larger loads can be achieved than with any other type of load test, enabling testing of production-size shaft in many cases.
- The side and base resistances may be isolated if multiple load cells are used or proper strain gauge instrumentation is installed. This may also allow for the side resistance in specific layers to be determined in some cases.
- Static loading can be maintained so that creep behavior can be observed.

Disadvantages of bi-directional load testing:

- The test shaft must be predetermined because load cells cannot be installed after construction takes place.
- If only a single load cell is used, the weaker portion of the shaft (i.e. above or below) will dictate the maximum load which can be achieved. This often prevents tests from reaching loads corresponding to the geotechnical strength limit state requirements.
- Elastic compression above the load cell must be accounted for theoretically in order to construct the equivalent top-down load-settlement curve.
- Current procedures for estimating side resistance in rock sockets are likely to be conservative.

Chapter 2

Measured Data

2.1 Database

The load test data employed for this study consists of 41 tests selected from the Nevada Deep Foundation Load Test Database (NDFLTD) ([Motamed et al., 2016](#)). These represent the tests that passed an initial screening of 45 tests to ensure that an associated GI report was obtainable and that enough movement was achieved to enable an estimate of the axial resistance corresponding to the geotechnical strength limit state. In the final data set, shaft diameters range from 2 to 8 ft with embedded lengths from 31.6 to 128.0 ft and all but one of the selected load tests involved a bi-directional load cell to induce movement (as opposed to a traditional top-down test). While some of the test shafts were constructed under dry conditions, the number of such cases was insufficient to separate the LRFD calibrations based on construction methods. Also, inspection of the measured responses reveals that there is no statistical basis for treating the dry constructed test shafts as outliers from the rest of the data. Figure [2.1](#) shows the approximate locations of the test shafts and histograms of shaft diameter, embedded length, and relative fractions of different soil types along shafts are given in Figure [2.2](#).

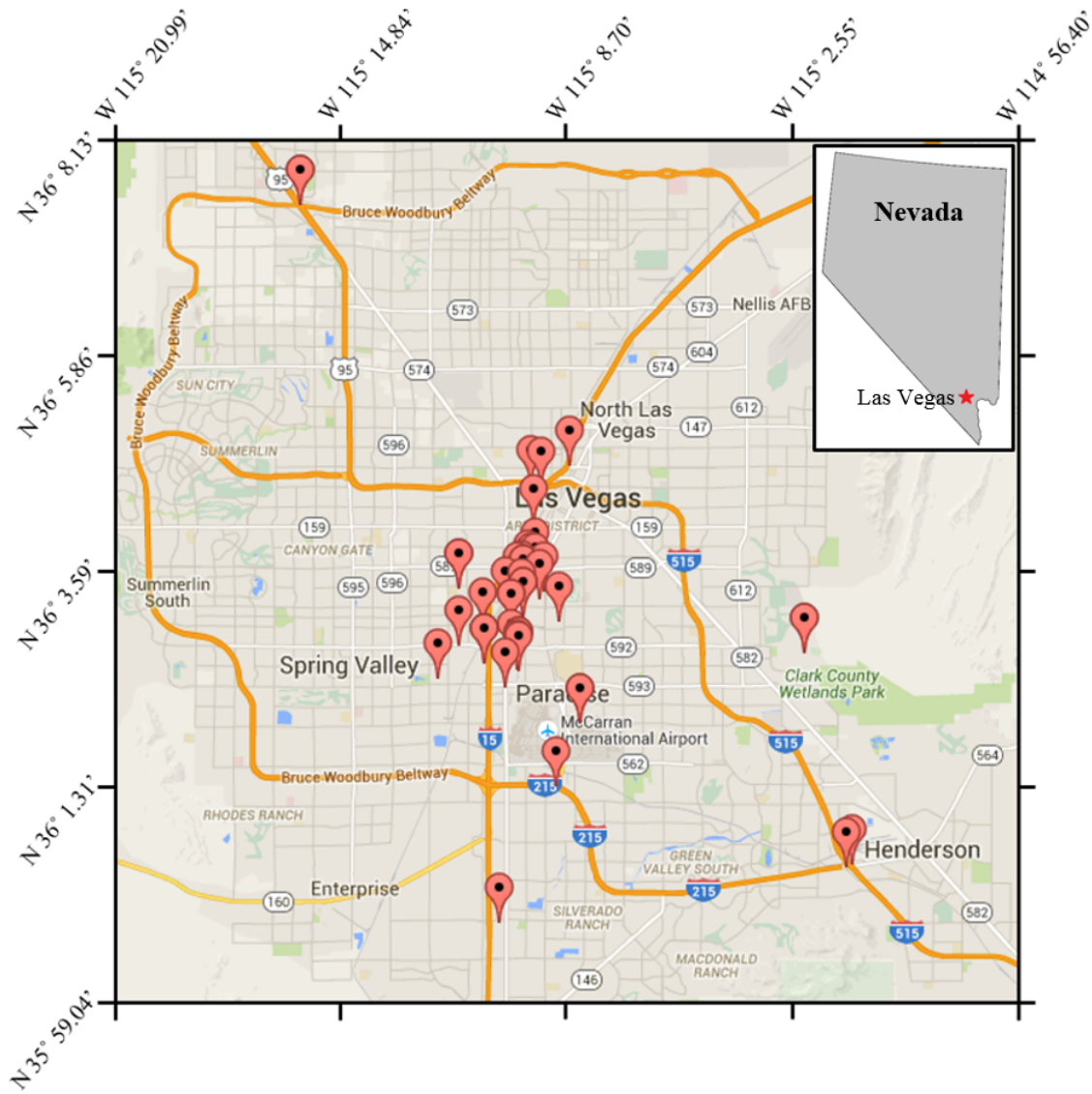


Figure 2.1: Approximate locations of the test shafts included in the study

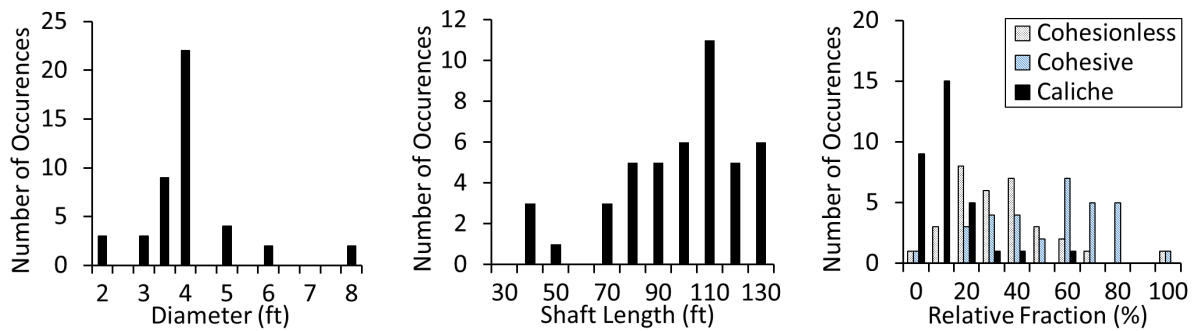


Figure 2.2 Distribution of select characteristics among the data employed for calibration

Microsoft Access and Visual Basic for Applications (VBA) is employed to develop the interface for the NDFLTD. Figure 2.3 depicts the finalized object components and information mapping. With this framework, the user can query foundation load test data and associated GI information. Drop down menus are also included to enable constrained searches based on the type of foundation, a specified range of diameters, and/or the presence of designated soil units. A screen-shot of the main search window is given in Figure 2.4.

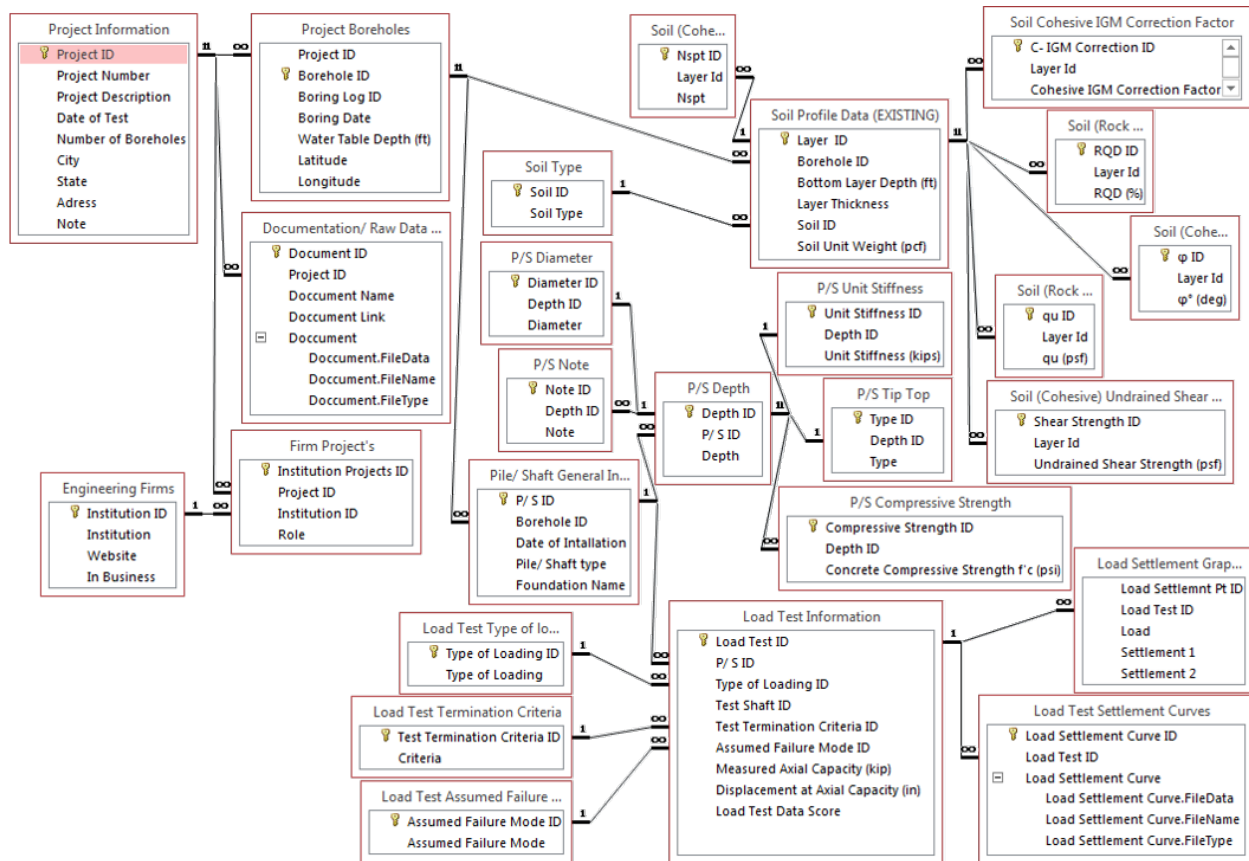


Figure 2.3: Object components and information mapping in the NDFLTD

Once a selection is made in the main search window, the user can choose to view the associated GI data, load test data, or plot up to 10 points at once on an interactive map. Examples of the GI and load test data report formats are given in Figures 2.5 and 2.6, respectively. All pages which display data include an active link to the original source of the information being presented. Additionally, the data may be exported to Microsoft Excel or to a Personal Data Form (PDF). The processed GI data, such as in the example from Figure 2.5, include the minimum parameters required for design against axial loading for the assumed units in each layer. Hence, additional information is sometimes available in the original reports which are linked on the same page.

Select Projects and Show a Report, or select nothing and show a Report with all Projects

Project Selection

Project Description	Boring Log ID	Foundation Name
I-215 Airport Connector	B-06	TS-01
I-15/ US 95 Interchange	B-2	TS-02
I-15/ US 95 Interchange	B-2	TS-03
I-15/ US 95 Interchange	B-3	TS-04
Encore Tower	B-2	TS-01
Planet Hollywood	B-1	TS-01
City Center	B-18	TS-01
City Center	B-13	TS-02
Fountainbleau	B-1	TS-01
Fountainbleau	B-2	TS-02

Foundation Type

Foundation Diameter Between (ft) And (ft)

Projects with with a thickness greater than (ft) and less than (ft)

Welcome Page

Show Borehole Logs

Show Foundation Data

Show Boreholes On Map (up to 10 points)

Figure 2.4: Main search window in the NDFLTD

PROJECT BOREHOLE LOGS Export to Excel Export PDF Menu

NEVADA DOT Project Name: **Planet Hollywood** Project Number **LT-9297** **N**

Borehole Log ID: **B-1** Raw Data Link: [Raw Data\Planet Hollywood](#) City, State: **Las Vegas, NV**

9/14/2005 **1** Borehole(s) Water Table Depth **20** (ft) Address: **3667 S Las Vegas Blvd**

Bottom Layer Depth (ft)	Layer Thickness	Soil Type	Soil Unit Weight (pcf)	ϕ° (deg)	N_{SPT} (Field)	Undrained Shear Strength (psf)	q_u (psf)	RQD (%)
2.5	2.5	Cohesive	124 ₁		16	3016		
5	2.5	Cohesionless (SM)	110 ₁	40	23			
7.5	2.5	Cohesionless (SM)	110 ₁	40	23			
16	8.5	Cohesive	116 ₁		4	534		
20	4	Cohesive	133 ₁		17	2060		
25	5	Cohesionless (GP)	140 ₁	43	42			
29	4	Caliche	140	40	R		625000	52
35	6	Cohesionless (SM)	132	42	42			
36	1	Caliche	140	40	R		625000	52
43	7	Cohesionless (GP)	132	41	44			
47	4	Caliche	140	40	R		625000	52
53.5	6.5	Cohesive	136 ₁		35	3920		
56	2.5	Caliche	140	40	R		625000	52
65	9	Cohesive	131		40	4175		
69	4	Caliche	140	40	R		625000	52
85	16	Cohesionless (SM)	130 ₁	41	40			
85.5	0.5	Caliche	140	40	R		625000	52
87	1.5	Cohesive	128		16	1450		
100	13	Cohesionless (SM)	129 ₁	37	16			
110	10	Caliche	140	40	R		625000	52

1 Denotes values from lab testing (others interpolated from NSPT)
 2 Denotes Soil with "Partial Cementation"

Figure 2.5: Example GI report in the NDFLTD

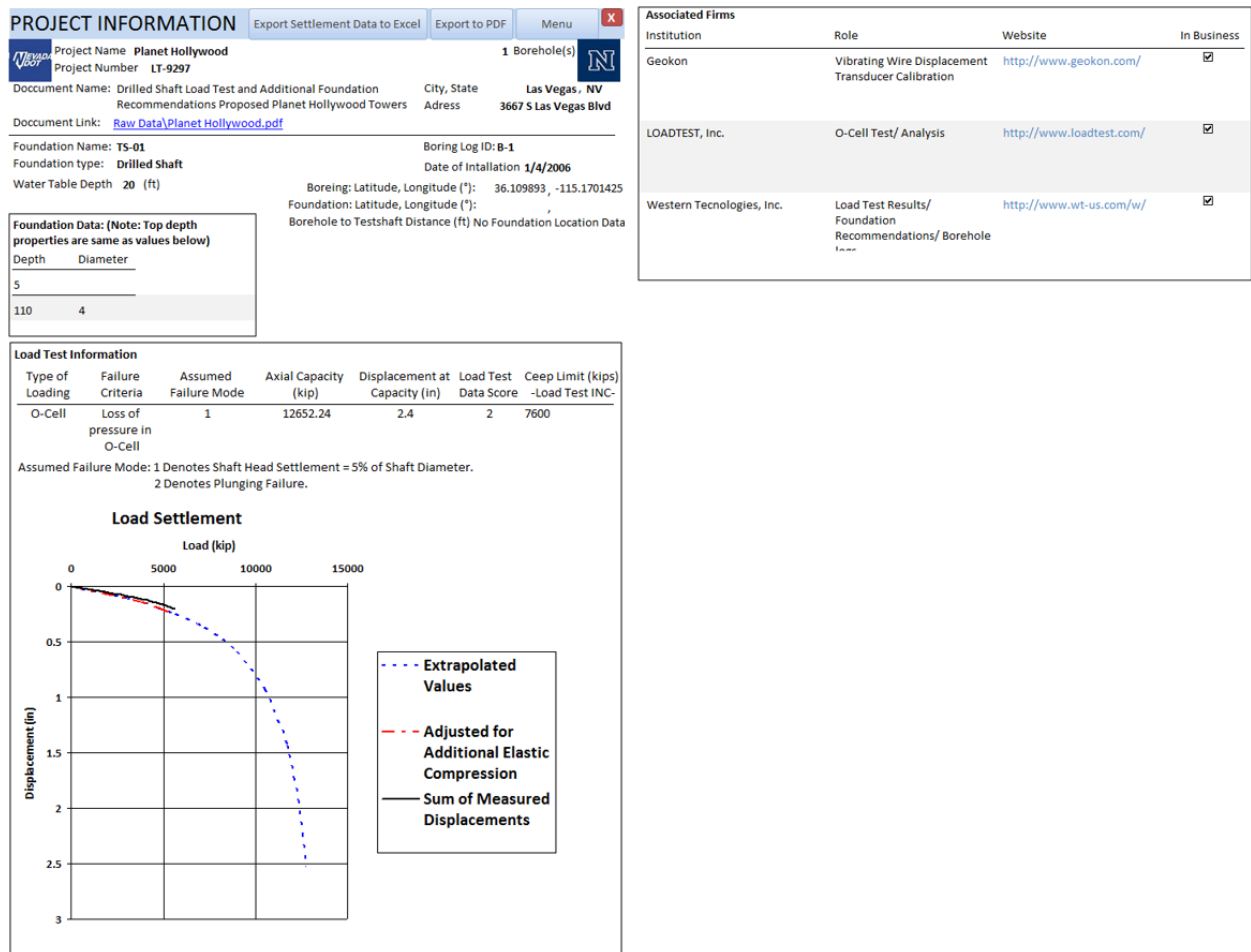


Figure 2.6: Example load test report in the NDFLTD

2.1.1 Sharing

The NDFLTD is available as an electronic supplement linked in Appendix A. Note that usage guidelines and a stand-alone ReadMe text file are accessible from within the database interface. Additionally, all of the interpreted soil boring logs are given in Appendix C and the original load test and associated geotechnical reports are available as an electronic supplement in Appendix B.

2.2 Interpretation of Bi-Directional Load Test Data

Bi-directional load test data consists of two components of load and displacement, one for movement above the load cell and one below. An example of this is shown in Figure 2.7 (upper plot). To estimate the measured capacity from this type of test, additional details about the test shaft must first be known so that the equivalent top-down curve can be constructed in a fashion that accounts for the elastic settlement which would have occurred in the upper portion of the shaft in a traditional top-down test. Namely, this information includes the buoyant weight of the test shaft above the load cell, the unit stiffness above the load cell, and the shaft geometry.

Construction of an equivalent top-down curve typically involves two phases: (1) computing the equivalent rigid top load-settlement and (2) correcting for the effects of elastic compression. Phase 1 requires summing the loads associated with equal movement above and below the load cell, as is shown in Figure 2.7.

Two methods of correcting for elastic compression above the load cell are considered in this study. It is important to note that the elastic compression below the load cell is not taken into account in either method because it is theoretically the same for both a bi-directional and top-down load test. The first method, hereafter referred to as the approximate method, accounts for the estimated pattern of developed side shear stress through coefficients known as centroid factors. This approach, described by Figure 2.8 and Equation 2.1, is often advantageous because it allows for any available data to be used in estimating the pattern of developed side shear. Kishida et al. (1992) and Ogura and Kishida (1996) offer validation for the approximate method.

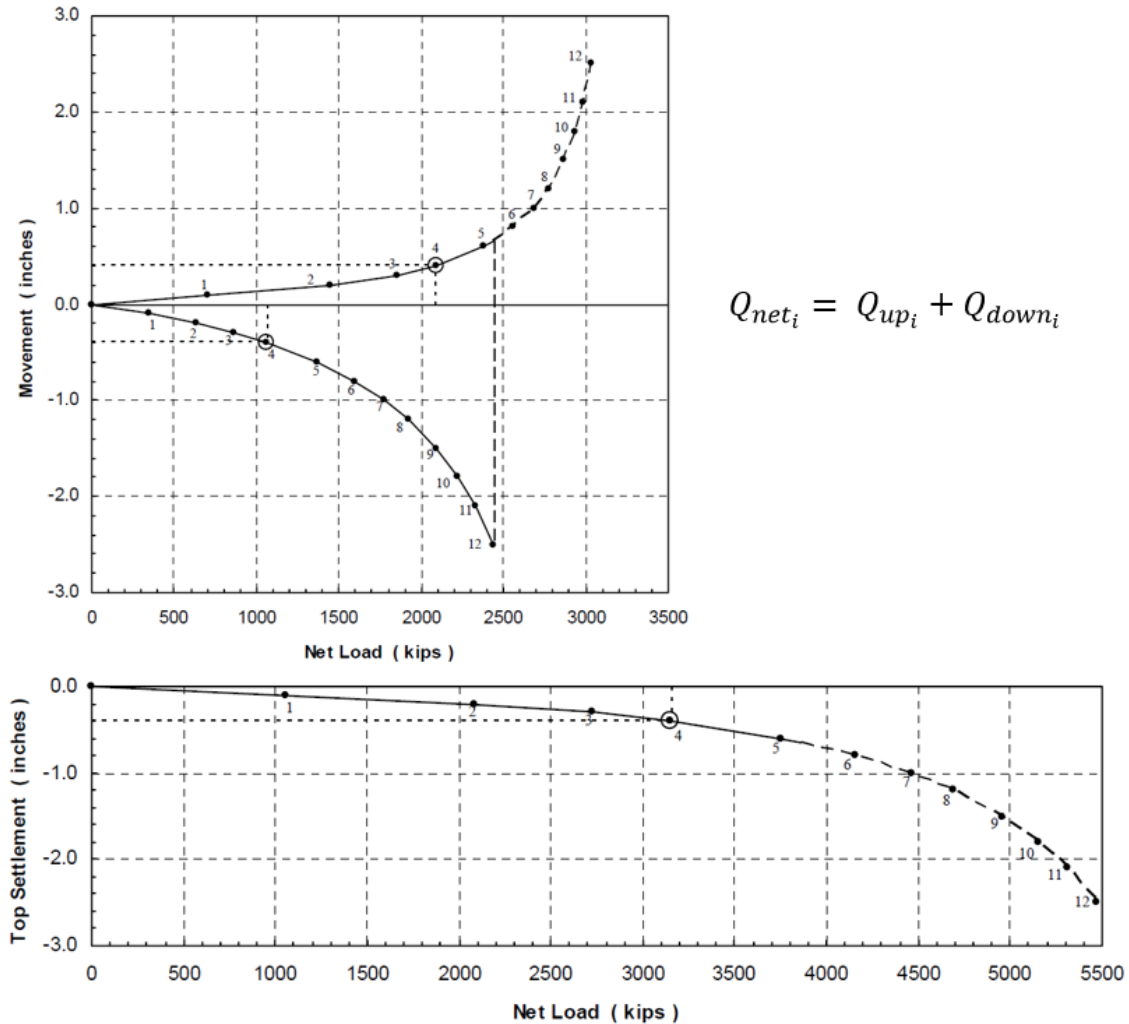


Figure 2.7: Determination of the rigid equivalent top-down load-settlement curve from bi-directional load test data where Q_{net_i} is the net load for movement increment i (modified from original figure provided by Loadtest Inc.)

$$\delta_{up} = C_1 \frac{Q'_{upA} (L_1 + L_2)}{AE} \quad (2.1)$$

where

δ_{up} = Elastic compression for a single stage bi-directional load test above load cell A

C_1 = Centroid factor (see Figure 2.8)

Q'_{upA} = Net upward load applied by the load cell (i.e. $Q_{upA} - w'_{L_0+L_1+L_2}$)

A = Cross-sectional area of the test shaft

E = Elastic modulus of the test shaft

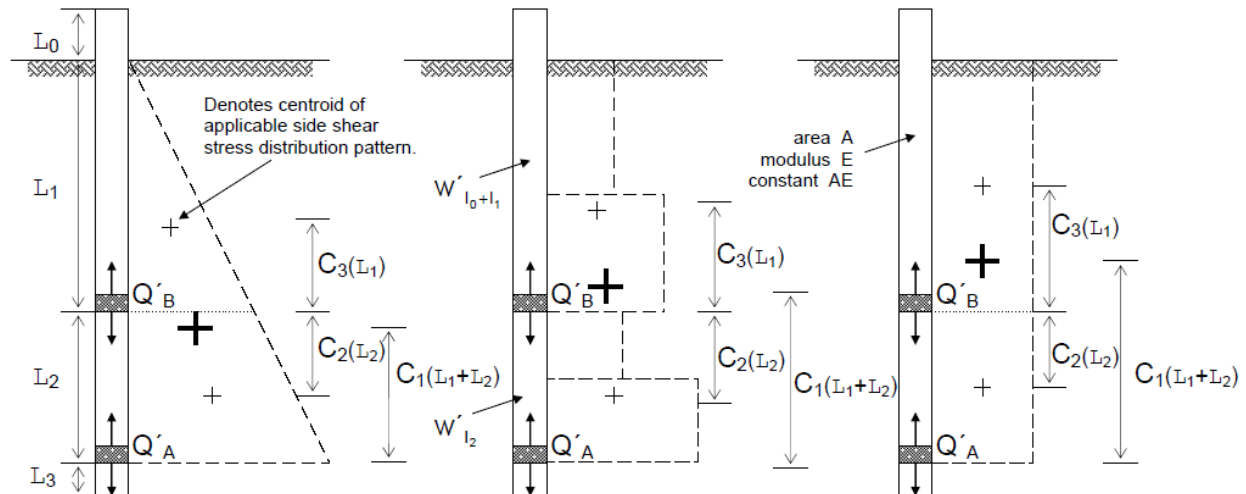


Figure 2.8: Example patterns of developed side shear stress and corresponding parameters needed to estimate elastic compression above the load cell(s) in a bi-directional load test, after [Loadtest Inc. \(2000\)](#). Note that w' denotes the buoyant weight when below the water table

If good quality and complete strain gauge data is available, then the second method of correcting for elastic compression may be applicable. This is hereafter referred to as the load-transfer method and is based on procedures and validations from [Lee and Park \(2008\)](#) and [Meyer et al. \(1975\)](#). The procedure is described by Figure 2.9 and Equations 2.2 through 2.4, which must be solved for in an iterative fashion for each section, i , until the computed displacements and loads match the measured values. Note that the load transfer in end-bearing (i.e. the q - z curve) must also be considered in the same way as the side load transfer in the above shaft sections.

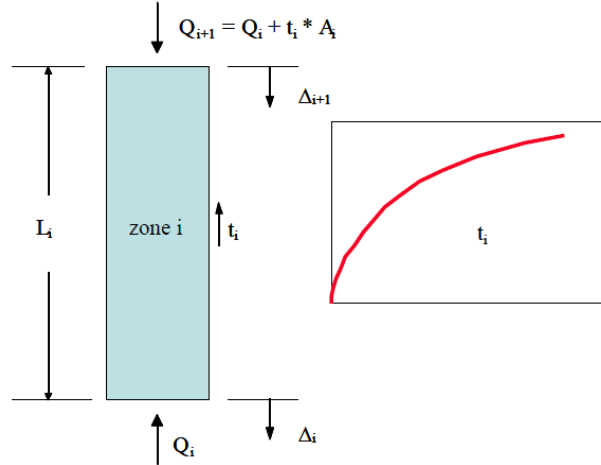


Figure 2.9: Analytical framework for a single shaft section in the t - z method for correcting bi-directional load test data for elastic compression above the load cell, after [Loadtest Inc. \(2000\)](#)

$$\delta_i = \frac{(Q_i + Q_{i+1}) L_i}{2A_i E_i} \quad (2.2)$$

$$\Delta_{i+1} = \Delta_i + \delta_i \quad (2.3)$$

$$Q_{i+1} = Q_i + t \left(\frac{\Delta_i + \Delta_{i+1}}{2} \right) A_i \quad (2.4)$$

where

δ_i = Elastic compression associated with section i

Q_i & Q_{i+1} = Load at the bottom and top of the section, respectively

Δ_i & Δ_{i+1} = Displacement at the bottom and top of the section, respectively

A_i = Cross-sectional area of the section

E_i = Elastic modulus of the section

In this study, the load-transfer method is preferred over the approximate method for constructing equivalent top-down load curves from bi-directional test data because it directly considers the accumulated strains to account for the pattern of developed side shear (as opposed to approximating it with the centroid factor). Once this step is complete, measured resistances are interpreted as the lesser of axial loads corresponding to: (a) settlement equal

to 5% of the shaft diameter or (b) the onset of plunging failure. Plunging is defined when movement occurs without the application of additional load. Also, the method from [Chin \(1970\)](#) is employed when extrapolation is required to reach the governing failure criteria. The finalized equivalent top-down load-settlement curves for all of the load tests in this study are presented in Appendix D.

2.3 Scoring System

A scoring system proposed by [Motamed et al. \(2016\)](#) is employed herein to quantify the quality of each load test and associated GI. This enables separate reliability calibrations to be carried out for three data quality bins: (a) all data, (b) mean score > 2 , and (c) mean score ≥ 3 . The scoring criteria, which is presented in Table 2.1, is setup such that a higher score indicates higher quality and considers factors such as the amount of extrapolation required to approximate the axial load at failure from the load test data, the thoroughness of the GI, and the distance from the GI to the test shaft. The precise distance from the borehole to the test shaft is known for 22 of 41 data points and an approximate distance is known for an additional 11 points. Figure 2.10 portrays the distribution of scores for the data included in this report and Table 2.2 tabulates this information along with basic test shaft properties and measured resistances. Note that the names of the load test projects are not included in order maintain confidentiality with the owners of some of the data.

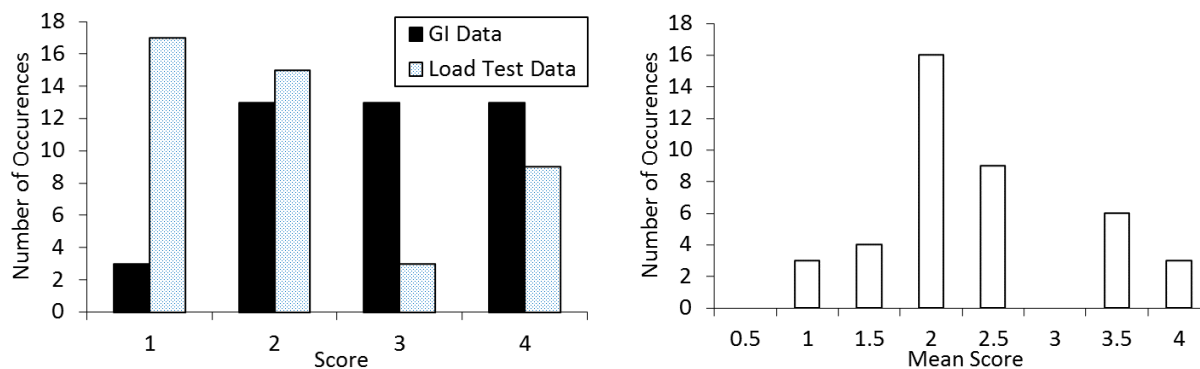


Figure 2.10: Load test and GI quality scores for the data included in this study

Table 2.1: Scoring criteria for load test and GI data quality.

Score	Scoring Criteria	
	Load Test Data	Geotechnical Investigation Data
1 (worst)	Extrapolation $> 2\%$ of the shaft diameter is required for both components of bi-directional movement or $> 3\%$ is required for a top-down test.	Incomplete boring logs with little to no SPT data or proper visual-manual classifications. No lab data.
2	Extrapolation $> 2\%$ of the shaft diameter is required for one component of bi-directional movement (second component may require $< 2\%$) or $> 2.5\%$ but $\leq 3\%$ is required for a top-down test.	Boring logs with minimal SPT data (i.e. missing for some geologic units) and useful visual-manual classifications. No lab data.
3	Extrapolation $< 2\%$ of the shaft diameter is required for both components of bi-directional movement or $> 2\%$ but $\leq 2.5\%$ is required for a top-down test.	Boring logs are complete with SPT data, visual-manual classifications and possibly torvane or pocket pen data. Limited lab data and/or additional in situ data is available.
4 (best)	Either no extrapolation is needed or extrapolation $\leq 2\%$ of the shaft diameter is required for only one component of load-cell movement or in total for a top-down test.	Complete boring logs with detailed material classifications, SPT data and possibly other data such as CPT or shear wave velocity measurements. Thorough lab data covering soil strengths is available.

Note: If a test shaft is not fully instrumented, the load test data score is reduced by 1. For every 150 ft a borehole is spaced from the test shaft, or if the distance is unknown, the GI data score is reduced by 1. If quality control is lacking or significant problems/irregularities are present in the constructed shaft, the load test data score is reduced by 2.

Figure 2.10 shows that there is a higher concentration of low quality load test data than GI data in the current data set. When combined, the mean data quality scores are predominately in the range of 2.0 to 2.5. From the data provided in Table 2.2, it can be determined that the average distance between the test shaft and GI is approximately 90 ft with a maximum distance of nearly 350 ft. Also, the load test data indicates plunging failure occurred before the shaft head settlement reached $5\%B$ in nearly half of load tests.

Table 2.2: Summary of test shaft and GI parameters.

Data Number	Load Test Quality Score	GI Quality Score	Const. Method	B (ft)	L (ft)	R_m (kip)	Failure Criteria ^a	Shaft to GI Dist. (ft)
1	2	2	Wet	4.00	103.00	10707	1	< 100
2	4	4	Dry	5.00	39.97	3423	2	90
3	1	4	Dry	7.67	74.43	13989	2	87
4	3	4	Dry	8.00	32.00	7905	2	12
5	3	4	Dry	2.00	31.60	1125	2	3
6	1	2	Dry	2.00	82.50	3812	1	5
7	1	4	Dry	2.00	43.00	1426	2	22
8	1	2	Wet	4.00	106.00	19299	1	< 165
9	2	2	Wet	4.00	105.00	12641	1	NA
10	2	2	Wet	4.00	116.80	10940	1	< 165
11	2	2	Dry	4.00	112.50	12699	1	< 165
12	2	3	Dry	4.00	123.00	20937	1	0 ^c
13	2	3	Wet	4.00	122.50	20109	1	0 ^c
14	1	3	Wet	3.00	102.00	5260	1	79
15	1	4	Wet	4.00	100.00	10616	1	85
16	1	4	Wet	4.00	101.00	11848	1	91
17	3	4	Wet	6.00	122.00	13215	2	0 ^c
18	2	2	Wet	4.00	121.70	8112	1	< 100
19	2	2	Wet	4.00	121.80	15935	1	< 100
20	1	3	Wet	3.50	90.70	22110	1	14
21	1	3	Wet	3.50	105.50	20669	1	< 150
22	1	2	Wet	4.00	128.00	15964	1	68
23	2	2	Wet	4.00	117.00	13286	2	347
24	1	3	Wet	3.50	100.00	12185	2	100
25	1	4	Wet	4.00	82.00	7142	2	< 150
26	4	4	Wet	4.00	90.50	3682	2	< 150
27	4	3	Wet	5.00	95.50	9965	2	NA
28	4	3	Wet	5.00	96.00	10822	2	NA
29	2	1	Wet	4.00	62.00	6611	2	10
30	1	3	Wet	4.00	101.60	8876	2	NA
31	1	3	Wet	6.00	112.70	18519	1	NA
32	2	2	Wet	3.75	104.33	15268	1	< 150
33	4	3	Dry	3.50	70.00	7923	2	< 165
34	2	2	Wet	3.50	70.00	10943	1	220
35	4	4	Wet	3.50	75.00	7712	1	0 ^c

36	2	3	Wet	3.50	105.50	16945	1	120
37	4	1	Wet	3.50	112.00	9918	2	NA
38	4	2	Wet	5.00	101.00	10276	1	NA
39	1	3	Wet	4.00	106.20	11001	2	NA
40	4	4	Wet	4.00	84.00	3376	2	83
41 ^b	4	4	Wet	3.00	83.00	2204	2	55

^a1=shaft head settlement equivalent to 5%B; 2=plunging

^bTop-down load test

^cBorehole is known to have been drilled prior to shaft installation in the same location

Chapter 3

Predicted Resistances

The design methodology described in [AASHTO \(2014\)](#) with 2015 and 2016 interim revisions, which is largely based on [Brown et al. \(2010\)](#), is employed to estimate the geotechnical strength limit state of the test shafts included in this study. However, there is currently no consensus among local practitioners or NDOT engineers regarding the proper treatment of cemented materials in Las Vegas. Thus, four different approaches regarding the treatment of cemented local geomaterials are evaluated hereafter.

In the context of this report, cemented materials are defined in accordance with the language from ASTM D 2488 ([ASTM, 2000](#)). This is presented in [Table 3.1](#). According to the experience of NDOT engineers, soil with weak cementation (defined by ASTM D 1586) can be sampled during a Standard Penetration Test (SPT) and a meaningful value for N_{SPT} may be obtained. Soil with moderate cementation (ASTM D 1586) can only be sampled partially during SPT (e.g. 50 blows per 4 inches) and a meaningful value of N_{SPT} cannot be achieved. Alternatively, soil with strong cementation cannot be penetrated under normal SPT hammer blows.

Table 3.1: Criteria for describing cementation (after [ASTM \(2000\)](#)).

Description	Criteria
Weak	Crumbles or breaks with handling or little finger pressure
Moderate	Crumbles or breaks with considerable finger pressure
Strong	Does not crumble or break with finger pressure

Based on [Table 3.1](#) and in consideration of the available evidence regarding the behavior of cemented material in Las Vegas, caliche is defined as strongly cemented material which also yields refusal in a standard penetration test (i.e. no penetration). In addition, it is not recommended to derive any strength from caliche in design if coring has not been performed to verify the composition and competency of the layer in question. If only weak to moderate

cementation is evident, but not enough to warrant classification of caliche, it is recommended that the behavior of the parent material (i.e. very dense sand or hard clay) be considered for design purposes.

While a few techniques for dealing with moderately cemented material have been proposed in the past (e.g. Rinne et al., 1996), preliminary analyses revealed that simply treating such material the same as the parent material is generally acceptable. That being said, in the proposed approach presented hereafter, a slightly modified model for moderately cemented material with $N_{SPT} \geq 50$ is found to be necessary to ensure that there is no dependence between the R_p and λ (which is required for a valid calibration of the resistance factor). It is emphasized that special treatment of non-caliche materials is for calibration purposes only and is not recommended for design.

The four potential design approaches investigated herein are summarized as follows:

- Current practice (caliche as very dense sand) - Method (M1)

This is the approach is meant to represent typical design outcomes in Las Vegas for cases in which full scale load test data is not available. Caliche is treated as very dense sand with $\gamma = 140$ pcf, $\phi' = 40^\circ$, and $N_{SPT} = 50$. This is mainly based on discussions with local practitioners.

- Caliche as cohesive IGM - Method (M2)

Caliche is treated according to procedures from Brown et al. (2010) for cohesive IGM. Unless site-specific data suggests otherwise, it is assumed that $q_u = 100$ ksf for caliche layers based on the maximum suggested by Brown et al. (2010) for a material classified as cohesive IGM.

- Caliche as rock - Method (M3)

Caliche is treated according to codified procedures from Brown et al. (2010) for rock with an assumed $q_u = 729$ ksf and $RQD = 70\%$, unless site-specific data suggests otherwise. Note that the value of q_u is assumed for calibration purposes only.

- Proposed approach - Method (M4)

Side resistance in caliche is computed with Equation 3.1. For the purpose of calibration only, it is assumed that $q_u = 729$ ksf for layers not associated with site-specific unconfined compression test data. Base resistance is taken as the value from the rock model or 100 ksf, whichever is lower. For calibration purposes only, material which is not strongly cemented with $N_{SPT} \geq 50$ is modeled with $f_{SN} = 6$ ksf. Otherwise, if $N_{SPT} < 50$, moderately cemented material is treated the same as the parent material.

Base resistance in moderately cemented material is always treated the same as the parent material.

For each design approach, a non-parametric correlation test (Spearman's ρ) was conducted to ensure that there is no dependence between the predicted resistance and bias for a level of significance of 0.05. The p-values associated with the null hypothesis that R_p and λ are independent are provided in Table 3.2. Thus, if the reported p-value is greater than 0.05, the null is accepted and independence is assumed (as is the case for all approaches).

Table 3.2: Spearman's ρ statistics to test for dependence between R_p and λ (assumed significance level of 0.05, null = independent).

Caliche Model	Spearman's ρ	p-value
M1	-0.2061	0.0962
M2	-0.1537	0.1656
M3	-0.0944	0.2752
M4	-0.2024	0.1002

The default q_u of caliche assumed for calibration of the resistance for M3 and M4 is based on the results of laboratory tests performed on 60 caliche core samples for projects in Las Vegas ([Western Technologies Inc., 1994](#); [Arup, 2011](#); [Rinne et al., 1996](#)). This data conforms to a lognormal distribution with a geometric mean of 729 ksf and COV of 0.59 (see Figure 3.1). In general, this supports the findings from [Cibor \(1983\)](#) which suggest that q_u of competent caliche in Las Vegas ranges between 576 and 1440 ksf. Thus, the data collected is accepted and the default q_u of caliche is set to 729 ksf for the analyses conducted hereafter. Any value much lower than this would prevent a meaningful calibration as the resistance factor would need to be uncommonly high to match the target reliability index, even for the least conservative design approaches considered herein.

It is important to clarify that the default value of $q_u = 729$ ksf is intended to serve as an upper bound for practitioners only after laboratory testing has been carried out to determine the actual unconfined compressive strengths of the caliche layers at a given site. Also, the estimated concrete compressive strength should also be considered as a limiting factor for assigning q_u . If for some reason such testing is not carried out or is inconclusive, the authors recommend a much more conservative value of $q_u = 100$ ksf which, following Equation 3.1, produces a nominal side resistance in caliche of approximately 12 ksf. Given the data in this study as well as the results of discussions with local practitioners, this assumption appears to represent a conservative path forward for engineers who are tasked with carrying out design in cemented soils in Las Vegas despite a lack of proper GI data. As Figure 3.1 shows, there is significant variation in caliche strength properties so assuming $f_{SN} > 12$ ksf without proper justification would not be acceptable.

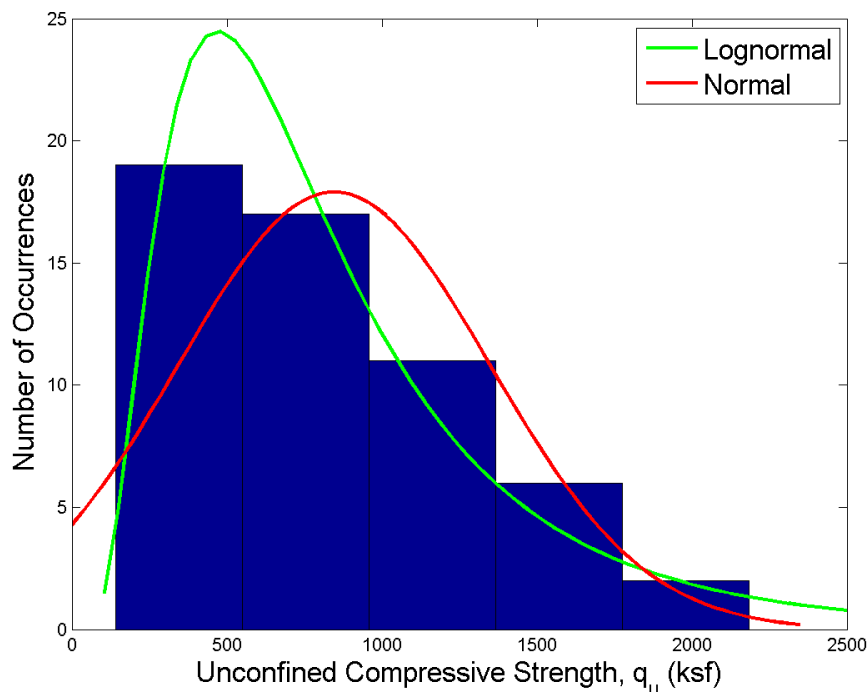


Figure 3.1: Histogram of unconfined compressive strengths of caliche core samples in Las Vegas reported by [Western Technologies Inc. \(1994\)](#), [Arup \(2011\)](#), and [Rinne et al. \(1996\)](#)

Inspection of the bias, λ , reveals that treating caliche as cohesive IGM or rock, produces generally low estimates of R_p . Given this, a modification to the codified procedure for rock is proposed herein to increase the likelihood that meaningful resistance factors will be obtained (i.e. $\phi_{RT} < 0.70$). The proposed approach (M4) employs Equation 3.1 to estimate skin resistance. Equation 3.1 is identical to Equation 10.8.3.5.4b-1 from [AASHTO \(2014\)](#) except that the coefficient, C , is set to 0.85 instead of 1.0. The value of $C = 1$ suggested for design of "normal" rock sockets in [AASHTO \(2014\)](#) is based on the results of regression analyses performed by [Kulhawey et al. \(2005\)](#). However, according to the Spearman's Rho test for the strength of association between two variables, a value of 0.85 is necessary to assume independence between R_p and λ at a significance level of 0.05 (which is assumed to be adequate for this study). A detailed description of a similar application of this non-parametric statistical test is provided in [Bathurst et al. \(2008\)](#).

$$\frac{f_{SN}}{p_a} = 0.85 \sqrt{\frac{q_u}{p_a}} \leq 15.8 \quad (3.1)$$

where

$$\begin{aligned} f_{SN} &= \text{Unit side resistance in caliche} \\ p_a &= \text{Atmospheric pressure} \\ q_u &= \text{Unconfined compressive strength of caliche} \end{aligned}$$

The limit placed on Equation 3.1 is to ensure that designers do not exceed upper bound of the unit side resistances considered for the resistance factor calibrations for M4 within this study. This corresponds to $f_{SN} = 33.4$ ksf based on the default assumptions for caliche strength. This also falls within the range suggested by [Brown et al. \(2010\)](#) that unit side resistance in Las Vegas caliche, based on bi-directional load test data, is typically between 30 to 55 ksf.

It is important to convey that the assumptions regarding caliche strength are employed for the purpose of calibration only and should not, under any circumstances, be applied in practice. In the context of calibration, it is conservative to assign the highest feasible predictions that might be generated in design so that the computed resistance factor encompasses all potential design outcomes. Again, the intent is that designers will always rely on appropriate site-specific data to validate the strength parameters required for the approximation of side resistance in caliche or any other geomaterial.

Regarding unit end-bearing in M4, a value equal to the lesser of 100 ksf or the value from M3 is assumed. Trial and error with a number of potential options reveals that this maximizes prediction accuracy for the cases in which the test shafts were tipped into caliche. This is also supported by the findings from [Stone \(2009\)](#).

To further improve prediction accuracy of the proposed design approach, moderately cemented material with $N_{SPT} \geq 50$ is modeled with $f_{SN} = 6$ ksf and is treated the same as the parent material otherwise (including base resistance). This was found to reduce the dependence between R_p and λ whereas the application of the recommendations from [Rinne et al. \(1996\)](#) had the opposite effect. Note that this approach is employed for calibration purposes only since assuming the behavior of the parent material is more conservative.

It should be noted that NDOT has also recognized a simplified alternative to M1 that some engineers use in Las Vegas to obtain a rough estimate of expected resistance without

conducting a GI. In this approach, which is hereafter referred to as M1a, all soil along the embedded length of the shaft is modeled with a unit side resistance of 4 ksf. Despite such a sweeping assumption, however, Figure 3.2 shows that M1a does produce results of similar, if not slightly improved, accuracy to M1. Nevertheless, M1a is not considered in the LRFD calibrations herein because it undermines all codified design procedures and introduces unnecessary epistemic uncertainty.

Figures 3.2 through 3.5 show the distributions of measured and predicted resistances developed with M1 through M4, respectively. From these plots, it appears that M4 is the most accurate on average and that the level of conservatism decreases from M1 to M4.

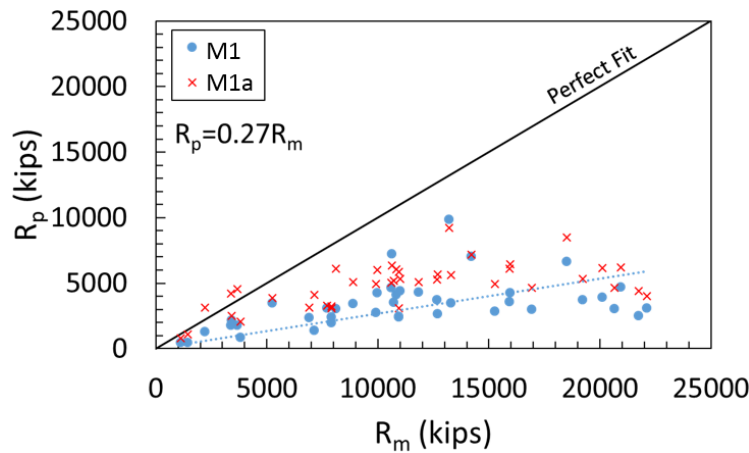


Figure 3.2: Measured and predicted resistances computed with M1 and M1a (trend line and equation pertains only to M1)

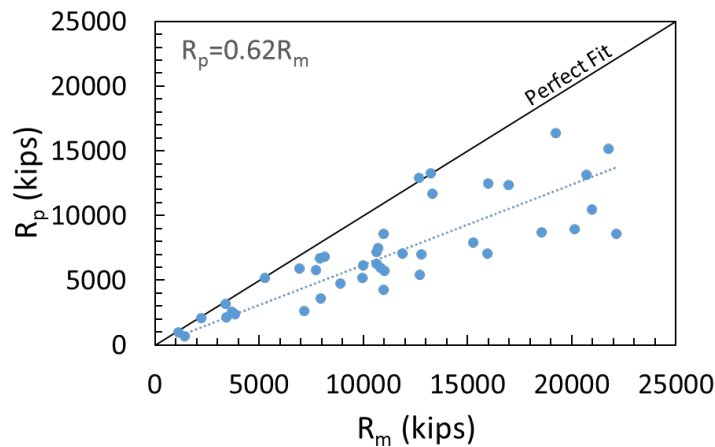


Figure 3.3: Measured and predicted resistances computed with M2

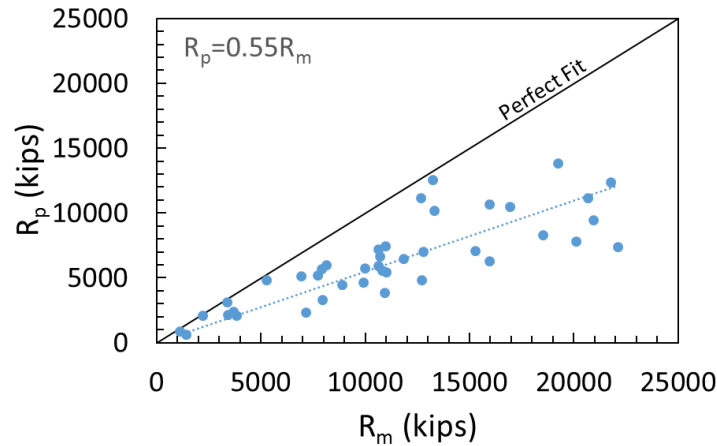


Figure 3.4: Measured and predicted resistances computed with M3

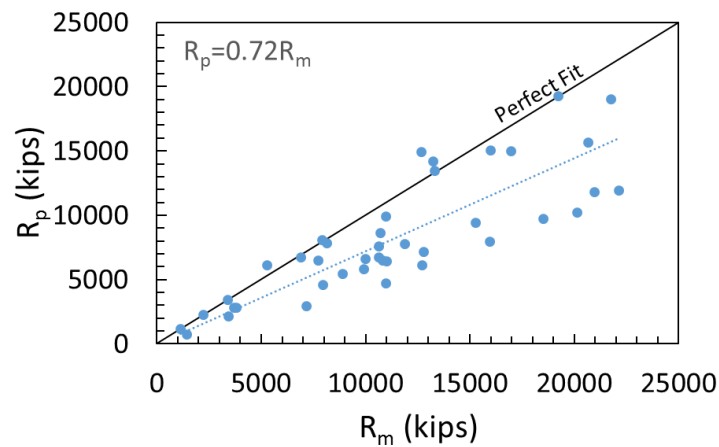


Figure 3.5: Measured and predicted resistances computed with M4

Figure 3.6 portrays the relationship between prediction bias and the relative amount of caliche present along the embedded lengths of the test shafts (caliche fraction) for each design approach, including M1a. The relatively steep positive slopes of the trend lines for M1 and M1a suggest that these methods underestimate the resistance in cemented soils compared to the other methods. M2, M3, and M4 all maintain relatively consistent bias for different levels of caliche fraction, although M4 is closest to $\lambda = 1.0$ on average. The distribution of bias is discussed in greater detail in the next chapter.

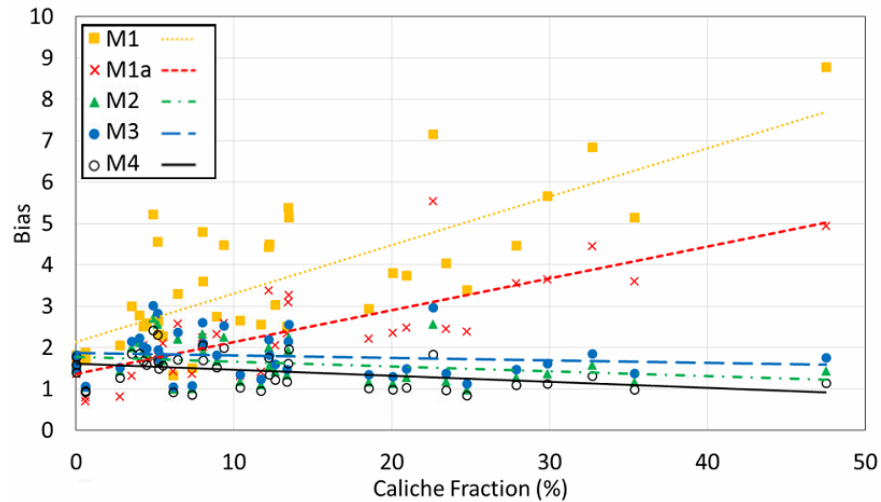


Figure 3.6: Relationship between bias and relative amount of caliche along the embedded lengths of the test shafts

Overall, Figures 3.2 to 3.6 suggest that M1 and M1a drastically underestimate R_p , especially for greater caliche fractions. M2 and M3 represent improvements over M1 and M1a because they produce consist bias for different amounts of caliche but both models still underestimate resistance in general.

Chapter 4

Calibration Procedures

Bi-directional load cells for test shafts in Las Vegas are often installed at a significant distance above the shaft base to promote equal movement above and below the load cell. This leaves a significant portion of the shaft below the load cell to contribute to skin friction (the average is 15.25 m for the shafts in this study) and makes it difficult to accurately differentiate between tip and side resistance when interpreting the measured data. While it is sometimes possible to use strain gauge readings to approximate the relative contribution of side and tip resistance below the load cell, in many cases such information is unavailable or not reliable enough to be used for that purpose. As a result, the LRFD calibrations in this study only produce total resistance factors, ϕ_{RT} , as opposed to separate factors for side and tip resistance.

Two approaches for implementing the MC method to calibrate ϕ_{RT} are carried out: L1 and L2. In L1, which may be considered the current state-of-the-art, the statistical characterization of the random variable representing resistance is based on "best-estimate" geomaterial properties. Alternatively, L2 employs nested MC simulations to capture the uncertainty associated with the interpretation of geomaterial properties from Standard Penetration Test (SPT) data and other information made available in Geotechnical Investigation (GI) reports such as boring logs and laboratory test results. Compared to L1, L2 is more robust because it considers an additional source of epistemic uncertainty. That being said, L2 is also more computationally demanding because dedicated MC simulations must be performed on many individual design parameters for each data point.

The generalized procedure for L1 is as follows:

1. Collect load test data and associated information required to estimate the resistance of each test foundation.
2. Determine the mean (λ_R), COV (COV_R), and distribution type for the resistance bias

using best-estimate geomaterial properties.

3. Assume a mean (λ_{LL} and λ_{DL}), COV (COV_{LL} and COV_{DL}), and distribution type for the dead and live load bias.
 - These values are taken from Paikowsky (2004) and are shown in Table 1.2.
4. For a given resistance factor, compute the limit state equation ($g = R - Q$) with values for R and Q assigned randomly following the statistical characterizations from steps 2 and 3.
 - This requires a dead to live load ratio be assumed ($Q_{DL}/Q_{LL} = 3$ herein).
5. Repeat step 4 until increasing the number of iterations no longer impacts the results.
6. Compute the probability of failure and reliability index, β for the given resistance factor.
7. Repeat steps 4 through 6 for a range of resistance factors to find the value which corresponds to the desired level of reliability.
8. Validate with an alternative procedure (e.g. FORM)

L2 is essentially the same as L1 except for the key feature that the bias computed in step 2 treats the "best-estimate" values of γ , q_u , ϕ' , s_u , and N_{SPT} as the means of random variables with COVs given in Table 4.1. These values were determined based on the data collected for this study and, while they are relied upon hereafter, they are also compared to similar values from published literature in Table 4.2. Thus, for L2, an additional MC simulation take place every time one of the aforementioned parameters enters the design. The number of iterations (N) required for the nested simulations is determined by increasing N until the mean R_p for each test shaft converges. For this study, $N = 500000$ is found to be sufficient. Hence, the bias statistics for the final MC simulation of L2 encompass 2.05×10^7 potential design outcomes (41×500000) as opposed to just 41 in L1.

The nested MC simulations for L2 are carried out with Microsoft Excel Visual Basic for Applications (Excel VBA) since the design of axially loaded drilled shafts can be readily performed within a spreadsheet environment. Alternatively, the final MC simulations for L1 and L2 are implemented in Matlab (MATLAB, 2014). FORM validations are performed with Matlab for each final MC simulation using the procedure from Ayyub et al. (2000).

Both L1 and L2 rely on statistical characterizations of the bias summarized in Table 4.3. Inspection of various distribution types fit to cumulative distributions of the bias as

well as in consideration of the goodness of fit statistics (Chi-Squared), a global lognormal distribution is determined to be the most appropriate for characterizing the data for all of the prediction methods. This is because it is globally accurate and maintains conservatism in the lower tail regions of the Cumulative Distribution Functions (CDFs). The normal distribution is also considered as well as the best fit to the lower tail, which is defined as described in Allen et al. (2005) and represents the region on the CDF where $R_m < R_p$. However, using the statistics from the best fit to tail is found to be nonconservative. The Probability Distribution Functions (PDFs) and CDFs of the bias for M1 through M4 are given in Figures 4.1 through 4.4, respectively.

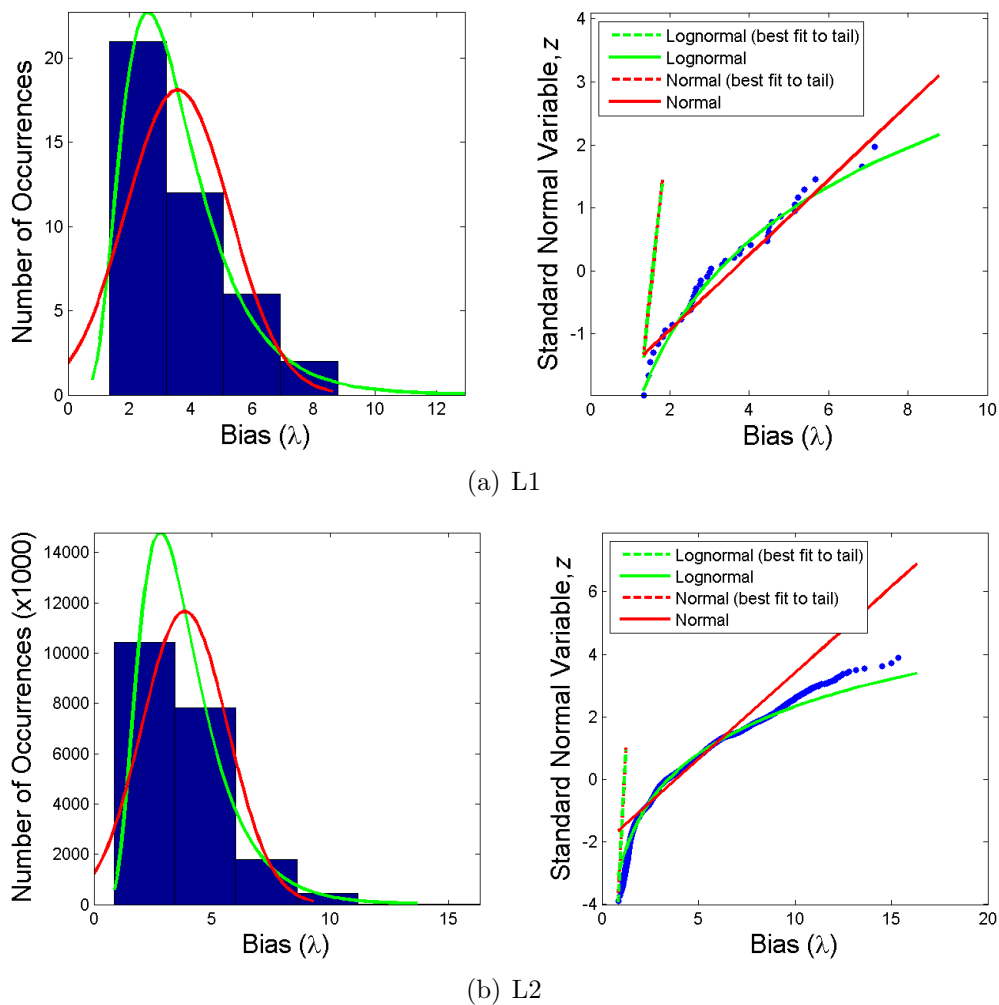
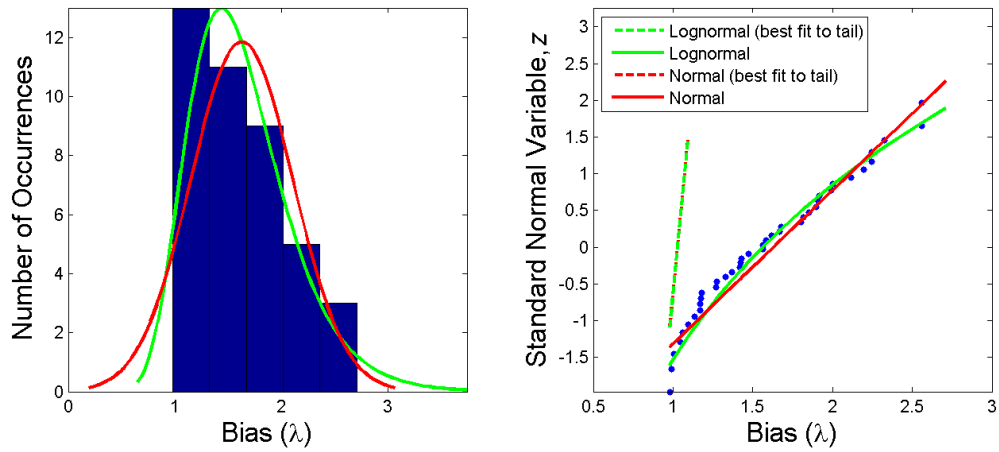
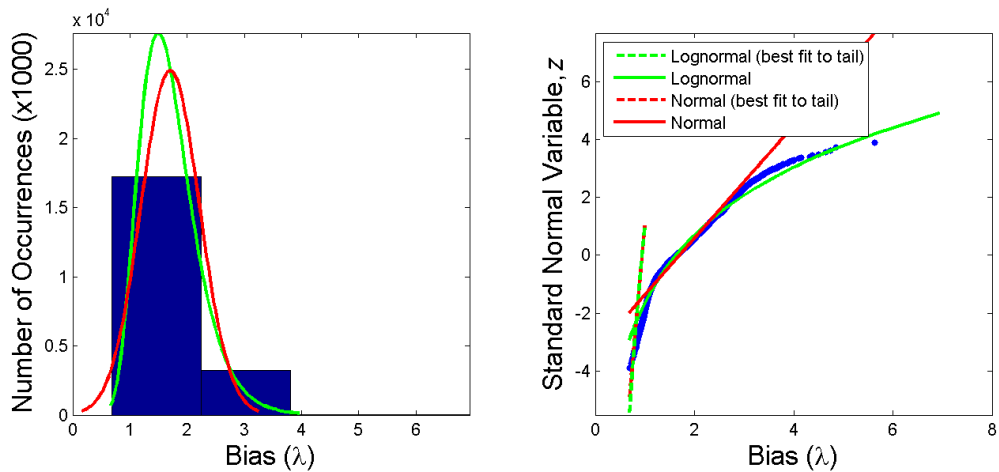


Figure 4.1: PDFs and CDFs of the bias developed with M1 for the L1 and L2 calibrations



(a) L1



(b) L2

Figure 4.2: PDFs and CDFs of the bias developed with M2 for the L1 and L2 calibrations

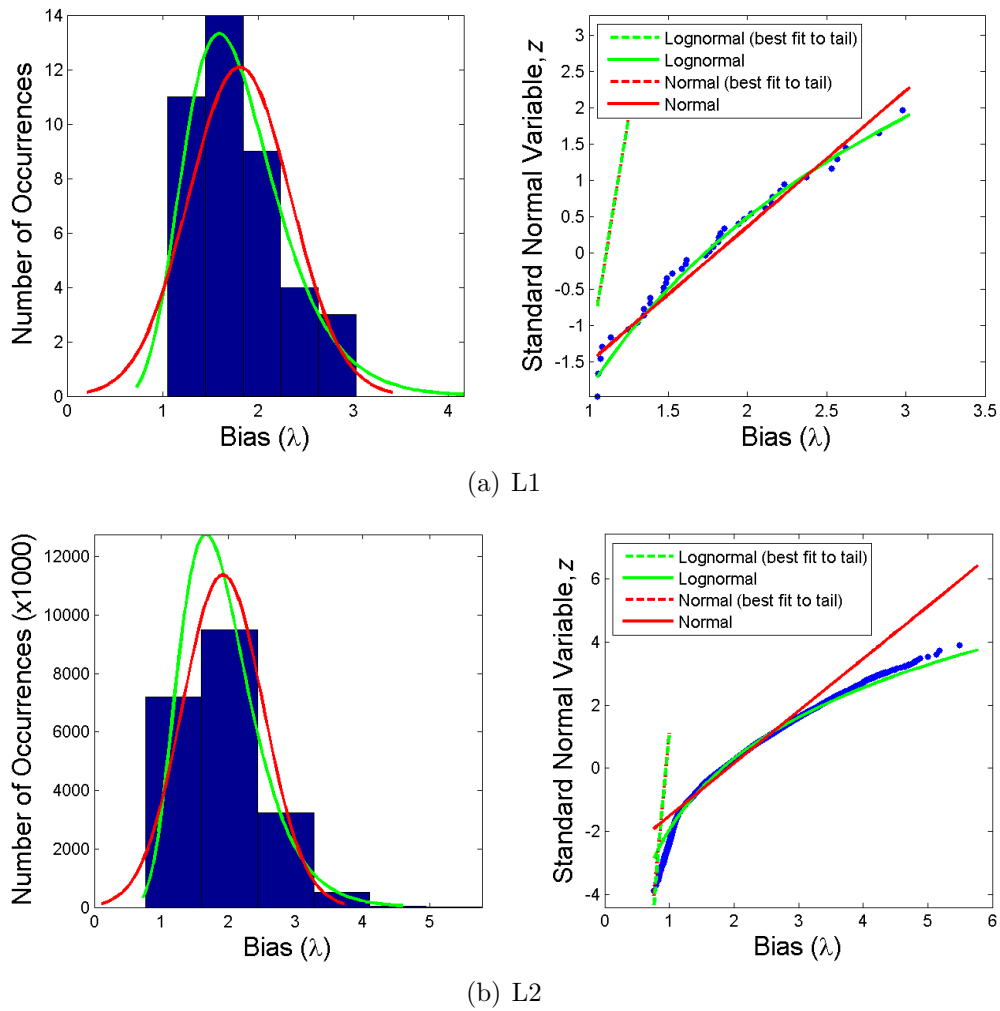


Figure 4.3: PDFs and CDFs of the bias developed with M3 for the L1 and L2 calibrations

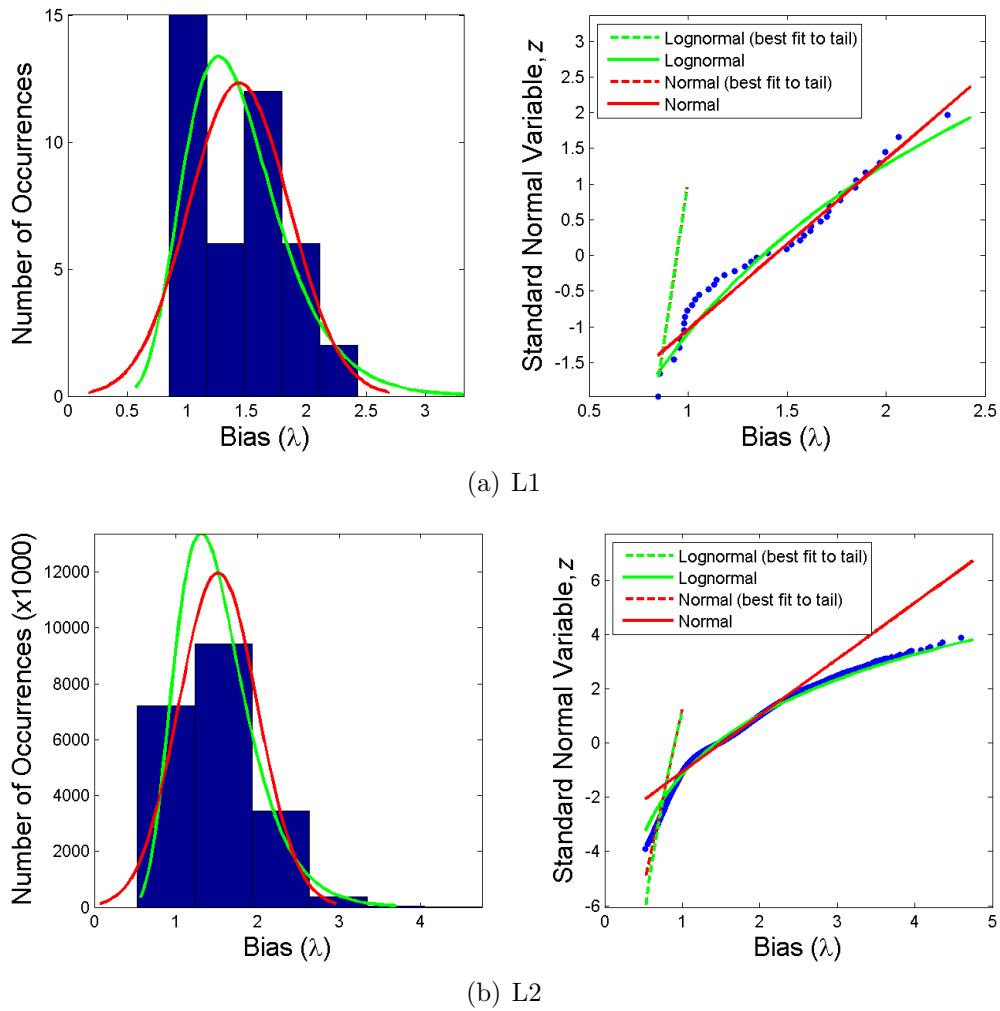


Figure 4.4: PDFs and CDFs of the bias developed with M4 for the L1 and L2 calibrations

Table 4.1: Assumed COV values for design parameters in the L2 LRFD calibrations.

Parameter	Measured (M) or Interpreted (I)	Number of Samples	COV (%)
γ	I	898	9.2
ϕ'	I	362	14.5
s_u	I	412	44.9
γ	M	208	8.6
ϕ'	M ¹	8	6.5
s_u	M	51	34.1
N_{SPT}	M	1105	37.4
q_u	M ²	60	59.0

¹COV obtained using Bayesian equivalent sampling

²Not all data is pertinent to the test shafts in this study

Table 4.2: Comparable COV values for design parameters from literature.

Measured or Interpreted Parameter	Mean COV (%)	Source	Notes
γ	5.0	Duncan (2000)	cited values range from 3 to 7%
ϕ'	7.5	Duncan (2000)	cited values range from 2 to 13%
s_u	26.5	Duncan (2000)	cited values range from 13 to 40%
N_{SPT}	30.0	Duncan (2000)	cited values range from 15 to 45%

Inspection of Figures 4.1 through 4.4 reveals that a lognormal distribution provides the most accurate characterization of the bias data in all cases. Thus, the values of the random variables for resistance are generated on each iteration within the MC simulations accordingly. This is accomplished through the use of random number generation functions available in Matlab and Excel VBA which are designed to output values following a lognormal distribution.

To further validate the final resistance factors, the inverse transformation method (e.g. [Au & Wang, 2014](#)) was also employed to generate values for the MC simulations directly from the empirical CDFs. However, this approach consistently produced greater resistance factors (i.e. less conservative) than those from the fitted lognormal distributions. Thus, the resistance factors from the lognormal fitting approach are reported hereafter.

Table 4.3: Summary of statistical parameters used to describe the bias for the L1 and L2 calibrations.

Calibration Level	Caliche Model	All Data		Mean Score > 2		Mean Score ≥ 3	
		Mean λ	COV	Mean λ	COV	Mean λ	COV
L1	M1	3.57 (1.48)	0.47 (0.07)	3.27 (1.61)	0.55 (0.13)	3.27 (1.61)	0.55 (0.13)
	M2	1.63 (1.00)	0.29 (0.03)	1.63 (1.05)	0.28 (0.04)	1.63 (1.05)	0.28 (0.04)
	M3	1.81 (1.07)	0.30 (0.01)	1.78 (1.11)	0.29 (0.09)	1.78 (1.11)	0.29 (0.09)
	M4	1.43 (0.94)	0.29 (0.06)	1.45 (0.95)	0.28 (0.02)	1.29 (0.95)	0.26 (0.02)
L2	M1	3.76 (1.19)	0.47 (0.06)	3.45 (1.16)	0.53 (0.06)	2.50 (1.16)	0.36 (0.06)
	M2	1.71 (0.98)	0.30 (0.01)	1.70 (0.98)	0.28 (0.01)	1.46 (0.98)	0.28 (0.01)
	M3	1.91 (0.98)	0.31 (0.02)	1.89 (0.98)	0.31 (0.02)	1.59 (0.98)	0.30 (0.02)
	M4	1.52 (0.92)	0.32 (0.07)	1.55 (0.93)	0.31 (0.07)	1.33 (0.93)	0.29 (0.07)

- Values in parenthesis represent the best fit to tail.

Chapter 5

Results

The results of the MC simulations for L1 and L2 are shown in Figure 5.1 and are summarized in Table 5.1. Additionally, the governing resistance factors for each design approach and calibration level are given in Table 5.2. These represent the lowest computed values of ϕ_{RT} among the three data quality bins (including both L1 and L2).

Figure 5.2 shows the impact of data quality and calibration level on the computed resistance factors. For M2, M3, and M4, the resistance factors from L1 are slightly greater than those from L2. However, the opposite is generally true for M1 and M2. In light of this, it is important to note that AASHTO (2014) and Brown et al. (2010) allow most design parameters to affect the outcome only if they fall within a certain range. For example, s_u is limited to $2.5p_a$ in the Alpha Method for cohesive soils Brown et al. (2010). Hence, if most of the assumed material properties happen to fall close to the effective upper limit, then the L2 calibration is likely to produce a greater ϕ_{RT} than L1 because any randomly generated values that fall above this threshold would not actually increase the predicted resistance. Alternatively, considering that q_u of caliche in M2, M3, and M4 has the potential to impact design outcomes for any value greater than zero, it is reasonable for L2 to produce lower resistance factors than L1 for these approaches.

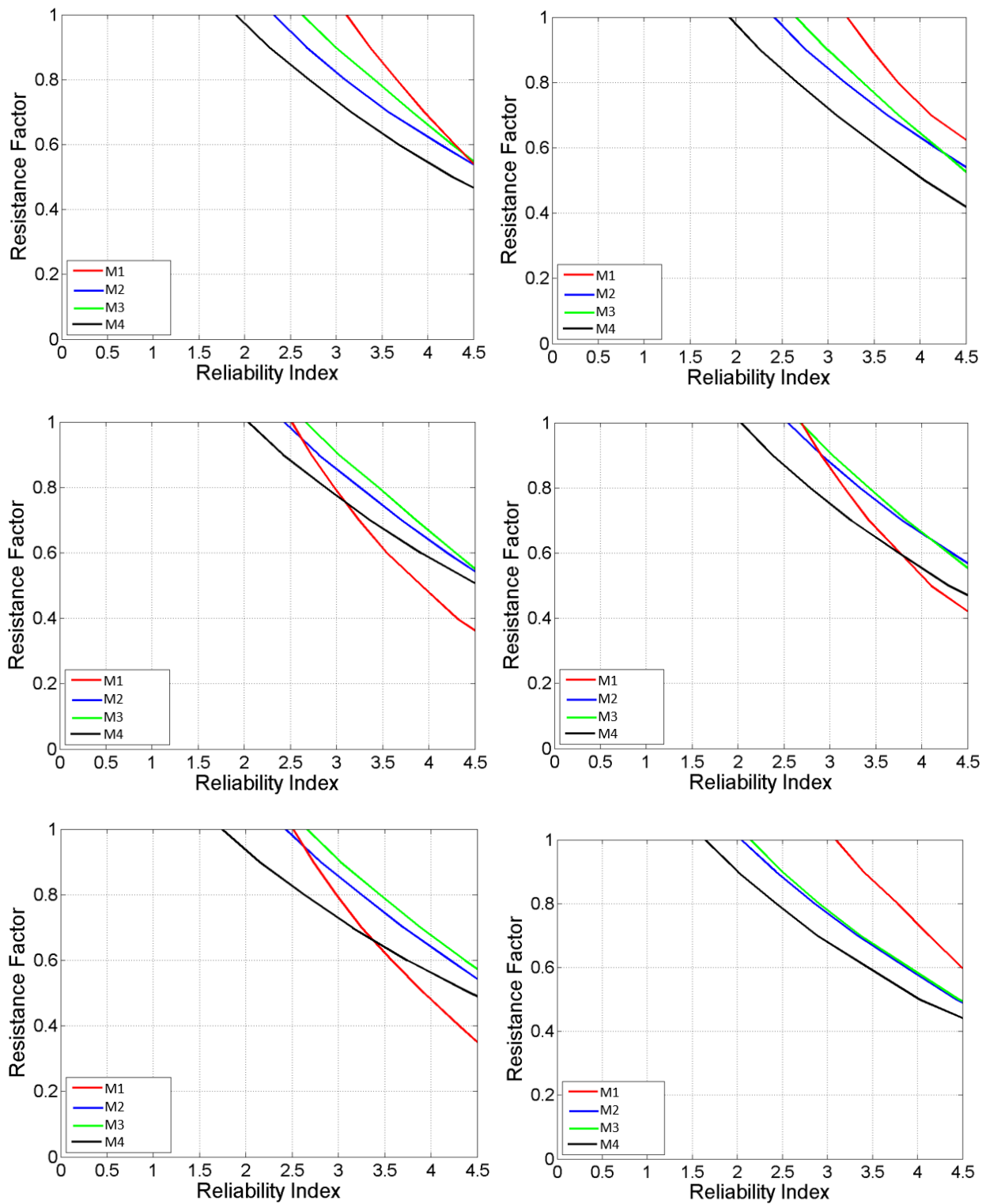


Figure 5.1: L1 and L2 calibration results for different data quality bins and design approaches (M1, M2, M3, and M4) based on [AASHTO \(2014\)](#)

Table 5.1: Resistance factors computed with the MC simulations for the L1 and L2 calibration (using the global lognormal bias statistics).

Design Method	Caliche Model	ϕ_{RT} at $\beta = 3$		
		All data	Mean Score > 2	Mean Score ≥ 3
L1	M1	1.05 (1.09)	0.78 (NR)	0.79 (NR)
	M2	0.81 (0.98)	0.85 (0.93)	0.85 (0.93)
	M3	0.90 (1.01)	0.91 (0.91)	0.91 (0.91)
	M4	0.73 (0.87)	0.77 (0.89)	0.72 (0.88)
L2	M1	1.09 (NR)	0.86 (NR)	1.02 (NR)
	M2	0.84 (0.96)	0.87 (0.96)	0.76 (0.96)
	M3	0.90 (0.95)	0.91 (0.95)	0.77 (0.96)
	M4	0.71 (0.84)	0.74 (0.85)	0.66 (0.85)

- Values in parenthesis represent the best fit to tail.

- NR = No result

Table 5.2: Governing LRFD resistance factors for all design approaches and calibration levels

Calibration Level	Governing ϕ_{RT} at $\beta = 3$			
	M1	M2	M3	M4
L1	0.78	0.81	0.90	0.72
L2	0.86	0.76	0.77	0.66

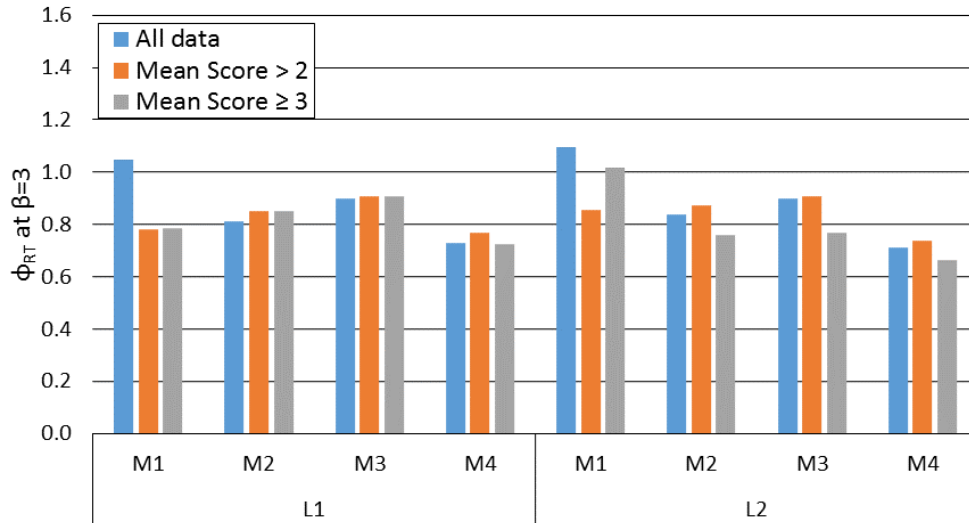


Figure 5.2: Impact of data quality and calibration level on the computed resistance factors

Inspection of Figure 5.2 suggests that the impact of data quality is dependent on the design method of choice. For example, the resistance factors from M2, M3, and M4 developed with L2 are governed by the data bin with a mean score ≥ 3 but those for M1 are governed by the data bin with a mean score > 2 . Additionally, while the governing resistance factors developed with all data qualities only vary slightly between L1 and L2, the difference is much greater for the other data quality bins.

Overall, the resistance factors computed with the MC method are in close agreement with those from FORM at $\beta = 3$. Both approaches also suggest that the resistance factor at the target level of reliability is not governed by the best fit to tail for any case. Thus, the results of the MC simulations are considered valid.

Chapter 6

Conclusions and Final Recommendations

A database (the NDFLTD) has been developed in Microsoft Access and employed to calibrate LRFD resistance factors for axially loaded drilled shafts in the Las Vegas Valley. Collected data includes 41 load tests and associated GI information. The framework of the NDFLTD will allow NDOT engineers to add to the current data in the future for the benefit of engineers and researchers involved with deep foundation design in state of Nevada.

The impact of data quality, assessed through the ranking system from Table 2.1, is found to be non-trivial. In fact, all of the governing resistance factors in this study were obtained by using one of the top two data quality bins (mean score > 2 or ≥ 3). Since it is impossible to tell which subset of the data is truly the most appropriate representation of the conditions in Las Vegas, it can be concluded that the final recommendations might have been non-conservative if no attempt had been made to address the impact of data quality.

The four design approaches considered in this report are summarized below. The results suggest that only the proposed approach (M4) and the associated resistance factor (0.66) is potentially adequate for design purposes.

- Current practice (caliche as very dense sand) - Method (M1)

This is the approach is meant to represent typical design outcomes in Las Vegas for cases in which full scale load test data is not available. Caliche is treated as dense sand with $\gamma = 140$ pcf, $\phi' = 40^\circ$, and $N_{SPT} = 50$.

- Caliche as cohesive IGM - Method (M2)

Caliche is treated according to procedures from [Brown et al. \(2010\)](#) for cohesive IGM. Unless site-specific data suggests otherwise, it is assumed that $q_u = 100$ ksf for

caliche layers based on the maximum suggested by [Brown et al. \(2010\)](#) for a material classified as cohesive IGM.

- Caliche as rock - Method (M3)

Caliche is treated according to codified procedures from [Brown et al. \(2010\)](#) for rock with an assumed $q_u = 729$ ksf and $RQD = 70\%$, unless site-specific data suggests otherwise. Note that the value of q_u is assumed for calibration purposes only.

- Proposed approach - Method (M4)

Side resistance in caliche is computed with Equation 3.1. For the purpose of calibration only, it is assumed that $q_u = 729$ ksf for layers not associated with site-specific unconfined compression test data. Base resistance is taken as the value from the rock model or 100 ksf, whichever is lower.

Two calibration techniques were used to develop total resistance factors: L1 and L2 (see Chapter 4). The results demonstrate that the application of a nested MC simulation to capture the uncertainty associated with the interpretation of material properties (i.e. L2) has the potential to produce lower resistance factors than more typical calibration procedures (i.e. L1). Also, of the four methods for treating problematic local geomaterials investigated herein, M1 is the only case for which the governing resistance factor came from L1. This suggests that the L2 style calibration should be considered in future studies of this nature.

The governing resistance factor for M4 is the only value which can be recommended for design purposes ($\phi_{RT} = 0.66$). This is because all of the other design approaches require a resistance factor greater than 0.70 to achieve the target reliability index of 3, in all cases. [Allen \(2005\)](#), which is cited in [AASHTO \(2014\)](#), suggests that the maximum value for drilled shaft design, even if field load testing has been conducted, should not exceed 0.70. Thus, treating caliche as dense sand (M1), cohesive IGM (M2), or rock (M3) does not appear to be compatible with accepted LRFD guidelines for drilled shafts in Las Vegas. That being said, the proposed approach is still relatively conservative and was only shown to require a resistance factor < 0.70 when the highest data quality bin was considered within the L3 framework.

Overall, the evidence presented herein suggests that the prevalence of caliche in the subsurface is one of the most influential factors regarding deep foundation performance in Las Vegas. Consequently, it is necessary to exercise extreme care so that such layers are accurately identified and conservatism is maintained. The authors therefore recommend that site investigations in the area be extended to prove the lateral extent and competence of cemented layers before considering them in design. Also, the unconfined compressive

strength of caliche layers must be verified using laboratory testing before employing Equation 3.1 for design.

6.1 Final Recommendations

Given the findings of this investigation, it is recommended that LRFD of axially loaded drilled shafts in the Las Vegas Valley, with respect to the strength limit state, be carried out using M4 with a total LRFD resistance factor, ϕ_{RT} , of 0.66. In the M4 design methodology, all subsurface materials except for caliche must be modeled according to the [AASHTO \(2014\)](#) design guidelines. Side resistance in caliche should be computed with Equation 3.1 after laboratory testing on cored samples is employed to determine the unconfined compressive strength, q_u , and the final q_u employed for design should not exceed 729 ksf under any circumstances. Also, the estimated concrete compressive strength should also be considered as a limiting factor for assigning q_u . If caliche layers cannot be associated with site-specific test data, a value of $q_u = 100$ ksf should be assumed to account for the exceptionally high variability in caliche strength. Base resistance in caliche should be evaluated using the [AASHTO \(2014\)](#) design methodology for rock. All material which is not strongly cemented is to be treated according to the codified guidelines for the parent material.

It is important to clarify that if any amount of caliche is to be considered in design, the proposed resistance factor should be applied to the sum of nominal base resistance and all of the nominal side resistances computed for the different soil layers along the embedded shaft length. Additionally, base resistance may be neglected if the pertinent properties of the tipping material are inconclusive based on the results of the GI. This would match current common practice and represents a conservative assumption.

Due to the nature of the data employed for the calibrations in this report, there are no direct comparisons which can be made between the resistance factors recommended in [AASHTO \(2014\)](#) the total resistance factor of 0.66 suggested herein. This is because separate resistance factors could not be determined herein for side and tip resistance or for different individual material types (due to a lack of necessary data). That being said, engineers may choose to use the [AASHTO \(2014\)](#) LRFD methodology and associated resistance factors if no caliche is considered in design.

The recommended LRFD procedure for drilled shafts in Las Vegas is described concisely in Appendix E and in an example provided in Appendix F.

6.2 Future Work

The analyses carried out for this report should be repeated in the future as additional load test and GI data becomes available in the Las Vegas Valley. With a large enough sample size, it may also be possible to separate the calibration procedures to provide resistance factors which are more ideal for different foundation geometries and construction methods. This could be accomplished, for example, by binning the data according shaft diameter before carrying out the calibrations to produce a table of appropriate resistance factors for various shaft diameters.

New data may also enable more robust empirical relationships to be developed between site investigation data and caliche strength parameters. This might require creating spatially dependent models for different areas within Las Vegas, which was not feasible herein due to limited data barring statistical significance. Furthermore, promoting more non-invasive exploration techniques to allow engineers to make use of V_s measurements in design may also prove beneficial in this regard.

It would also be advantageous for the database to be published online. This would allow more practitioners to benefit from it and may also speed up the accumulation of additional data since more potential sources will be aware of its existence.

There is a need for load tests to be performed for research purposes only. This is because the goals of field load tests conducted for industry are very different from those of researchers attempting to solve broader problems concerning foundation design methods. For example, simply proving that a test shaft provides a specified level of axial resistance does not necessarily require the load test to be carried out to failure. Researchers are also often forced to contend with limited GI data which is usually collected by a third party. Thus, it would be useful for at least a few tests to be associated with a GI which was designed to be as thorough as possible for research purposes.

References

- AASHTO. (2014). AASTHO LRFD Bridge Design Specifications, U.S. Customary Units with 2015 and 2016 Interim Revisions (7th Edition). *American Association of State Highway and Transportation Officials, Washington DC*.
- Abu-Farsakh, M., Yu, X., & Zhang, Z. (2012). Calibration of side, tip, and total resistance factors for load and resistance factor design of drilled shafts. *Transportation Research Record: Journal of the Transportation Research Board*, 2310, 38–48.
- Abu-Hejleh, N., Abu-Farsakh, M., Suleiman, M. T., & Tsai, C. (2015). State of Practices in Databases for Deep Foundation Load Tests. In *Ifcee 2015* (pp. 237–246). San Antonio, TX.
- Allen, T. M. (2005). *Development of geotechnical resistance factors and downdrag load factors for lrfd foundation strength limit state design: Reference manual*. US Department of Transportation, Federal Highway Administration, National Highway Institute.
- Allen, T. M., Nowak, A. S., & Bathurst, R. J. (2005). Calibration to determine load and resistance factors for geotechnical and structural design. *Transportation Research E-Circular*(E-C079).
- Arup. (2011). *Vegas high roller - geotechnical interpretative report* (Tech. Rep. No. 210193). Prepared for Caesar’s Entertainment.
- ASTM. (2000). *ASTM D 2488, Standard Practice for Description and Identification of Soil (Visual-Manual Procedure)* (Tech. Rep.). ASTM, West Conshohocken.
- Atabey, E., Atabey, N., & Kara, H. (1998). Sedimentology of caliche (calcrete) occurrences of the kirşehir region. *Bulletin of the Mineral Research and Exploration*, 120, 6980.
- Au, S.-K., & Wang, Y. (2014). *Engineering risk assessment with subset simulation*. John Wiley & Sons.
- Ayyub, B., Assakkaf, I., & Atua, K. (2000). Reliability-Based Load and Resistance Factor Design (LRFD) of Hull Girders for Surface Ships. *Naval Engineers Journal*, 112(4), 279–296.
- Barker, R., Duncan, J., Rojiani, K., Ooi, P., Tan, C., & Kim, S. (1991). Manuals for the design of bridge foundations. *NCHRP Report*, 343.

- Bathurst, R. J., Allen, T. M., & Nowak, A. S. (2008). Calibration concepts for load and resistance factor design (lrfd) of reinforced soil walls. *Canadian Geotechnical Journal*, 45(10), 1377–1392.
- Brown, D., Turner, J., & Castelli, R. (2010). *Drilled Shafts: Construction Procedures and LRFD Design Methods* (Tech. Rep. No. FHWA NHI-10-016). Federal Highway Administration.
- Chin, F. (1970). Estimation of the ultimate load of piles not carried to failure. In *Proceedings of the 2nd southeast asian conference on soil engineering* (pp. 81–90).
- Cibor, J. M. (1983). Geotechnical considerations of las vegas valley. In *Geological environmental and soil properties* (pp. 351–373).
- Duncan, J. M. (2000). Factors of safety and reliability in geotechnical engineering. *Journal of geotechnical and geoenvironmental engineering*, 126(4), 307–316.
- Garder, J. A., Ng, K. W., Sritharan, S., & Roling, M. J. (2012). *Development of a Database for Drilled SHAft Foundation Testing (DSHAFT)* (Tech. Rep. No. InTrans 10-366).
- Hannigan, P. J., Goble, G. G., Thendean, G., Likins, G. E., & Rausche, F. (1997). *Design and construction of driven pile foundations-volume ii* (Tech. Rep.).
- Hasofer, A. M., & Lind, N. C. (1974). Exact and invariant second-moment code format. *Journal of the Engineering Mechanics division*, 100(1), 111–121.
- Kishida, H., Tsubakihara, Y., & Ogura, T. (1992). Pile loading tests at osaka amenity park project. *preprint by Mitsubishi Co.*
- Kluzniak, B., Karakouzian, M., & Afsharhasani, R. (2014). Case History: Drilled Shaft Foundation System in Cemented Soils, Las Vegas, Nevada. In *39th annual conference on deep foundations* (pp. 365–372). Atlanta, GA.
- Kulhawy, F. H., Prakoso, W. A., & Akbas, S. O. (2005). Evaluation of capacity of rock foundation sockets. In *Proceedings of the 40th united states symposium on rock mechanics*.
- Lee, J.-S., & Park, Y.-H. (2008). Equivalent pile load–head settlement curve using a bi-directional pile load test. *Computers and Geotechnics*, 35(2), 124–133.
- Lemieux, C. (2009). *Monte Carlo and Quasi-Monte Carlo Sampling*. Springer Science & Business Media.
- Liang, R., & Li, J. (2009). Resistance Factors Calibrated from FHWA Drilled Shafts Static Top-down Test Database. In *Proc., international foundation congress and equipment expo: Contemporary topics in in situ testing, analysis, and reliability of foundations* (pp. 15–19).
- Loadtest Inc. (2000). *Construction of the equivalent top-loaded load-settlement curve from the results of an o-cell load test* (Tech. Rep.).

- Long, J., Hendrix, J., & Baratta, A. (2009). *Evaluation/modification of IDOT foundation piling design and construction policy* (Tech. Rep. No. ICT-09-037). Illinois Center for Transportation (ICT).
- Luke, B., Calderón-Macías, C., Huynh, M., Culligan, P., Einstein, H., & Whittle, A. (2003). Inverting Surface Wave Data from a Site Containing Cemented Inclusions. In (pp. 157–162). Verlag Glückauf GMBH, Essen.
- MATLAB. (2014). *Version 8.3.0.532 (R2014a)*. Natick, Massachusetts: The MathWorks Inc.
- McVay, M., Hoit, M., Hughes, E., Nguyen, T., & Lai, P. (2005). Development of a web based design, and construction bridge substructure database. In *Transportation research board 84th annual meeting* (pp. 9–13).
- McVay, M. C., Kuo, C. L., & Singletary, W. A. (1998). *Calibrating Resistance Factors in the Load and Resistance Factor Design for Florida Foundations* (Tech. Rep. No. FHWA Report No. WPI0510772). Raleigh, North Carolina: University of Florida, Florida Department of Transportation.
- Melchers, R. (1987). *Structural reliability: Analysis and prediction*. UK: Ellis Horwood Limited.
- Meyer, P. L., Holmquist, D. V., Matlock, H. L., et al. (1975). Computer predictions for axially-loaded piles with nonlinear supports. In *Proceedings of the 7th offshore technology conference*. Houston, TX.
- Motamed, R., Stanton, K., Elfass, S., & Kluzniak, B. (2016). Development of the Nevada Deep Foundations Load Test Database: Drilled Shaft Component. In *Transportation research board 95th annual meeting* (p. 12). Washington D.C..
- Murvosh, H., Luke, B., Taylor, W. J., & Wagoner, J. (2013). Three-dimensional shallow shear-wave velocity model for the las vegas valley. *Environmental & Engineering Geoscience*, 19(2), 115–134.
- Ogura, S., & Kishida, Y. (1996). Application of the pile toe test to cast-in-place and precast piles. *Translated by Karkee, Foundation Drilling Magazine*.
- Paikowsky, S. G. (2004). *Load and resistance factor design (LRFD) for deep foundations* (Tech. Rep. No. 507). Transportation Research Board.
- Rahman, M. S., Gabr, M., Sarica, R., & Hossain, M. (2002). *Load and Resistance Factor Design (LRFD) for analysis/design of piles axial capacity* (Tech. Rep. No. FHWA/NC/2005-08). Raleigh, North Carolina: North Carolina State University.
- Rinne, E., Thompson, J., & Vanderpool, W. (1996). *I-15/US 95 Load Test Program, Las Vegas, Nevada* (Tech. Rep. No. 31-215903-07A). Las Vegas, Nevada: Parsons Brinckerhoff.

- Roling, M. J., Sritharan, S., & Suleiman, M. T. (2011). Introduction to PILOT database and establishment of LRFD resistance factors for the construction control of driven steel H-piles. *Journal of Bridge Engineering*, 16(6), 728–738.
- Schmertmann, J. H., & Hayes, J. A. (1997). The osterberg cell and bored pile testing—a symbiosis. In *Proceedings: 3rd international geotechnical engineering conference, cairo university, cairo, egypt* (pp. 3–12).
- Smith, T., Banas, A., Gummer, M., & Jin, J. (2011). *Recalibration of the GRLWEAP LRFD Resistance Factor for Oregon DOT* (Tech. Rep. No. OR-RD-98-00). Salem, Oregon: Oregon Department of Transportation, Research Unit.
- Stokoe, K. H., Wright, S., Bay, J., Roesset, J., et al. (1994). Characterization of geotechnical sites by sasw method. *Geophysical Characterization of Sites*, 15–25.
- Stone, R. C. (2009). *Analysis of a Caliche Stiffened Pile Foundation* (Ph.D. Dissertation). University of Nevada, Las Vegas.
- Thiros, S., Bexfield, L., Anning, D., & Huntington, J. (2010). *Conceptual Understanding and Groundwater Quality of Selected Basin-Fill Aquifers in the Southwestern United States* (Tech. Rep. No. 1781). National Water Quality Assessment Program, USGS.
- Vanderpool, W. E., Chesnut, R. L., & McGettigan, M. E. (2011). Geotechnical exploration phase drilled shaft load testing. *DFI Journal-The Journal of the Deep Foundations Institute*, 5(2), 16–22.
- Werle, J., & Luke, B. (2007). Engineering with heavily cemented soils in Las Vegas, Nevada. *Geo-Denver*, 1–9.
- Western Technologies Inc. (1994). *Geotechnical Exploration, Fremont Street Experience* (Tech. Rep. No. Project No. 4123JZ254). Las Vegas, Nevada.
- Wyman, R. V., Karakouzian, M., Bax-Valentine, V., Slemmons, D. B., Peterson, L., & Palmer, S. (1993). Geology of las vegas, nevada, united states of america. *Bulletin of the Association of Engineering Geologists*, 30(1), 33–78.

Appendix A

NDFLTD

The NDFLTD may be opened from this [link](#) if the appropriate files have been saved to the same path as the current document. The link will not work if this report file was obtained as a stand alone document. For further assistance, please contact the Nevada Department of Transportation.

Appendix B

Collected Load Tests and GI Reports

The original load test and GI reports may be found at this [link](#) if the appropriate files have been saved to the same path as the current document. The link will not work if this report file was obtained as a stand alone document. For further assistance, please contact the Nevada Department of Transportation.

Appendix C

Interpreted Stratigraphy and Geomaterial Properties

Tables [C.1](#) through [C.41](#) describe the assumed stratigraphy and material properties employed for the estimation of nominal axial capacity and load-settlement behavior of the test shafts in the NDFLTD. Note that the unconfined compressive strength of caliche, which is not given in the following tables, was set to 729 ksf for all cases for calibration purposes. Also, the superscript PCM indicates that a given layer was noted in the boring log as being partially cemented (i.e. not caliche but exhibiting some level of cementation).

APPENDIX C. INTERPRETED STRATIGRAPHY AND GEOMATERIAL
PROPERTIES

Table C.1: Assumed stratigraphy and material properties for data number 1 (water table depth = 85 ft).

Bottom Layer Depth (ft)	Soil Type	B (ft)	γ (pcf)	ϕ°	N_{SPT}	s_u (psf)
2	Cohesionless (GP)	4	98	43	25	-
4	Cohesionless (SM)	4	98	43	25	-
8	Cohesive	4	111	-	19	2992
11.5	Cohesionless (GP)	4	110	43	39	-
13.5	Cohesive ^{PCM}	4	111	-	45	5453
16.5	Caliche	4	140	40	-	-
18	Cohesive	4	111	-	45	5112
19	Caliche	4	140	40	-	-
22	Caliche	4	140	40	-	-
27	Cohesionless (SM)	4	101	40	21	-
30	Cohesionless (SM) ^{PCM}	4	117	44	50	-
36.5	Caliche	4	140	40	-	-
42	Cohesive	4	119	-	6	718
47	Cohesionless (SM)	4	115	39	16	-
57	Cohesionless (SM)	4	114	38	15	-
60	Cohesive ^{PCM}	4	131	-	50	4806
62	Caliche	4	140	40	-	-
64.5	Cohesionless (SM)	4	119	41	30	-
65	Cohesive	4	131	-	24	2225
68	Cohesionless (SM)	4	119	41	30	-
69.5	Caliche	4	140	40	-	-
74.5	Cohesive	4	131	-	19	1671
79.5	Cohesive	4	131	-	19	1630
84.5	Cohesive	4	129	-	18	1507
86	Cohesive	4	131	-	40	3301
87.5	Cohesionless (SM)	4	108	36	11	-
90	Cohesionless (SM)	4	108	36	11	-
94	Cohesive	4	126	-	15	1209
97	Cohesive	4	131	-	25	1987
99	Cohesionless (SM)	4	108	36	11	-
100.5	Cohesionless (SM)	4	102	35	8	-

*APPENDIX C. INTERPRETED STRATIGRAPHY AND GEOMATERIAL
PROPERTIES*

122	Cohesionless (SM)	4	116	39	25	-
-----	-------------------	---	-----	----	----	---

APPENDIX C. INTERPRETED STRATIGRAPHY AND GEOMATERIAL
PROPERTIES

Table C.2: Assumed stratigraphy and material properties for data number 2 (water table depth = 101 ft).

Bottom Layer Depth (ft)	Soil Type	B (ft)	γ (pcf)	ϕ°	N_{SPT}	s_u (psf)
45.03	Cohesionless (SM)	5	131	44	50	-
53	Cohesive	5	111	-	30	5800
58	Cohesionless (SM)	5	125	43	50	-
60	Cohesive	5	114	-	40	7830
67	Cohesive	5	114	-	20	6590
77	Cohesive	5	125	-	50	7800
84	Cohesive	5	112	-	22	4850
85	Cohesionless (SM)	5	121	42	50	-

APPENDIX C. INTERPRETED STRATIGRAPHY AND GEOMATERIAL
PROPERTIES

Table C.3: Assumed stratigraphy and material properties for data number 3 (water table depth = 101 ft).

Bottom Layer Depth (ft)	Soil Type	B (ft)	γ (pcf)	ϕ°	N_{SPT}	s_u (psf)
10.47	Cohesionless (SM)	7.67	140	45	50	-
20.67	Cohesionless (SM)	7.67	131	44	50	-
34	Cohesionless (SM) ^{PCM}	6	115	40	50	-
44	Cohesionless (SM)	6	122	33	50	-
69	Cohesionless (SM)	6	115	33	50	-
79	Cohesionless (SM)	6	120	44	50	-
84.9	Cohesionless (SM)	6	123	42	50	-

APPENDIX C. INTERPRETED STRATIGRAPHY AND GEOMATERIAL
PROPERTIES

Table C.4: Assumed stratigraphy and material properties for data number 4 (water table depth = 10 ft).

Bottom Layer Depth (ft)	Soil Type	B (ft)	γ (pcf)	ϕ°	N_{SPT}	s_u (psf)
3.5	Cohesionless (SM)	8	91	28	19	-
9	Cohesive	8	114	-	25	4200
10	Cohesive	8	125	-	13	1770
12	Cohesive	8	125	-	13	1675
13.5	Cohesionless (SM) ^{PCM}	8	115	39	13	-
21	Caliche	8	140	40	-	-
32	Cohesionless (SM) ^{PCM}	8	136	45	50	-

APPENDIX C. INTERPRETED STRATIGRAPHY AND GEOMATERIAL
PROPERTIES

Table C.5: Assumed stratigraphy and material properties for data number 5 (water table depth = 7 ft).

Bottom Layer Depth (ft)	Soil Type	B (ft)	γ (pcf)	ϕ°	N_{SPT}	s_u (psf)
0.5	Cohesionless (SM)	2	97	38	8	-
7	Cohesive	2	111	-	10	1794
8.5	Cohesive	2	132	-	18	1428
14	Cohesionless (SM)	2	130	41	18	-
17	Caliche	2	140	40	-	-
18.5	Cohesionless (SM)	2	119	41	20	-
22	Cohesive	2	112	-	24	820
26	Cohesive	2	125	-	38	582
29	Cohesionless (SM)	2	126	44	45	-
30.5	Cohesive	2	131	-	11	1706
31.2	Caliche	2	140	40	-	-
31.6	Cohesive	2	131	-	50	7952

APPENDIX C. INTERPRETED STRATIGRAPHY AND GEOMATERIAL
PROPERTIES

Table C.6: Assumed stratigraphy and material properties for data number 6 (water table depth = 7 ft).

Bottom Layer Depth (ft)	Soil Type	B (ft)	γ (pcf)	ϕ°	N_{SPT}	s_u (psf)
0.5	Cohesionless (SM)	2	97	38	8	-
7	Cohesive	2	111	-	10	1794
8.5	Cohesive	2	132	-	18	1428
14	Cohesionless (SM)	2	130	41	18	-
17	Caliche	2	140	40	-	-
18.5	Cohesionless (SM)	2	119	41	20	-
22	Cohesive	2	112	-	24	820
26	Cohesive	2	125	-	38	582
29	Cohesionless (SM)	2	126	45	45	-
30.5	Cohesive	2	131	-	11	1706
31.2	Caliche	2	140	40	-	-
31.6	Cohesive	2	131	-	50	7952
34	Caliche	2	140	40	-	-
34.5	Cohesionless (SM)	2	107	45	50	-
37.5	Caliche	2	140	40	-	-
40	Cohesive	2	149	-	30	1407
43	Cohesive	2	109	-	8	608
44	Caliche	2	140	40	-	-
82.5	Cohesive	2	107	33	27	3252

APPENDIX C. INTERPRETED STRATIGRAPHY AND GEOMATERIAL
PROPERTIES

Table C.7: Assumed stratigraphy and material properties for data number 7 (water table depth = 12 ft).

Bottom Layer Depth (ft)	Soil Type	B (ft)	γ (pcf)	ϕ°	N_{SPT}	s_u (psf)
1	Cohesionless (SM)	2	105	42	19	-
3.5	Cohesionless (GP)	2	120	43	25	-
7	Cohesionless (SM)	2	99	40	13	-
9.5	Cohesive	2	105	-	11	1237
12	Cohesionless (SM)	2	105	42	31	-
12.5	Cohesionless (SM)	2	125	42	31	-
13	Caliche	2	140	40	-	-
20	Cohesionless (SM)	2	130	42	24	-
21	Cohesive	2	115	-	46	504
22	Caliche	2	140	40	-	-
26.5	Cohesionless (GP)	2	139	43	32	-
30	Cohesive	2	115	-	12	551
34	Cohesionless (SM)	2	135	44	45	-
35.5	Cohesive	2	137	-	50	1319
37	Cohesionless (SM)	2	137	44	50	-
40.5	Cohesive	2	119	-	16	1084
43	Cohesionless (SM)	2	132	41	22	-

APPENDIX C. INTERPRETED STRATIGRAPHY AND GEOMATERIAL
PROPERTIES

Table C.8: Assumed stratigraphy and material properties for data number 8 (water table depth = 22 ft).

Bottom Layer Depth (ft)	Soil Type	B (ft)	γ (pcf)	ϕ°	N_{SPT}	s_u (psf)
4	Cohesionless (SM)	4	106	42	22	-
8	Cohesionless (SM)	4	140	45	50	-
12	Cohesionless (GP)	4	111	43	43	-
18	Cohesionless (GP)	4	126	44	50	-
20	Caliche	4	140	40	-	-
21	Caliche	4	140	40	-	-
24	Cohesive	4	131	-	40	5349
32.5	Caliche	4	140	40	-	-
38.5	Cohesionless (GP)	4	116	44	50	-
42	Caliche	4	140	40	-	-
47	Cohesive	4	124	-	16	1899
48.5	Caliche	4	140	40	-	-
50.5	Cohesionless (GP)	4	133	43	50	-
52.5	Caliche	4	140	40	-	-
53	Cohesive	4	131	30	50	5563
53.5	Caliche	4	140	40	-	-
57.5	Cohesionless (SM)	4	149	43	50	-
62.5	Cohesive	4	131	-	38	3996
63.5	Caliche	4	140	40	-	-
65	Cohesive	4	131	-	30	3070
67	Cohesionless (GP)	4	129	43	50	-
70.5	Cohesive	4	131	-	43	4287
78	Cohesionless (SM)	4	123	40	28	-
79	Caliche	4	140	40	-	-
83.5	Cohesive	4	134	-	50	4529
84.5	Caliche	4	140	40	-	-
88	Cohesive	4	124	-	50	4561
88.5	Caliche	4	140	40	-	-
92.5	Cohesive	4	132	-	34	2755
99	Cohesionless (GP)	4	133	42	50	-
101	Caliche	4	140	40	-	-
108.5	Cohesive	4	126	-	40	3361

*APPENDIX C. INTERPRETED STRATIGRAPHY AND GEOMATERIAL
PROPERTIES*

114.5	Caliche	4	140	40	-	-
117	Cohesive	4	121	-	15	1206
126	Caliche	4	140	40	-	-

APPENDIX C. INTERPRETED STRATIGRAPHY AND GEOMATERIAL
PROPERTIES

Table C.9: Assumed stratigraphy and material properties for data number 9 (water table depth = 20 ft).

Bottom Layer Depth (ft)	Soil Type	B (ft)	γ (pcf)	ϕ°	N_{SPT}	s_u (psf)
2.5	Cohesive	4	124	-	16	3016
5	Cohesionless (SM)	4	110	40	23	-
7.5	Cohesionless (SM)	4	110	40	23	-
16	Cohesive	4	116	-	4	534
20	Cohesive	4	133	-	17	2060
25	Cohesionless (GP)	4	140	43	42	-
29	Caliche	4	140	40	-	-
35	Cohesionless (SM)	4	132	42	42	-
36	Caliche	4	140	40	-	-
43	Cohesionless (GP)	4	132	41	44	-
47	Caliche	4	140	40	-	-
53.5	Cohesive	4	136	-	35	3920
56	Caliche	4	140	40	-	-
65	Cohesive	4	131	-	40	4175
69	Caliche	4	140	40	-	-
85	Cohesionless (SM)	4	130	41	40	-
85.5	Caliche	4	140	40	-	-
87	Cohesive	4	128	-	16	1450
100	Cohesionless (SM)	4	129	37	16	-
110	Caliche	4	140	40	-	-

APPENDIX C. INTERPRETED STRATIGRAPHY AND GEOMATERIAL
PROPERTIES

Table C.10: Assumed stratigraphy and material properties for data number 10 (water table depth = 20 ft).

Bottom Layer Depth (ft)	Soil Type	B (ft)	γ (pcf)	ϕ°	N_{SPT}	s_u (psf)
5.2	Cohesionless (SP)	4	112	42	19	-
6	Cohesionless (SP)	4	111	41	19	-
9	Cohesionless (GP)	4	101	41	19	-
10.5	Cohesionless (SP)	4	135	44	50	-
16.5	Cohesionless (SP)	4	140	44	50	-
19	Caliche	4	140	40	-	-
20	Cohesionless (SM)	4	103	41	30	-
25	Cohesionless (SM)	4	125	42	30	-
32.5	Cohesionless (SM)	4	126	37	11	-
36	Caliche	4	140	40	-	-
44	Cohesive	4	131	-	18	2286
50.5	Cohesionless (SP)	4	140	44	50	-
59.5	Cohesive	4	123	-	9	1095
69	Cohesive	4	131	-	50	5218
71	Cohesive	4	131	-	50	5039
90	Cohesive	4	131	-	37	3447
98	Cohesive	4	131	-	50	4452
100.5	Cohesionless (SP)	4	118	36	11	-
122	Cohesive	4	120	-	9	676

APPENDIX C. INTERPRETED STRATIGRAPHY AND GEOMATERIAL
PROPERTIES

Table C.11: Assumed stratigraphy and material properties for data number 11 (water table depth = 24.5 ft).

Bottom Layer Depth (ft)	Soil Type	B (ft)	γ (pcf)	ϕ°	N_{SPT}	s_u (psf)
9	Cohesionless (SM)	4	99	39	11	-
10	Cohesionless (SM)	4	97	38	11	-
14	Cohesive	4	111	-	50	7064
19.5	Caliche	4	140	40	50	-
26	Cohesive	4	131	-	31	4410
29.5	Cohesionless (SM)	4	140	44	50	-
33	Cohesive	4	131	-	41	5764
38	Cohesionless (GP) ^{PCM}	4	140	44	50	-
45	Cohesive	4	131	-	42	4736
54	Cohesive	4	124	-	9	1061
56	Caliche	4	140	40	-	-
66	Cohesive	4	131	-	31	3384
67	Caliche	4	140	40	-	-
69.5	Cohesive	4	131	-	50	5172
78	Cohesive	4	96	-	4	339
78.5	Caliche	4	140	40	-	-
92	Cohesive	4	114	-	4	388
100	Cohesive	4	122	-	10	928
110	Cohesive	4	122	-	10	805
121.5	Cohesive ^{PCM}	4	131	-	50	4275

APPENDIX C. INTERPRETED STRATIGRAPHY AND GEOMATERIAL
PROPERTIES

Table C.12: Assumed stratigraphy and material properties for data number 12 (water table depth = 18 ft).

Bottom Layer Depth (ft)	Soil Type	B (ft)	γ (pcf)	ϕ°	N_{SPT}	s_u (psf)
1.5	Cohesionless (SP)	4	117	43	25	-
8	Cohesive	4	111	-	50	9362
12	Cohesionless (SP)	4	109	40	21	-
12.5	Cohesive	4	111	-	40	4702
13.5	Cohesive	4	111	-	40	5173
15	Cohesionless (GP)	4	112	43	40	-
18.5	Cohesionless (SM)	4	140	44	50	-
20	Cohesive	4	131	-	40	4993
22	Cohesionless (SM)	4	140	44	48	-
29	Cohesive	4	131	-	32	4509
29.5	Cohesionless (SM)	4	131	43	40	-
33	Cohesive	4	131	-	30	4346
38.5	Cohesionless (GP)	4	140	44	50	-
39	Cohesive	4	131	-	40	5291
40.5	Cohesionless (GP)	4	140	44	50	-
41.5	Caliche	4	140	40	-	-
43	Cohesionless (GP)	4	129	43	40	-
45	Caliche	4	140	40	-	-
48	Cohesionless (SM)	4	138	44	50	-
49	Cohesive	4	131	-	35	4205
54.5	Cohesionless (SM)	4	126	42	37	-
57	Cohesive	4	131	-	24	2730
58.5	Cohesionless (GP)	4	127	42	40	-
59.5	Cohesive	4	130	-	24	2668
61	Caliche	4	140	40	-	-
63	Cohesive	4	131	-	30	3261
64	Cohesionless (SM)	4	126	42	40	-
66	Cohesive	4	131	-	45	4797
69.5	Cohesionless (SM)	4	130	43	50	-
73	Cohesive	4	131	-	50	5126
79	Cohesionless (SM)	4	129	43	50	-
80	Cohesive	4	131	-	45	4405

APPENDIX C. INTERPRETED STRATIGRAPHY AND GEOMATERIAL
PROPERTIES

Table C.12: Assumed stratigraphy and material properties for data number 12 (water table depth = 18 ft). (continued)

Bottom Layer Depth (ft)	Soil Type	B (ft)	γ (pcf)	ϕ°	N_{SPT}	s_u (psf)
84	Cohesionless (SM)	4	128	43	50	-
87	Cohesive	4	130	-	28	2656
89.5	Cohesionless (SM)	4	120	41	33	-
94	Cohesive	4	131	-	38	3500
97.5	Cohesive	4	131	-	23	2078
98.5	Cohesionless (GP)	4	122	42	40	-
100	Cohesive	4	131	-	23	2046
103	Caliche	4	140	40	-	-
107	Cohesive	4	131	-	50	4327
109	Cohesionless (SM)	4	126	42	50	-
112	Cohesive	4	131	-	50	4231
113.5	Cohesionless (SM)	4	119	41	35	-
117	Cohesive	4	129	-	18	1496
118.5	Cohesionless (GP)	4	116	39	25	-
120	Cohesive	4	130	-	30	2457
125	Caliche	4	140	40	-	-
129.5	Cohesive ^{PCM}	4	131	-	50	3979
132	Cohesive	4	131	-	50	3922
133	Caliche	4	140	40	-	-
134	Cohesive	4	131	-	30	2326
135.5	Caliche	4	140	40	-	-

APPENDIX C. INTERPRETED STRATIGRAPHY AND GEOMATERIAL
PROPERTIES

Table C.13: Assumed stratigraphy and material properties for data number 13 (water table depth = 15.5 ft).

Bottom Layer Depth (ft)	Soil Type	B (ft)	γ (pcf)	ϕ°	N_{SPT}	s_u (psf)
9.5	Cohesionless (SP)	4	140	45	50	-
13	Cohesive	4	110	-	14	1556
15	Cohesionless (SM)	4	124	44	50	-
17	Cohesionless (SM)	4	139	44	50	-
24	Cohesive	4	131	-	47	6736
30.5	Cohesive	4	131	-	34	4689
34.5	Cohesive	4	131	-	50	6835
35.5	Cohesionless (SM)	4	113	38	10	-
36.5	Cohesive	4	131	-	50	6609
38.5	Caliche	4	140	40	-	-
39.5	Cohesive	4	131	-	35	4481
41.5	Caliche	4	140	40	-	-
43.5	Cohesive	4	131	-	35	4330
45	Cohesionless (SM)	4	129	43	40	-
50.5	Cohesionless (GP)	4	136	44	50	-
54.5	Caliche	4	140	40	-	-
57.5	Cohesionless (SM)	4	107	36	8	-
59.5	Cohesionless (GP)	4	116	39	17	-
60.5	Caliche	4	140	40	-	-
61	Cohesionless (SM)	4	128	43	45	4896
63	Caliche	4	140	40	-	-
68.5	Cohesive	4	131	-	50	5215
73	Cohesive	4	131	-	50	5059
77.5	Cohesive	4	130	-	27	2662
82	Cohesionless (SM)	4	122	41	36	-
88	Cohesive	4	131	-	50	4696
88.5	Caliche	4	140	40	-	-
89.5	Cohesive	4	131	-	45	4141
90	Caliche	4	140	40	-	-
93	Cohesive	4	126	-	14	1273
93.5	Caliche	4	140	40	-	-
94.5	Cohesionless (SM)	4	120	41	35	-

APPENDIX C. INTERPRETED STRATIGRAPHY AND GEOMATERIAL
PROPERTIES

Table C.13: Assumed stratigraphy and material properties for data number 13 (water table depth = 15.5 ft). (continued)

Bottom Layer Depth (ft)	Soil Type	B (ft)	γ (pcf)	ϕ°	N_{SPT}	s_u (psf)
96.5	Cohesive	4	131	-	50	4468
102	Cohesive	4	131	-	27	2371
102.5	Caliche	4	140	40	-	-
108.5	Cohesive	4	126	-	15	1290
113.5	Cohesive	4	130	-	29	2427
119	Cohesive	4	127	-	16	1313
123.5	Cohesive	4	131	-	45	3625
126.5	Caliche	4	140	40	-	-
127	Cohesive	4	131	-	45	3547
127.5	Caliche	4	140	40	-	-
129.5	Cohesive	4	131	-	40	3133
130.5	Cohesionless (SM)	4	114	38	20	-
132	Cohesive	4	131	-	44	3416

APPENDIX C. INTERPRETED STRATIGRAPHY AND GEOMATERIAL
PROPERTIES

Table C.14: Assumed stratigraphy and material properties for data number 14 (water table depth = 23 ft).

Bottom Layer Depth (ft)	Soil Type	B (ft)	γ (pcf)	ϕ°	N_{SPT}	s_u (psf)
2.5	Cohesionless (GP)	3	104	42	20	-
8.5	Cohesionless (SM)	3	99	40	12	-
13.5	Cohesionless (SM)	3	102	41	22	-
18	Cohesionless (SM)	3	101	41	21	-
20.5	Cohesionless (SM)	3	108	43	32	-
23	Cohesive	3	111	-	48	7076
30	Cohesive	3	131	-	50	6814
31	Cohesive	3	131	-	50	7182
34	Caliche	3	140	40	-	-
35	Cohesive	3	131	-	45	6150
35.5	Caliche	3	140	40	-	-
37.5	Cohesive	3	131	-	45	6017
40	Caliche	3	140	40	-	-
45.5	Cohesive	3	131	-	27	3417
48	Cohesionless (SM)	3	127	43	38	-
55	Cohesionless (SM)	3	135	44	50	-
59.5	Cohesionless (GP)	3	132	43	50	-
60.5	Caliche	3	140	40	-	-
68.5	Cohesive	3	131	-	39	4135
72	Cohesionless (SM)	3	127	43	44	-
75	Cohesive	3	131	-	39	3918
78	Cohesionless (SM)	3	118	40	27	-
81.5	Cohesionless (GP) ^{PCM}	3	128	43	50	-
86.5	Cohesive	3	131	-	50	4283
88.5	Cohesionless (SM)	3	127	43	50	-
96.5	Cohesive	3	131	-	50	3573
99.5	Cohesionless (SM)	3	126	42	50	-
105.5	Cohesive	3	130	-	50	3927
107.5	Cohesionless (SM)	3	126	42	50	-
108	Caliche	3	140	40	-	-
118	Cohesionless (SM) ^{PCM}	3	125	42	50	-
129	Cohesive	3	131	-	50	4024

*APPENDIX C. INTERPRETED STRATIGRAPHY AND GEOMATERIAL
PROPERTIES*

132	Cohesive	3	131	-	50	3709
-----	----------	---	-----	---	----	------

APPENDIX C. INTERPRETED STRATIGRAPHY AND GEOMATERIAL
PROPERTIES

Table C.15: Assumed stratigraphy and material properties for data number 15 (water table depth = 24 ft).

Bottom Layer Depth (ft)	Soil Type	B (ft)	γ (pcf)	ϕ°	N_{SPT}	s_u (psf)
2	Cohesionless (GP)	4	105	42	20	-
6	Cohesionless (SM)	4	113	43	30	-
8	Cohesive	4	111	-	30	4679
19	Cohesionless (GP)	4	140	44	50	-
21.5	Cohesionless (SM)	4	135	44	50	-
22.5	Caliche	4	140	40	-	-
24	Cohesive	4	111	-	50	6367
27	Cohesive	4	131	-	50	6177
36	Cohesionless (SM)	4	140	44	50	-
37	Cohesive	4	131	-	50	6089
40	Cohesionless (SM)	4	123	42	32	-
41.5	Cohesionless (SM)	4	123	42	32	-
47	Cohesive	4	131	-	34	3906
48.5	Cohesionless (SM)	4	124	42	35	-
53	Cohesive	4	131	-	39	4278
57	Cohesionless (GP) ^{PCM}	4	131	43	50	-
59.5	Caliche	4	140	40	-	-
63	Cohesive	4	131	-	50	5114
68.5	Cohesionless (SM)	4	123	28	37	-
72	Cohesive	4	131	-	50	4877
81	Cohesionless (SM)	4	128	43	50	-
82	Cohesive	4	131	-	50	4610
83	Cohesionless (SM)	4	123	42	40	-
93.5	Cohesive	4	131	-	46	2127
95	Cohesionless (SM)	4	126	42	50	-
96	Cohesive	4	131	-	49	4241
99.5	Cohesionless (SM)	4	125	42	49	-
106.5	Cohesive	4	130	-	30	2518
111	Cohesionless (GP)	4	125	42	50	-
120	Cohesive	4	131	-	35	2804
124	Cohesionless (SM)	4	118	40	34	-
127	Caliche	4	140	40	-	-

*APPENDIX C. INTERPRETED STRATIGRAPHY AND GEOMATERIAL
PROPERTIES*

135	Cohesionless (SM)	4	123	42	50	-
140	Cohesive	4	131	-	50	3730

APPENDIX C. INTERPRETED STRATIGRAPHY AND GEOMATERIAL
PROPERTIES

Table C.16: Assumed stratigraphy and material properties for data number 16 (water table depth = 20 ft).

Bottom Layer Depth (ft)	Soil Type	B (ft)	γ (pcf)	ϕ°	N_{SPT}	s_u (psf)
10	Cohesionless (GP)	4	140	45	50	-
13	Cohesionless (SM)	4	111	43	50	-
20	Cohesionless (GP)	4	116	44	50	-
30	Cohesive	4	131	-	50	6473
36	Caliche	4	140	40	50	-
44.5	Cohesionless (SM)	4	131	43	45	-
48.5	Cohesive	4	131	-	50	5208
54.5	Cohesionless (SM)	4	127	43	50	-
57.5	Caliche	4	140	40	50	-
60	Cohesive	4	131	-	50	5319
62.5	Cohesionless (SM)	4	130	43	50	-
68	Cohesive	4	131	-	50	4596
69.5	Cohesionless (SM)	4	129	43	50	-
75	Cohesive	4	131	-	50	4906
78.5	Cohesive	4	111	-	32	3073
83	Cohesive	4	101	-	50	4738
89	Cohesive	4	131	-	34	3153
93	Cohesionless (SM)	4	124	41	38	-
98	Cohesive	4	131	-	39	3464
102	Cohesive	4	131	-	24	2089
104	Cohesionless (SM)	4	116	40	25	-
106	Cohesive	4	131	-	39	3329
113	Cohesionless (SM)	4	114	38	18	-
117.5	Cohesive	4	130	-	40	3297
122	Cohesionless (SM)	4	135	37	50	-
126	Cohesive	4	131	-	50	3989
131	Cohesive	4	131	-	50	4239

APPENDIX C. INTERPRETED STRATIGRAPHY AND GEOMATERIAL
PROPERTIES

Table C.17: Assumed stratigraphy and material properties for data number 17 (water table depth = 20.5 ft).

Bottom Layer Depth (ft)	Soil Type	B (ft)	γ (pcf)	ϕ°	N_{SPT}	s_u (psf)
10	Cohesionless (SM)	6	127	44	38	-
13.5	Cohesive	6	125	-	41	5815
19	Cohesive	6	125	-	50	6149
20.5	Cohesionless (SM)	6	115	44	47	-
22	Cohesionless (SM)	6	140	44	47	-
30	Cohesionless (SM)	6	140	44	50	230000
34	Cohesive	6	131	-	50	6570
37	Caliche	6	140	40	-	-
39.5	Cohesionless (GP) ^{PCM}	6	139	44	50	-
42	Cohesionless (SM)	6	110	37	9	-
43	Cohesive	6	131	-	35	4186
50	Cohesionless (SM)	6	134	44	50	-
55	Cohesive	6	130	-	22	2432
59.5	Cohesionless (SM)	6	131	43	50	-
64	Caliche	6	140	40	-	-
68	Cohesive	6	102	-	48	4866
72.5	Cohesionless (SM)	6	128	43	49	-
75	Cohesive	6	131	-	40	3902
79	Cohesionless (SM)	6	128	43	50	-
82	Cohesive	6	131	-	50	4711
86	Cohesionless (SM)	6	122	42	41	-
86.5	Cohesive	6	122	-	41	3764
89.5	Cohesionless (SM)	6	122	42	41	-
94.5	Cohesive	6	131	-	20	1790
98	Cohesionless (SM)	6	123	42	43	-
101	Cohesionless (SM)	6	126	42	50	-
104	Cohesive	6	131	-	45	3849
111.5	Cohesionless (SM)	6	125	42	50	-
112	Cohesive	6	131	-	50	4130
114	Cohesionless (SM)	6	119	41	35	-
115	Cohesive	6	131	-	45	3682
120	Cohesionless (SM)	6	122	42	45	-

*APPENDIX C. INTERPRETED STRATIGRAPHY AND GEOMATERIAL
PROPERTIES*

126	Cohesive	6	131	-	50	3973
132	Cohesive	6	128	-	18	1401
136.5	Cohesionless (SM)	6	117	40	30	-
138.5	Cohesive	6	131	-	45	3414
148.5	Cohesionless (SM)	6	123	42	50	-
152	Cohesive	6	130	-	36	2636

APPENDIX C. INTERPRETED STRATIGRAPHY AND GEOMATERIAL
PROPERTIES

Table C.18: Assumed stratigraphy and material properties for data number 18 (water table depth = 15 ft).

Bottom Layer Depth (ft)	Soil Type	B (ft)	γ (pcf)	ϕ°	N_{SPT}	s_u (psf)
45	Cohesionless (SM)	4	140	45	50	-
47.5	Cohesive	4	131	-	40	5155
50	Cohesive	4	131	-	44	5539
50.5	Caliche	4	140	40	-	-
51.25	Cohesionless (SM)	4	132	43	45	-
52	Caliche	4	140	40	-	-
53.5	Cohesive	4	131	-	45	5461
54	Caliche	4	140	40	-	-
57	Cohesive	4	131	-	45	5334
57.75	Caliche	4	140	40	-	-
59.5	Cohesive	4	131	-	50	5778
62.5	Cohesionless (SM)	4	121	41	30	-
62.75	Caliche	4	140	40	-	-
67.5	Cohesive	4	127	-	12	1327
72.25	Cohesionless (SM)	4	120	41	30	-
75	Cohesionless (SM)	4	125	42	40	-
80.5	Cohesive	4	119	-	7	720
81	Caliche	4	140	40	-	-
87	Cohesive	4	131	-	41	4076
91	Cohesive	4	121	-	9	872
91.2	Caliche	4	140	40	-	-
95	Cohesive	4	131	-	50	4744
95.25	Caliche	4	140	40	-	-
96.75	Cohesive	4	131	-	45	4206
97	Caliche	4	140	40	-	-
98	Cohesionless (SM)	4	117	40	25	-
98.2	Caliche	4	140	40	-	-
100	Cohesive	4	123	-	11	1014
103	Cohesive	4	127	-	15	1368
105	Cohesionless (GP) ^{PCM}	4	117	40	27	-
106	Cohesive	4	131	-	25	2242
106.5	Caliche	4	140	40	-	-

APPENDIX C. INTERPRETED STRATIGRAPHY AND GEOMATERIAL
PROPERTIES

Table C.18: Assumed stratigraphy and material properties for data number 18 (water table depth = 15 ft). (continued)

Bottom Layer Depth (ft)	Soil Type	B (ft)	γ (pcf)	ϕ°	N_{SPT}	s_u (psf)
107	Cohesive	4	131	-	35	3120
107.25	Caliche	4	140	40	-	-
109	Cohesive	4	131	-	50	4429
110	Caliche	4	140	40	-	-
111.5	Cohesive	4	131	-	45	3937
111.75	Caliche	4	140	40	-	-
113	Cohesive	4	131	-	45	3908
113.25	Caliche	4	140	40	-	-
116	Cohesive	4	131	-	50	4300
118	Caliche	4	140	40	-	-
120	Cohesionless (SM)	4	124	42	46	-
120.5	Caliche	4	140	40	-	-
122	Cohesive	4	131	-	45	3763
122.25	Caliche	4	140	40	-	-
123	Cohesionless (SM)	4	115	39	20	-
123.25	Caliche	4	140	40	-	-
125	Cohesionless (SM)	4	115	39	20	-
125.25	Caliche	4	140	40	-	-
127	Cohesive	4	131	-	23	1890
127.25	Caliche	4	140	40	-	-
130	Cohesive	4	131	-	27	2197
131	Caliche	4	140	40	-	-
132.5	Cohesive	4	130	-	20	1608
132.75	Caliche	4	140	40	-	-
136	Cohesive	4	126	-	16	1274
136.75	Caliche	4	140	40	-	-
137.5	Cohesive	4	122	-	12	947
138.25	Caliche	4	140	40	-	-
166.7	Cohesive	4	120	-	10	754

APPENDIX C. INTERPRETED STRATIGRAPHY AND GEOMATERIAL
PROPERTIES

Table C.19: Assumed stratigraphy and material properties for data number 19 (water table depth = 15 ft).

Bottom Layer Depth (ft)	Soil Type	B (ft)	γ (pcf)	ϕ°	N_{SPT}	s_u (psf)
54.2	Cohesionless (SP)	4	140	45	50	-
55	Caliche	4	140	40	-	-
56	Cohesive	4	131	-	45	5289
57	Caliche	4	140	40	-	-
59	Cohesive	4	131	-	50	5767
59.5	Caliche	4	140	40	-	-
60	Cohesive	4	131	-	45	5111
67	Cohesionless (SM)	4	121	41	30	-
68.25	Caliche	4	140	40	-	-
72	Cohesive	4	120	-	7	746
73	Cohesionless (SM)	4	118	40	25	-
76	Cohesive	4	123	-	10	1040
78	Cohesionless (SM)	4	124	42	39	-
83.5	Cohesive	4	131	-	39	3915
92	Cohesive	4	131	-	21	2027
92.5	Caliche	4	140	40	-	-
95	Cohesive	4	131	-	21	1964
95.5	Caliche	4	140	40	-	-
97	Cohesive	4	131	-	21	1939
97.25	Caliche	4	140	40	-	-
98.5	Cohesionless (SM)	4	113	38	15	-
99	Caliche	4	140	40	-	-
100	Cohesionless (GP)	4	111	37	13	-
100.2	Caliche	4	140	40	-	-
104	Cohesive	4	131	-	20	1800
105	Cohesionless (SM)	4	116	39	21	-
105.8	Cohesive	4	131	-	20	1775
106	Caliche	4	140	40	-	-
107	Cohesive	4	131	-	20	1766
107.25	Caliche	4	140	40	-	-
110.5	Cohesive	4	127	-	15	1311
111.25	Caliche	4	140	40	-	-

APPENDIX C. INTERPRETED STRATIGRAPHY AND GEOMATERIAL
PROPERTIES

Table C.19: Assumed stratigraphy and material properties for data number 19 (water table depth = 15 ft). (continued)

Bottom Layer Depth (ft)	Soil Type	B (ft)	γ (pcf)	ϕ°	N_{SPT}	s_u (psf)
112.5	Cohesive	4	121	-	10	863
112.75	Caliche	4	140	40	-	-
114.5	Cohesive	4	120	-	9	771
115.5	Cohesionless (SM)	4	105	35	9	-
116.5	Caliche	4	140	40	-	-
117	Cohesive	4	121	-	10	847
117.75	Caliche	4	140	40	-	-
119	Cohesive	4	131	-	45	3787
119.45	Caliche	4	140	40	-	-
120	Cohesive	4	131	-	45	3765
120.5	Caliche	4	140	40	-	-
122	Cohesive	4	131	-	45	3741
122.5	Caliche	4	140	40	-	-
123	Cohesionless (SM)	4	125	42	50	-
123.25	Caliche	4	140	40	-	-
124	Cohesive	4	131	-	45	3706
124.5	Caliche	4	140	40	-	-
125	Cohesive	4	131	-	45	3688
125.25	Caliche	4	140	40	-	-
127	Cohesive	4	131	-	45	3668
127.25	Caliche	4	140	40	-	-
128	Cohesive	4	131	-	45	3647
128.25	Caliche	4	140	40	-	-
132	Cohesive	4	121	-	10	804
137	Cohesionless (SM)	4	124	42	50	-
176	Cohesionless (SM)	4	100	34	8	-

APPENDIX C. INTERPRETED STRATIGRAPHY AND GEOMATERIAL
PROPERTIES

Table C.20: Assumed stratigraphy and material properties for data number 20 (water table depth = 24 ft).

Bottom Layer Depth (ft)	Soil Type	B (ft)	γ (pcf)	ϕ°	N_{SPT}	s_u (psf)
10	Cohesionless (SM)	3.5	110	42	22	-
18.5	Cohesionless (SM)	3.5	140	46	50	-
24	Caliche	3.5	140	40	-	-
29.5	Caliche	3.5	140	40	-	-
30	Cohesionless (SM)	3.5	136	44	50	-
34	Caliche	3.5	140	40	-	-
36	Cohesionless (SM)	3.5	140	44	50	-
52	Cohesionless (SP)	3.5	140	43	50	-
53	Cohesionless (SM)	3.5	131	43	50	-
53.5	Caliche	3.5	140	40	-	-
60	Cohesive	3.5	134	-	47	4880
62.5	Cohesive	3.5	122	-	13	1314
69.5	Cohesionless (SM)	3.5	134	43	50	-
71	Caliche	3.5	140	40	-	-
77.5	Cohesive	3.5	120	-	27	2544
82.5	Cohesionless (GP)	3.5	127	43	50	-
87.5	Cohesionless (SM)	3.5	124	40	29	-
92.5	Cohesive	3.5	124	-	39	3433
96	Caliche	3.5	140	40	-	-
100.7	Cohesive	3.5	118	-	14	1190

APPENDIX C. INTERPRETED STRATIGRAPHY AND GEOMATERIAL
PROPERTIES

Table C.21: Assumed stratigraphy and material properties for data number 21 (water table depth = 20 ft).

Bottom Layer Depth (ft)	Soil Type	B (ft)	γ (pcf)	ϕ°	N_{SPT}	s_u (psf)
10	Cohesionless (SP)	3.5	131	39	12	-
12.5	Cohesive	3.5	126	-	13	1472
19	Cohesionless (SM)	3.5	135	43	41	-
20	Cohesionless (SP)	3.5	120	43	50	-
30	Caliche	3.5	140	40	-	-
33.5	Cohesionless (SM)	3.5	148	44	50	-
34.5	Caliche	3.5	140	40	-	-
35.5	Cohesive	3.5	131	-	50	6244
39	Caliche	3.5	140	40	-	-
42.5	Cohesive	3.5	131	-	45	5330
47.5	Cohesionless (SM)	3.5	136	38	14	-
52.5	Cohesionless (SM)	3.5	137	40	24	-
56	Cohesionless (SM)	3.5	146	43	50	-
59	Caliche	3.5	140	40	-	-
72.5	Cohesive	3.5	124	-	11	1093
76	Cohesionless (SM)	3.5	131	43	50	-
77.5	Caliche	3.5	140	40	-	-
85	Cohesionless (SM)	3.5	126	40	24	-
86	Cohesionless (SM)	3.5	131	42	40	-
87	Caliche	3.5	140	40	-	-
94	Cohesive	3.5	114	-	31	2739
95.5	Caliche	3.5	140	40	-	-
99	Cohesive	3.5	131	-	40	3441
101	Caliche	3.5	140	40	-	-
104.5	Cohesive	3.5	131	-	40	3359
115.5	Caliche	3.5	140	40	-	-

APPENDIX C. INTERPRETED STRATIGRAPHY AND GEOMATERIAL
PROPERTIES

Table C.22: Assumed stratigraphy and material properties for data number 22 (water table depth = 14 ft).

Bottom Layer Depth (ft)	Soil Type	B (ft)	γ (pcf)	ϕ°	N_{SPT}	s_u (psf)
2	Cohesionless (GP)	4	98	39	10	-
6	Cohesionless (SM)	4	114	44	31	-
10	Caliche	4	140	40	-	-
12	Cohesionless (SM) ^{PCM}	4	116	44	50	-
14	Caliche	4	140	40	-	-
16	Cohesionless (SM) ^{PCM}	4	140	44	50	-
18.25	Caliche	4	140	40	-	-
20	Cohesionless (SM)	4	137	44	50	-
29.5	Cohesionless (SM) ^{PCM}	4	117	39	50	-
31	Cohesive	4	131	-	45	6610
36	Cohesionless (SM) ^{PCM}	4	140	44	50	-
36.5	Caliche	4	140	40	-	-
40	Cohesionless (SM) ^{PCM}	4	140	44	50	-
45	Caliche	4	140	40	-	-
51	Cohesive ^{PCM}	4	131	-	50	6021
51.5	Caliche	4	140	40	-	-
59	Cohesive	4	131	-	45	5115
61	Cohesionless (SM)	4	100	43	50	-
62	Cohesive ^{PCM}	4	131	-	45	4922
63	Caliche	4	140	40	-	-
71	Cohesive ^{PCM}	4	131	-	50	5268
72	Caliche	4	140	40	-	-
75	Cohesive	4	131	-	50	5058
76	Caliche	4	140	40	-	-
90	Cohesive	4	113	-	26	2517
93	Cohesionless (SM) ^{PCM}	4	119	41	30	-
95.5	Caliche	4	140	40	-	-
100	Cohesionless (SM) ^{PCM}	4	118	41	30	-
108	Cohesive	4	130	-	18	1594
109	Cohesionless (SM) ^{PCM}	4	112	38	15	-
111.5	Caliche	4	140	40	-	-
115	Cohesive	4	126	-	15	1276

*APPENDIX C. INTERPRETED STRATIGRAPHY AND GEOMATERIAL
PROPERTIES*

118	Cohesionless (SM) ^{PCM}	4	118	40	30	-
119.5	Caliche	4	140	40	-	-
121	Cohesionless (SM)	4	125	42	50	-
122	Caliche	4	140	40	-	-
124	Cohesive	4	130	-	20	1640
126	Caliche	4	140	40	-	-
128	Cohesionless (SM) ^{PCM}	4	122	41	45	-

APPENDIX C. INTERPRETED STRATIGRAPHY AND GEOMATERIAL
PROPERTIES

Table C.23: Assumed stratigraphy and material properties for data number 23 (water table depth = 14 ft).

Bottom Layer Depth (ft)	Soil Type	B (ft)	γ (pcf)	ϕ°	N_{SPT}	s_u (psf)
2	Cohesionless (GP)	4	98	39	10	-
6	Cohesionless (SM)	4	113	43	30	-
10	Caliche	4	140	40	-	-
12	Cohesionless (SM) ^{PCM}	4	116	42	35	-
14	Caliche	4	140	40	-	-
16	Cohesionless (SM)	4	140	44	50	-
18.25	Caliche	4	140	40	-	-
20	Cohesionless (SM)	4	137	40	20	-
29.5	Cohesionless (SM)	4	117	44	50	-
31	Cohesive	4	131	-	35	5145
36	Cohesionless (SM)	4	140	44	50	-
36.5	Caliche	4	140	40	-	-
40	Cohesionless (SM)	4	127	43	35	-
45	Caliche	4	140	40	-	-
45.5	Cohesionless (SM) ^{PCM}	4	140	44	50	-
46	Cohesive ^{PCM}	4	131	-	50	6173
48	Cohesionless (SM)	4	138	44	50	-
51	Cohesive	4	131	-	50	5969
51.5	Caliche	4	140	40	-	-
59	Cohesive	4	131	-	30	3421
61	Cohesionless (SM)	4	100	43	50	-
62	Cohesive ^{PCM}	4	131	-	35	3840
63	Caliche	4	140	40	-	-
71	Cohesive	4	131	-	30	3170
72	Caliche	4	140	40	-	-
75	Cohesive	4	131	-	30	3043
76	Caliche	4	140	40	-	-
90	Cohesive	4	113	-	26	2523
93	Cohesionless (SM)	4	119	41	30	-
95.4	Caliche	4	140	40	-	-
100	Cohesionless (SM)	4	118	41	30	-
108	Cohesive	4	130	-	18	1597

*APPENDIX C. INTERPRETED STRATIGRAPHY AND GEOMATERIAL
PROPERTIES*

109	Cohesionless (SM)	4	112	38	15	-
111.75	Caliche	4	140	40	-	-

APPENDIX C. INTERPRETED STRATIGRAPHY AND GEOMATERIAL
PROPERTIES

Table C.24: Assumed stratigraphy and material properties for data number 24 (water table depth = 24 ft).

Bottom Layer Depth (ft)	Soil Type	B (ft)	γ (pcf)	ϕ°	N_{SPT}	s_u (psf)
10	Cohesionless (SM)	3.5	138	30	25	-
13	Cohesive	3.5	111	-	22	2426
18	Cohesive	3.5	130	-	50	6169
23	Cohesionless (SP)	3.5	138	44	50	-
24	Caliche	3.5	140	40	-	-
41.5	Caliche	3.5	140	40	-	-
48	Cohesive	3.5	113	29	29	3256
49	Caliche	3.5	140	40	-	-
50	Cohesive	3.5	131	-	20	2182
54.5	Caliche	3.5	140	40	-	-
60	Cohesive	3.5	132	-	50	5166
65.5	Cohesive	3.5	130	-	30	3000
68	Cohesionless (SM)	3.5	129	37	13	-
77	Caliche	3.5	140	40	-	-
81.5	Cohesive	3.5	122	-	12	1096
84.5	Caliche	3.5	140	40	-	-
85.5	Cohesive	3.5	131	-	50	4442
91	Caliche	3.5	140	40	-	-
99.5	Cohesive	3.5	130	-	50	4236
100.5	Caliche	3.5	140	40	-	-
102	Cohesive	3.5	126	-	15	1240
107	Caliche	3.5	140	40	-	-
110	Cohesionless (SM)	3.5	128	37	16	-

APPENDIX C. INTERPRETED STRATIGRAPHY AND GEOMATERIAL
PROPERTIES

Table C.25: Assumed stratigraphy and material properties for data number 25 (water table depth = 30 ft).

Bottom Layer Depth (ft)	Soil Type	B (ft)	γ (pcf)	ϕ°	N_{SPT}	s_u (psf)
8	Cohesionless (SP)	4	117	43	25	-
9	Caliche	4	140	40	-	-
12.5	Cohesive	4	125	-	27	3254
15	Cohesive	4	107	-	9	1235
18	Caliche	4	140	40	-	-
25	Cohesive	4	111	-	50	6836
30	Cohesive	4	123	-	7	850
31.5	Cohesive	4	118	-	5	639
38	Cohesive	4	128	-	12	1129
43	Cohesive	4	119	-	6	710
48.5	Cohesive	4	125	-	10	1142
53	Cohesive	4	106	-	1	111
60	Cohesive	4	131	-	27	2896
65	Cohesive	4	131	-	50	5161
70	Cohesive	4	131	-	27	2705
75	Cohesive	4	127	-	14	1365
80	Cohesive	4	131	-	47	4464
85	Cohesive	4	122	-	10	928
90	Cohesive	4	129	-	17	1542

APPENDIX C. INTERPRETED STRATIGRAPHY AND GEOMATERIAL
PROPERTIES

Table C.26: Assumed stratigraphy and material properties for data number 26 (water table depth = 28 ft).

Bottom Layer Depth (ft)	Soil Type	B (ft)	γ (pcf)	ϕ°	N_{SPT}	s_u (psf)
5	Cohesive	4	111	-	15	2828
6.5	Cohesive	4	111	-	50	8582
8	Caliche	4	140	40	-	-
10	Cohesionless (SM)	4	100	40	20	-
12.5	Cohesive	4	104	-	8	977
16	Cohesive ^{PCM}	4	111	-	50	6993
17	Caliche	4	140	40	-	-
20	Cohesive	4	111	-	50	6097
25	Cohesive	4	111	-	24	3319
28	Cohesive	4	102	-	6	767
30	Cohesive	4	120	-	6	741
35	Cohesionless (SM)	4	116	39	14	-
40	Cohesive	4	125	-	9	1148
45	Cohesive	4	118	-	7	859
55	Cohesive	4	114	-	11	1286
60	Cohesive	4	117	-	22	2463
65	Cohesive	4	124	-	10	1087
70	Cohesive	4	121	-	8	845
75	Cohesive	4	119	-	7	720
77	Cohesive	4	131	-	27	2726
85.5	Cohesionless (SM)	4	123	42	38	-
90.5	Cohesive	4	131	-	21	1995

APPENDIX C. INTERPRETED STRATIGRAPHY AND GEOMATERIAL
PROPERTIES

Table C.27: Assumed stratigraphy and material properties for data number 27 (water table depth = 62 ft).

Bottom Layer Depth (ft)	Soil Type	B (ft)	γ (pcf)	ϕ°	N_{SPT}	s_u (psf)
4.5	Cohesive	5	111	-	24	4525
14	Cohesive	5	111	-	30	4601
16.8	Cohesionless (SM)	5	109	43	36	-
19	Cohesionless (GP)	5	119	44	50	-
21.5	Cohesionless (SM)	5	140	44	50	-
23.8	Cohesionless (GP)	5	129	44	49	-
24.5	Cohesive	5	111	-	50	6566
26	Cohesionless (SM)	5	106	42	32	-
27.5	Cohesive	5	111	-	35	4382
30	Cohesionless (SM)	5	116	44	50	-
33	Cohesive	5	111	-	50	6340
34.5	Cohesive	5	111	-	38	4704
37	Cohesive	5	111	-	20	2408
39	Cohesive	5	111	-	45	5260
40.5	Cohesionless (GP)	5	104	42	31	-
42	Cohesive	5	111	-	50	5623
43.5	Cohesive	5	111	-	45	4973
48	Cohesive	5	111	-	35	3742
49.5	Cohesionless (GP)	5	102	41	31	-
51	Cohesive	5	111	-	44	4499
52.5	Cohesionless (GP)	5	99	39	20	-
54	Cohesionless (GP)	5	108	43	45	-
57	Cohesionless (GP)	5	109	43	50	-
62	Caliche	5	140	40	-	-
66	Cohesive	5	131	-	35	3170
69	Cohesive	5	125	-	13	1159
72	Cohesive	5	131	-	50	4401
76	Cohesive	5	131	-	26	2254
78.5	Cohesive	5	130	-	19	1624
81	Cohesive	5	131	-	50	4230
91	Cohesive	5	131	-	50	4125
93	Cohesive	5	131	-	36	2902

*APPENDIX C. INTERPRETED STRATIGRAPHY AND GEOMATERIAL
PROPERTIES*

100	Cohesive	5	131	-	50	3965
-----	----------	---	-----	---	----	------

APPENDIX C. INTERPRETED STRATIGRAPHY AND GEOMATERIAL
PROPERTIES

Table C.28: Assumed stratigraphy and material properties for data number 28 (water table depth = 81.2 ft).

Bottom Layer Depth (ft)	Soil Type	B (ft)	γ (pcf)	ϕ°	N_{SPT}	s_u (psf)
4.5	Cohesive	5	111	-	24	4525
14	Cohesive	5	111	-	30	4601
16.8	Cohesionless (SM)	5	109	43	36	-
19	Cohesionless (GP)	5	119	44	50	-
21.5	Cohesionless (SM)	5	140	44	50	-
23.8	Cohesionless (GP)	5	129	44	49	-
24.5	Cohesive	5	111	-	50	6566
26	Cohesionless (SM)	5	106	42	32	-
27.5	Cohesive	5	111	-	35	4382
30	Cohesionless (SM)	5	116	44	50	-
33	Cohesive	5	111	-	50	6340
34.5	Cohesive	5	111	-	38	4704
37	Cohesive	5	111	-	20	2408
39	Cohesive	5	111	-	45	5260
40.5	Cohesionless (GP)	5	104	42	31	-
42	Cohesive	5	111	-	50	5623
43.5	Cohesive	5	111	-	45	4973
48	Cohesive	5	111	-	35	3742
49.5	Cohesionless (GP)	5	102	41	31	-
51	Cohesive	5	111	-	44	4499
52.5	Cohesionless (GP)	5	99	39	20	-
54	Cohesionless (GP)	5	108	43	45	-
57	Cohesionless (GP)	5	109	43	50	-
62	Caliche	5	140	40	-	-
66	Cohesive	5	131	-	35	3170
69	Cohesive	5	125	-	13	1159
72	Cohesive	5	131	-	50	4401
76	Cohesive	5	131	-	26	2254
78.5	Cohesive	5	130	-	19	1624
81	Cohesive	5	131	-	50	4230
91	Cohesive	5	131	-	50	4125
93	Cohesive	5	131	-	36	2902

*APPENDIX C. INTERPRETED STRATIGRAPHY AND GEOMATERIAL
PROPERTIES*

100	Cohesive	5	131	-	50	3965
-----	----------	---	-----	---	----	------

APPENDIX C. INTERPRETED STRATIGRAPHY AND GEOMATERIAL
PROPERTIES

Table C.29: Assumed stratigraphy and material properties for data number 29 (water table depth = 18 ft).

Bottom Layer Depth (ft)	Soil Type	B (ft)	γ (pcf)	ϕ°	N_{SPT}	s_u (psf)
8	Cohesive	4	130	-	-	5000
10	Cohesionless (SM)	4	130	39	35	-
11	Caliche	4	140	40	-	-
13	Cohesionless (SM)	4	105	42	35	-
14.5	Caliche	4	140	40	-	-
17	Cohesionless (GP)	4	109	43	40	-
18	Cohesive	4	111	-	35	4167
41	Cohesive	4	131	-	35	4656
42	Caliche	4	140	40	-	-
46	Cohesionless (SM) ^{PCM}	4	128	43	40	-
52	Cohesive	4	131	-	40	4666
56	Caliche	4	140	40	-	-
58	Cohesionless (SM)	4	129	43	45	-
60	Cohesive	4	131	-	40	4324
64.5	Cohesive	4	131	-	40	4232
68.5	Caliche	4	140	40	-	-
70	Cohesive	4	131	-	40	4040

APPENDIX C. INTERPRETED STRATIGRAPHY AND GEOMATERIAL
PROPERTIES

Table C.30: Assumed stratigraphy and material properties for data number 30 (water table depth = 48.1 ft).

Bottom Layer Depth (ft)	Soil Type	B (ft)	γ (pcf)	ϕ°	N_{SPT}	s_u (psf)
15	Cohesionless (SP)	4	133	44	40	-
18.5	Cohesionless (SM)	4	125	42	30	-
20	Cohesive	4	111	-	20	2332
22.5	Cohesionless (SM)	4	109	36	11	-
25.5	Cohesive	4	130	-	20	2638
28	Cohesionless (GP)	4	114	44	46	-
29	Cohesionless (SM)	4	102	41	25	-
32.5	Cohesive	4	100	-	27	3534
33.5	Caliche	4	140	40	-	-
36.5	Cohesionless (GP)	4	112	42	32	-
37	Caliche	4	140	40	-	-
39	Cohesive	4	111	-	50	5931
40	Cohesionless (SM)	4	114	44	50	-
41.5	Cohesive ^{PCM}	4	111	-	50	5744
42.5	Caliche	4	140	40	-	-
48.1	Cohesive	4	124	-	31	3373
53	Cohesionless (SM)	4	114	38	14	-
59	Cohesive	4	104	-	30	3069
64	Cohesive	4	131	-	20	1999
64.5	Caliche	4	140	40	-	-
68	Cohesionless (SM)	4	130	43	50	-
72	Cohesive	4	131	-	20	1916
74	Cohesionless (SM)	4	123	42	40	-
76.5	Cohesive	4	125	-	26	4234
81	Cohesive	4	131	-	40	3688
82.5	Caliche	4	140	40	-	-
86.5	Cohesionless (SM)	4	129	43	50	-
92	Cohesionless (SM)	4	124	42	44	-
98	Cohesive	4	121	-	32	2767
100	Cohesionless (GP)	4	123	42	45	-
102.5	Cohesive ^{PCM}	4	131	-	50	4232
108	Cohesive ^{PCM}	4	131	-	50	4170

*APPENDIX C. INTERPRETED STRATIGRAPHY AND GEOMATERIAL
PROPERTIES*

114	Cohesive	4	131	-	23	1879
115.5	Cohesionless (SM)	4	114	38	20	-

APPENDIX C. INTERPRETED STRATIGRAPHY AND GEOMATERIAL
PROPERTIES

Table C.31: Assumed stratigraphy and material properties for data number 31 (water table depth = 5 ft).

Bottom Layer Depth (ft)	Soil Type	B (ft)	γ (pcf)	ϕ°	N_{SPT}	s_u (psf)
14.3	Cohesionless (SP)	6	133	44	40	-
18.5	Cohesionless (SM)	6	125	42	30	-
20	Cohesive	6	111	-	20	2332
22.5	Cohesionless (SM)	6	109	36	11	-
25.5	Cohesive	6	130	-	20	2638
28	Cohesionless (GP)	6	114	44	46	-
29	Cohesionless (SM)	6	102	41	25	-
32.5	Cohesive	6	100	-	27	3534
33.5	Caliche	6	140	40	-	-
36.5	Cohesionless (GP)	6	112	42	32	-
37	Caliche	6	140	40	-	-
39	Cohesive	6	111	-	50	5931
40	Cohesionless (SM)	6	114	44	50	-
41.5	Cohesive ^{PCM}	6	111	-	50	5744
42.5	Caliche	6	140	40	-	-
48.1	Cohesive	6	124	-	31	3373
53	Cohesionless (SM)	6	114	38	14	-
59	Cohesive	6	104	-	30	3069
64	Cohesive	6	131	-	20	1999
64.5	Caliche	6	140	40	-	-
68	Cohesionless (SM)	6	130	43	50	-
72	Cohesive	6	131	-	20	1916
74	Cohesionless (SM)	6	123	42	40	-
76.5	Cohesive	6	125	-	26	4234
81	Cohesive	6	131	-	40	3688
82.5	Caliche	6	140	40	-	-
86.5	Cohesionless (SM)	6	129	43	50	-
92	Cohesionless (SM)	6	124	42	44	-
98	Cohesive	6	121	-	32	2767
100	Cohesionless (GP)	6	123	42	45	-
102.5	Cohesive	6	131	-	50	4232
108	Cohesive	6	131	-	50	4170

*APPENDIX C. INTERPRETED STRATIGRAPHY AND GEOMATERIAL
PROPERTIES*

114	Cohesive	6	131	-	23	1879
117	Cohesionless (SM)	6	114	38	20	-
123	Cohesive	6	131	-	50	4712
127	Cohesive	6	131	-	50	4606

APPENDIX C. INTERPRETED STRATIGRAPHY AND GEOMATERIAL
PROPERTIES

Table C.32: Assumed stratigraphy and material properties for data number 32 (water table depth = 19 ft).

Bottom Layer Depth (ft)	Soil Type	B (ft)	γ (pcf)	ϕ°	N_{SPT}	s_u (psf)
3	Cohesionless (SM)	3.75	106	42	21	-
7.5	Cohesive	3.75	111	-	34	6187
9.67	Cohesionless (SM)	3.75	108	43	33	-
13.5	Cohesionless (SM)	3.75	108	43	33	-
16	Cohesionless (SP)	3.75	140	44	50	-
17.5	Cohesive	3.75	111	-	45	5752
19	Cohesionless (SP)	3.75	126	44	50	-
24.5	Cohesionless (GP) ^{PCM}	3.75	140	44	50	-
27	Caliche	3.75	140	40	-	-
28	Cohesive	3.75	131	-	40	5235
29	Caliche	3.75	140	40	-	-
31	Cohesive	3.75	131	-	29	3873
33.5	Caliche	3.75	140	40	-	-
38	Cohesionless (SM)	3.75	123	42	29	-
42.5	Cohesionless (SM)	3.75	121	41	27	-
50	Cohesive	3.75	131	-	50	6047
51.5	Caliche	3.75	140	40	-	-
60	Cohesive	3.75	131	-	50	5605
63	Cohesive	3.75	131	-	19	2046
69.5	Cohesive	3.75	131	-	14	1462
71	Caliche	3.75	140	40	-	-
74	Cohesive	3.75	131	-	30	3013
76	Cohesionless (GP)	3.75	129	43	50	-
76.5	Caliche	3.75	140	40	-	-
85	Cohesive	3.75	130	-	28	2687
88.5	Cohesive	3.75	131	-	20	1861
89.5	Caliche	3.75	140	40	-	-
92.5	Cohesionless (GP)	3.75	126	42	48	-
98	Cohesive	3.75	131	-	46	4112
105	Cohesive	3.75	131	-	50	4346
106.5	Cohesive	3.75	129	-	18	1536
108.5	Caliche	3.75	140	40	-	-

*APPENDIX C. INTERPRETED STRATIGRAPHY AND GEOMATERIAL
PROPERTIES*

110.5	Cohesive	3.75	131	-	50	4198
111.5	Caliche	3.75	140	40	-	-
113.5	Cohesive	3.75	131	-	50	4146
114	Caliche	3.75	140	40	-	-

APPENDIX C. INTERPRETED STRATIGRAPHY AND GEOMATERIAL
PROPERTIES

Table C.33: Assumed stratigraphy and material properties for data number 33 (water table depth = 20 ft).

Bottom Layer Depth (ft)	Soil Type	B (ft)	γ (pcf)	ϕ°	N_{SPT}	s_u (psf)
2	Cohesionless (SP)	3.5	136	44	35	-
6	Cohesionless (SM)	3.5	140	45	50	-
10	Cohesionless (SP)	3.5	134	44	50	-
12	Cohesionless (SP)	3.5	121	43	50	-
20	Cohesionless (SM)	3.5	116	44	50	-
25	Cohesionless (SM)	3.5	140	44	50	-
27.5	Cohesive	3.5	131	-	35	4437
30	Cohesionless (SP)	3.5	140	44	50	-
39	Cohesionless (SM) ^{PCM}	3.5	135	39	50	-
45	Cohesive	3.5	131	-	33	3949
49.5	Caliche	3.5	130	40	-	-
56	Cohesive	3.5	131	-	50	5515
61	Cohesive	3.5	131	-	37	3296
66	Cohesive	3.5	131	-	30	3085
71	Cohesive	3.5	131	-	27	2695
76.5	Cohesive	3.5	131	-	32	3102
77	Cohesionless (SP)	3.5	138	43	50	-
80	Cohesive	3.5	131	-	45	4253

APPENDIX C. INTERPRETED STRATIGRAPHY AND GEOMATERIAL
PROPERTIES

Table C.34: Assumed stratigraphy and material properties for data number 34 (water table depth = 20 ft).

Bottom Layer Depth (ft)	Soil Type	B (ft)	γ (pcf)	ϕ°	N_{SPT}	s_u (psf)
3.5	Cohesionless (SP)	3.5	152	45	50	-
8.5	Cohesionless (SM)	3.5	105	42	25	-
11	Caliche	3.5	140	40	-	-
13	Cohesive	3.5	111	-	25	2822
15	Cohesionless (SM)	3.5	137	43	41	-
19	Cohesionless (SM)	3.5	137	43	41	-
21	Caliche	3.5	140	40	-	-
24	Cohesive	3.5	131	-	30	4009
30	Cohesive	3.5	120	-	41	5221
35	Cohesive	3.5	126	-	33	4417
40	Cohesionless (SM)	3.5	117	42	28	-
41.5	Caliche	3.5	140	40	-	-
48	Cohesive	3.5	123	-	49	5927
53	Cohesive	3.5	129	-	50	5794
60	Cohesive	3.5	130	-	43	4770
61	Cohesive	3.5	123	-	19	2052
66.5	Caliche	3.5	140	40	-	-
74	Cohesive	3.5	131	-	50	5057
84.5	Cohesive	3.5	131	-	50	4808
86	Cohesionless (SM)	3.5	116	38	16	-
90	Cohesive	3.5	131	-	25	2303
91	Cohesionless (SM)	3.5	125	42	40	-
97	Caliche	3.5	140	40	-	-
98.5	Cohesive	3.5	131	-	45	3948
101	Caliche	3.5	140	40	-	-
103	Cohesive	3.5	131	-	45	3870
105	Caliche	3.5	140	40	-	-

APPENDIX C. INTERPRETED STRATIGRAPHY AND GEOMATERIAL
PROPERTIES

Table C.35: Assumed stratigraphy and material properties for data number 35 (water table depth = 15.5 ft).

Bottom Layer Depth (ft)	Soil Type	B (ft)	γ (pcf)	ϕ°	N_{SPT}	s_u (psf)
1	Cohesionless (GP)	3.5	105	42	20	-
8	Cohesionless (SP)	3.5	127	43	26	-
15	Cohesionless (GP) ^{PCM}	3.5	135	44	50	-
15.5	Cohesionless (GP) ^{PCM}	3.5	135	44	50	-
17	Cohesionless (GP) ^{PCM}	3.5	135	44	50	-
24	Caliche	3.5	140	45	50	230000
27	Cohesionless (SM)	3.5	118	36	19	-
37	Cohesive	3.5	142	-	50	6789
43	Cohesive	3.5	123	-	11	1375
46	Caliche	3.5	140	45	50	230000
48.5	Cohesive	3.5	131	-	16	1880
67	Cohesionless (SM)	3.5	138	36	50	-
75	Cohesionless (SM)	3.5	121	41	33	-
90	Cohesionless (SM)	3.5	128	43	50	-

APPENDIX C. INTERPRETED STRATIGRAPHY AND GEOMATERIAL
PROPERTIES

Table C.36: Assumed stratigraphy and material properties for data number 36 (water table depth = 17.5 ft).

Bottom Layer Depth (ft)	Soil Type	B (ft)	γ (pcf)	ϕ°	N_{SPT}	s_u (psf)
1	Cohesionless (SM)	3.5	120	40	35	-
5	Cohesionless (SM)	3.5	133	4	15	-
10	Cohesive	3.5	129	-	8	1111
12.5	Cohesive	3.5	126	-	13	1478
17.5	Cohesionless (SM)	3.5	135	43	41	-
19	Cohesionless (SM)	3.5	135	43	41	-
23	Cohesionless (SP)	3.5	140	44	50	-
30	Caliche	3.5	140	40	-	-
33.5	Cohesionless (SM)	3.5	148	44	50	-
34.5	Caliche	3.5	140	40	-	-
35.5	Cohesive	3.5	131	-	50	6422
39	Caliche	3.5	140	40	-	-
42.5	Cohesive	3.5	131	-	40	4894
47.5	Cohesionless (SM)	3.5	136	39	14	-
52.5	Cohesionless (GP)	3.5	118	41	24	-
56	Cohesionless (SM)	3.5	146	43	50	-
59	Caliche	3.5	140	40	-	-
70	Cohesive	3.5	127	-	13	1337
72.5	Cohesive	3.5	122	-	9	892
76	Cohesionless (SM)	3.5	131	38	50	-
77.5	Caliche	3.5	140	40	-	-
83	Cohesionless (SM)	3.5	117	40	24	-
86	Cohesionless (SM)	3.5	123	42	40	-
87	Caliche	3.5	140	40	-	-
94	Cohesive	3.5	114	-	31	2813
95.5	Caliche	3.5	140	40	-	-
99	Cohesive	3.5	131	-	40	3529
101	Caliche	3.5	140	40	-	-
104.5	Cohesive	3.5	131	-	40	3441
115.5	Caliche	3.5	140	40	-	-

APPENDIX C. INTERPRETED STRATIGRAPHY AND GEOMATERIAL
PROPERTIES

Table C.37: Assumed stratigraphy and material properties for data number 37 (water table depth = 20 ft).

Bottom Layer Depth (ft)	Soil Type	B (ft)	γ (pcf)	ϕ°	N_{SPT}	s_u (psf)
6	Cohesionless (GP)	3.5	127	44	35	-
9	Cohesionless (SM)	3.5	109	43	35	-
14.5	Cohesionless (SM)	3.5	108	43	35	-
17	Caliche	3.5	140	40	-	-
20	Cohesive	3.5	11	-	35	4306
21.5	Cohesive	3.5	131	-	35	5292
28	Caliche	3.5	140	40	-	-
35	Cohesionless (GP)	3.5	140	44	45	-
40	Cohesive	3.5	131	-	35	4635
121	Cohesive	3.5	131	-	35	3389

APPENDIX C. INTERPRETED STRATIGRAPHY AND GEOMATERIAL
PROPERTIES

Table C.38: Assumed stratigraphy and material properties for data number 38 (water table depth = 15 ft).

Bottom Layer Depth (ft)	Soil Type	B (ft)	γ (pcf)	ϕ°	N_{SPT}	s_u (psf)
1.5	Cohesionless (GP)	5	127	44	35	-
3	Cohesionless (SM)	5	119	41	17	-
5	Cohesive	5	111	-	50	9426
6.5	Caliche	5	140	40	-	-
12.5	Cohesive	5	111	-	29	3734
15	Cohesionless (SM)	5	102	41	22	-
17	Cohesionless (SM)	5	119	41	22	-
26	Cohesionless (SM)	5	138	44	45	6079
28.5	Cohesionless (SP) ^{PCM}	5	140	44	50	-
35	Cohesionless (SM)	5	120	44	50	-
36.5	Cohesionless (SP)	5	140	44	50	-
40	Cohesionless (SM)	5	126	42	33	-
42.5	Cohesive	5	131	-	33	4295
49	Cohesionless (SM)	5	134	44	46	-
52	Cohesionless (SM)	5	136	44	50	-
58	Cohesionless (SM)	5	122	41	30	-
116	Cohesionless (SM)	5	123	42	40	-

APPENDIX C. INTERPRETED STRATIGRAPHY AND GEOMATERIAL
PROPERTIES

Table C.39: Assumed stratigraphy and material properties for data number 39 (water table depth = 80.5 ft).

Bottom Layer Depth (ft)	Soil Type	B (ft)	γ (pcf)	ϕ°	N_{SPT}	s_u (psf)
15	Cohesionless (SP)	4	133	44	40	-
18.5	Cohesionless (SM)	4	125	42	30	-
20	Cohesive	4	111	-	20	2332
22.5	Cohesionless (SM)	4	109	36	11	-
25.5	Cohesive	4	130	-	20	2638
28	Cohesionless (GP)	4	114	44	46	-
29	Cohesionless (SM)	4	102	41	25	-
32.5	Cohesive	4	100	-	27	3534
33.5	Caliche	4	140	40	-	-
36.5	Cohesionless (GP)	4	112	42	32	-
37	Caliche	4	140	40	-	-
39	Cohesive	4	111	-	50	5931
40	Cohesionless (SM)	4	114	44	50	-
41.5	Cohesive ^{PCM}	4	111	-	50	5744
42.5	Caliche	4	140	40	-	-
48.1	Cohesive	4	124	-	31	3373
53	Cohesionless (SM)	4	114	38	14	-
59	Cohesive	4	104	-	30	3069
64	Cohesive	4	131	-	20	1999
64.5	Caliche	4	140	40	-	-
68	Cohesionless (SM)	4	130	43	50	-
72	Cohesive	4	131	-	20	1916
74	Cohesionless (SM)	4	123	42	40	-
76.5	Cohesive	4	125	-	26	4234
81	Cohesive	4	131	-	40	3688
82.5	Caliche	4	140	40	-	-
86.5	Cohesionless (SM)	4	129	43	50	-
92	Cohesionless (SM)	4	124	42	44	-
98	Cohesive	4	121	-	32	2767
100	Cohesionless (GP)	4	123	42	45	-
102.5	Cohesive ^{PCM}	4	131	-	50	4232
108	Cohesive ^{PCM}	4	131	-	50	4170

*APPENDIX C. INTERPRETED STRATIGRAPHY AND GEOMATERIAL
PROPERTIES*

114	Cohesive	4	131	-	23	1879
117	Cohesionless (SM)	4	114	38	20	-
121.2	Cohesive	4	131	-	50	4712

APPENDIX C. INTERPRETED STRATIGRAPHY AND GEOMATERIAL
PROPERTIES

Table C.40: Assumed stratigraphy and material properties for data number 40 (water table depth = 16 ft).

Bottom Layer Depth (ft)	Soil Type	B (ft)	γ (pcf)	ϕ°	N_{SPT}	s_u (psf)
2	Cohesive	4	111.35	-	20	1250
8	Cohesive	4	133	-	31	4000
13	Cohesive	4	121	-	5	250
16	Cohesive	4	119	-	12	1250
17	Cohesive	4	116	-	12	1375
23	Cohesive	4	116	-	12	1375
27	Cohesive	4	113	-	5	250
33	Cohesive	4	113	-	14	1625
37	Cohesive	4	120	-	23	2375
42	Cohesive	4	117	-	28	3250
49	Cohesive ^{PCM}	4	122	-	50	5500
55	Cohesionless (SM)	4	124	42	30	-
60	Cohesionless (GP)	4	138	44	50	-
63	Cohesive	4	118	-	15	2625
68	Cohesive	4	131	-	21	2320
73	Cohesive	4	120	-	25	1850
80	Cohesive	4	134	-	50	1650
83.5	Cohesionless (GP)	4	126	43	50	-
84	Caliche	4	140	40	-	-

APPENDIX C. INTERPRETED STRATIGRAPHY AND GEOMATERIAL
PROPERTIES

Table C.41: Assumed stratigraphy and material properties for data number 41 (water table depth = 16 ft).

Bottom Layer Depth (ft)	Soil Type	B (ft)	γ (pcf)	ϕ°	N_{SPT}	s_u (psf)
2	Cohesive	3	111.35	-	20	1250
8	Cohesive	3	133	-	31	4000
13	Cohesive	3	121	-	5	250
16	Cohesive	3	119	-	12	1250
17	Cohesive	3	116	-	12	1375
23	Cohesive	3	116	-	12	1375
27	Cohesive	3	113	-	5	250
33	Cohesive	3	113	-	14	1625
37	Cohesive	3	120	-	23	2375
42	Cohesive	3	117	-	28	3250
49	Cohesive ^{PCM}	3	122	-	50	5500
55	Cohesionless (SM)	3	124	42	30	-
60	Cohesionless (GP)	3	138	44	50	-
63	Cohesive	3	118	-	15	2625
68	Cohesive	3	131	-	21	2320
73	Cohesive	3	120	-	25	1850
80	Cohesive	3	134	-	50	1650
82.5	Cohesionless (GP)	3	126	43	50	-
83	Caliche	3	140	40	-	-

Appendix D

Equivalent Top-Down Load-Settlement Curves

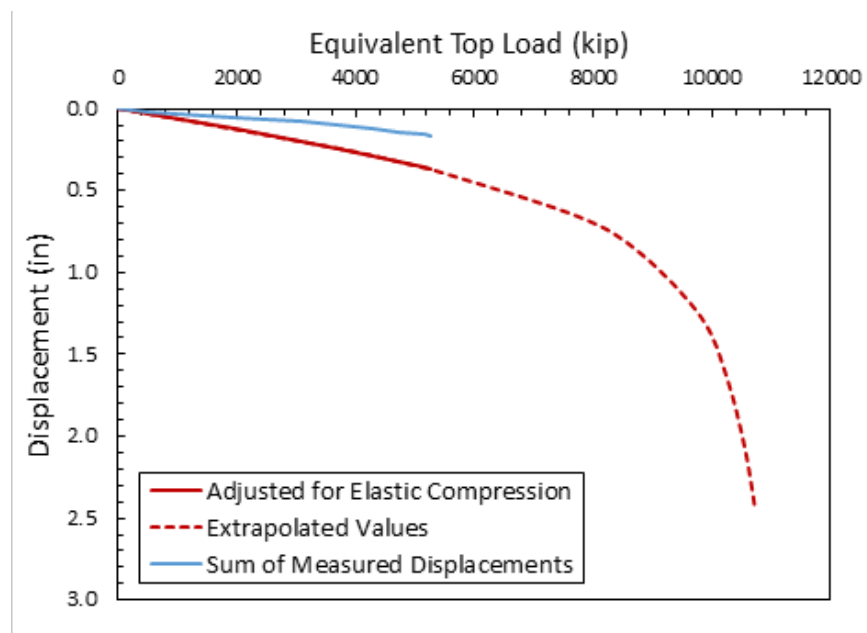


Figure D.1: Equivalent top-down load-settlement curve for data number 1

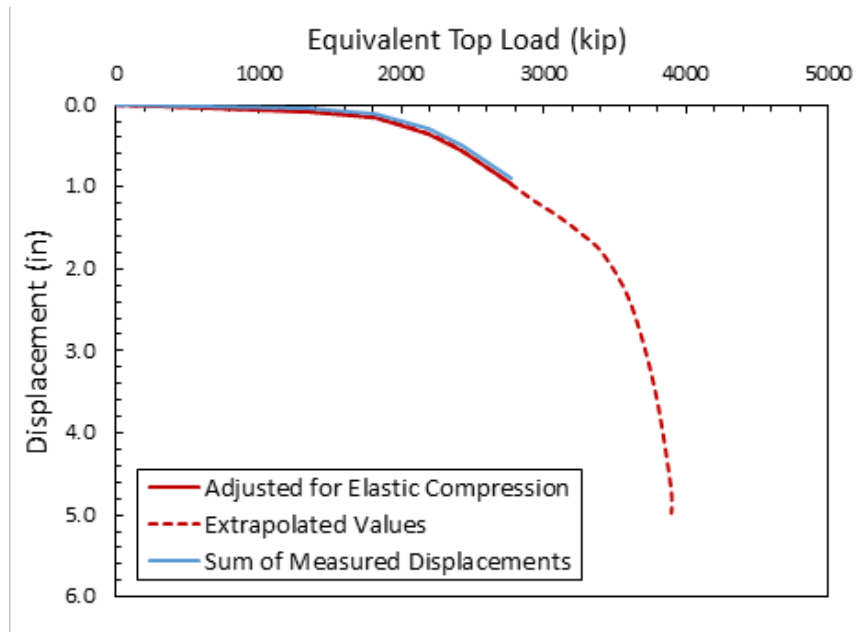


Figure D.2: Equivalent top-down load-settlement curve for data number 2

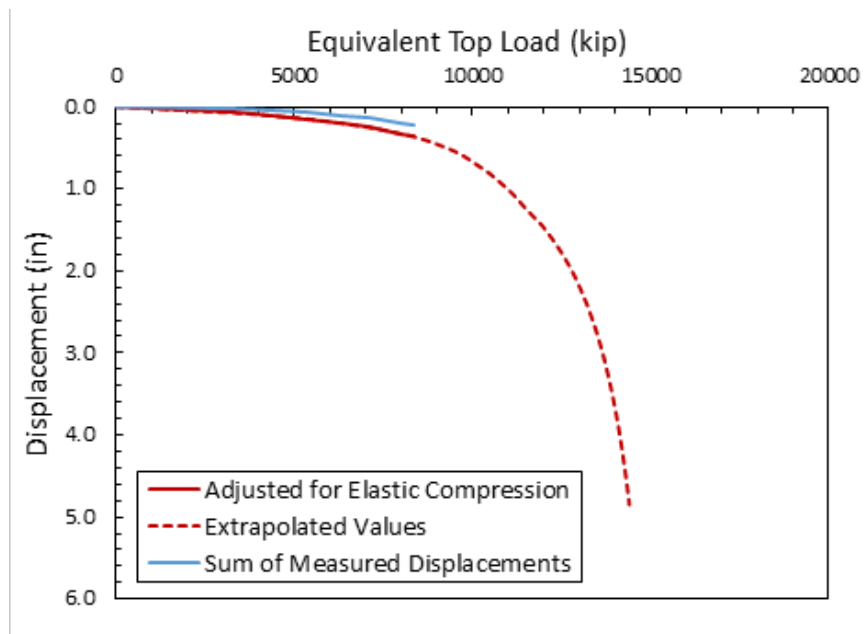


Figure D.3: Equivalent top-down load-settlement curve for data number 3

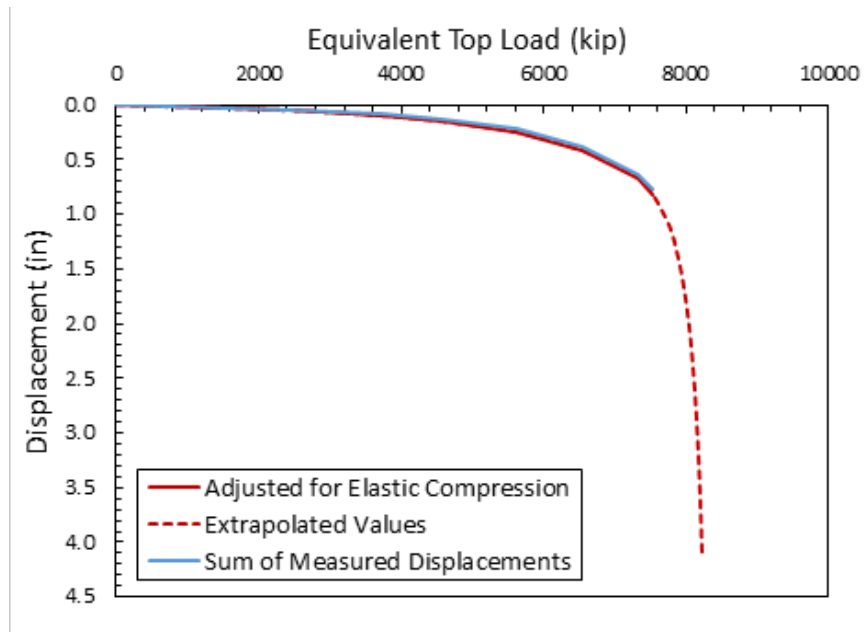


Figure D.4: Equivalent top-down load-settlement curve for data number 4

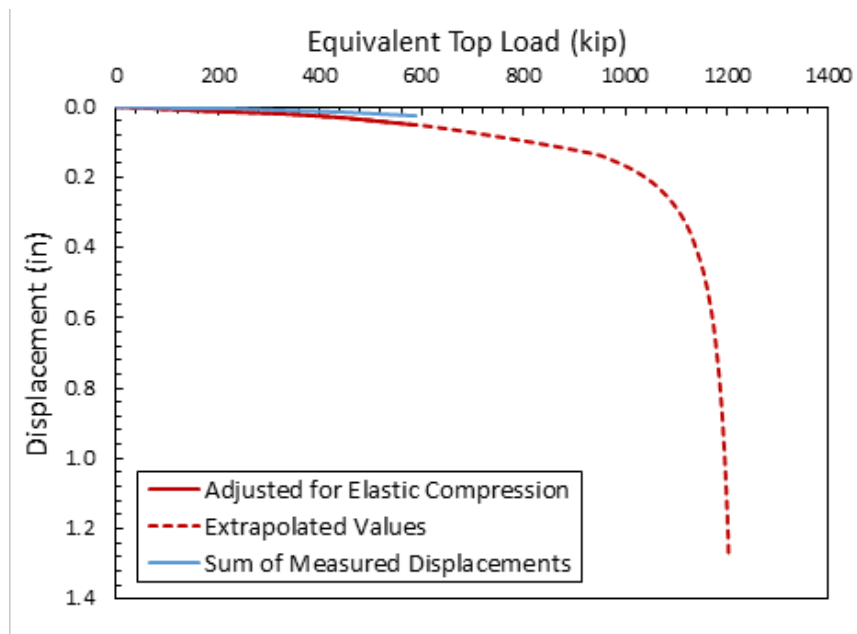


Figure D.5: Equivalent top-down load-settlement curve for data number 5

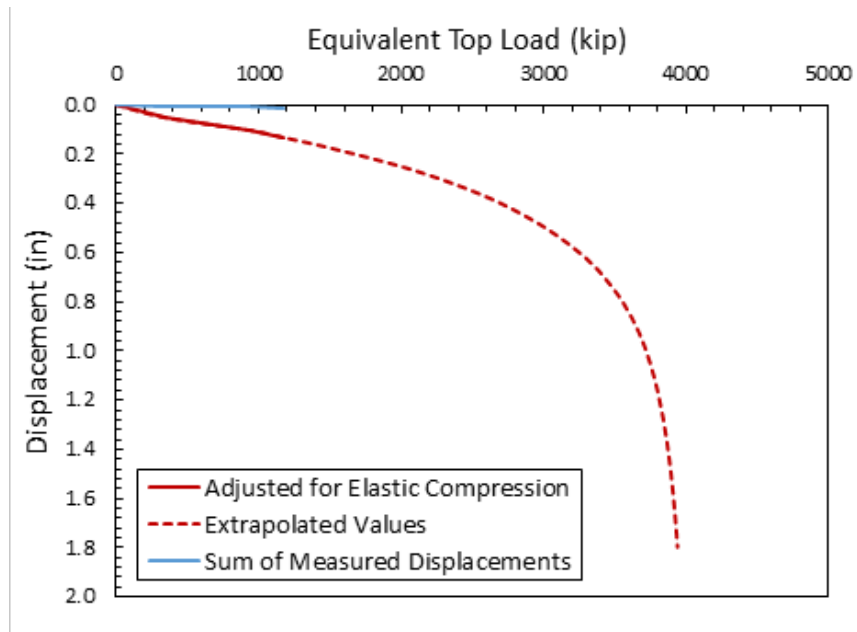


Figure D.6: Equivalent top-down load-settlement curve for data number 6

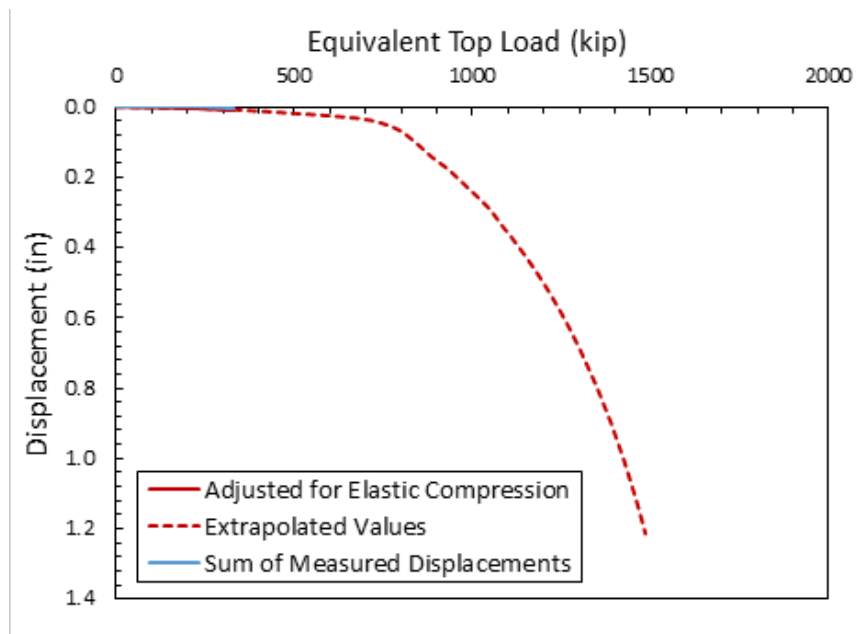


Figure D.7: Equivalent top-down load-settlement curve for data number 7

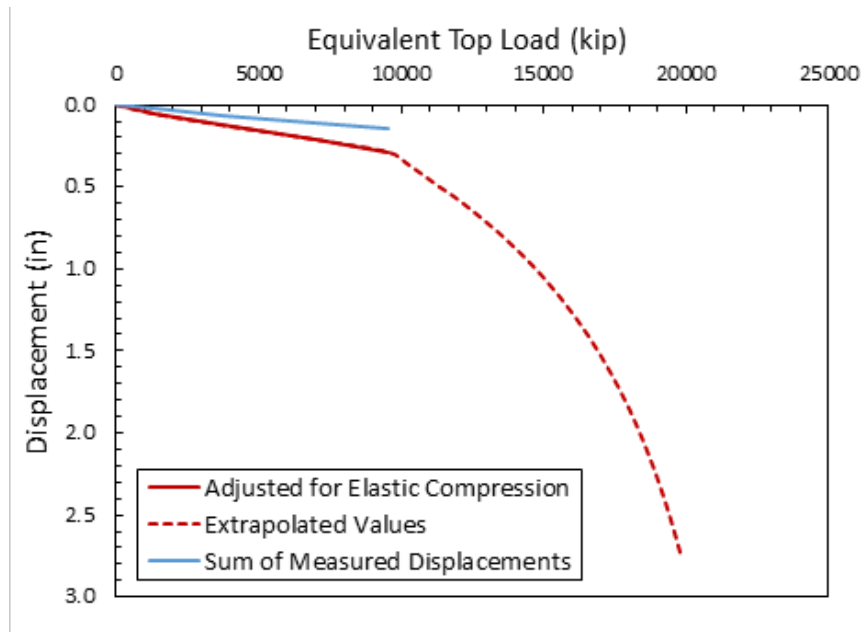


Figure D.8: Equivalent top-down load-settlement curve for data number 8

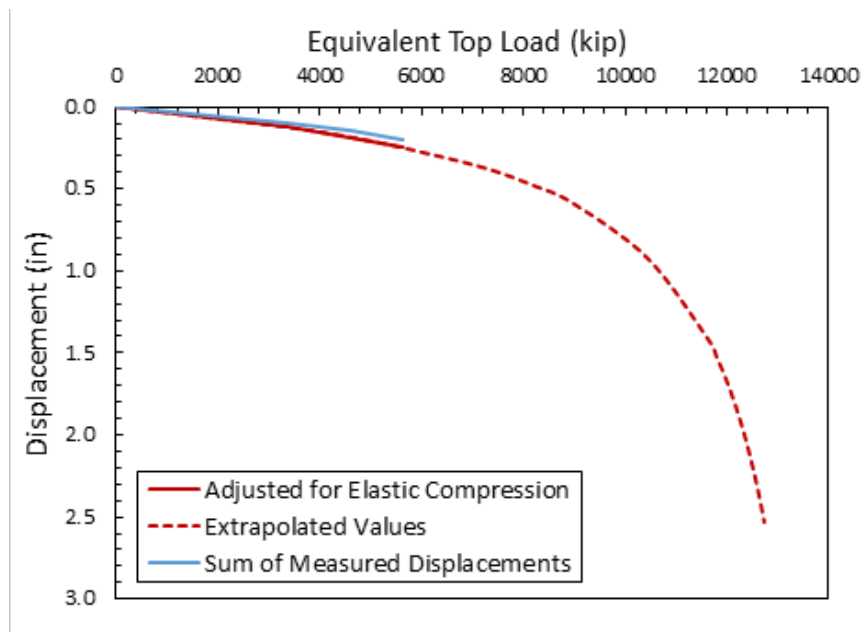


Figure D.9: Equivalent top-down load-settlement curve for data number 9

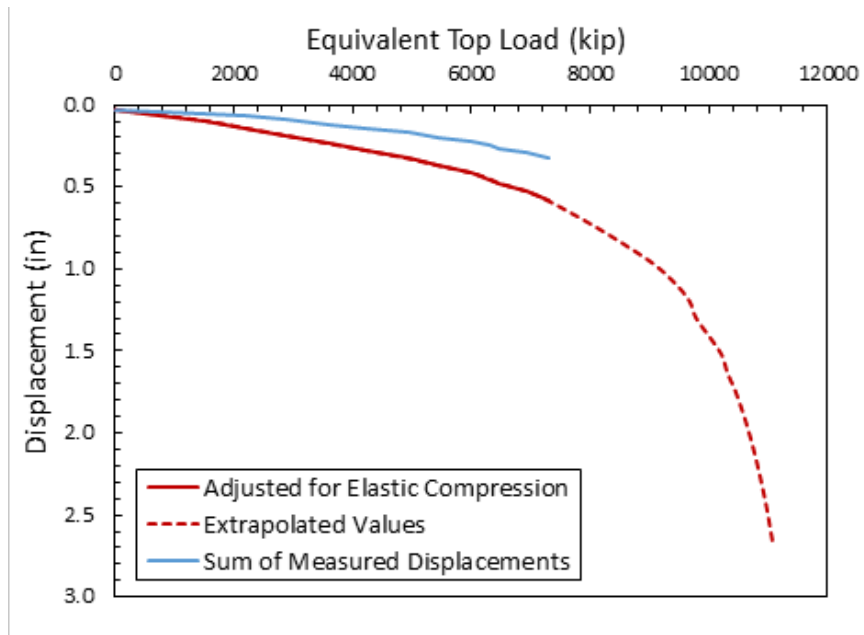


Figure D.10: Equivalent top-down load-settlement curve for data number 10

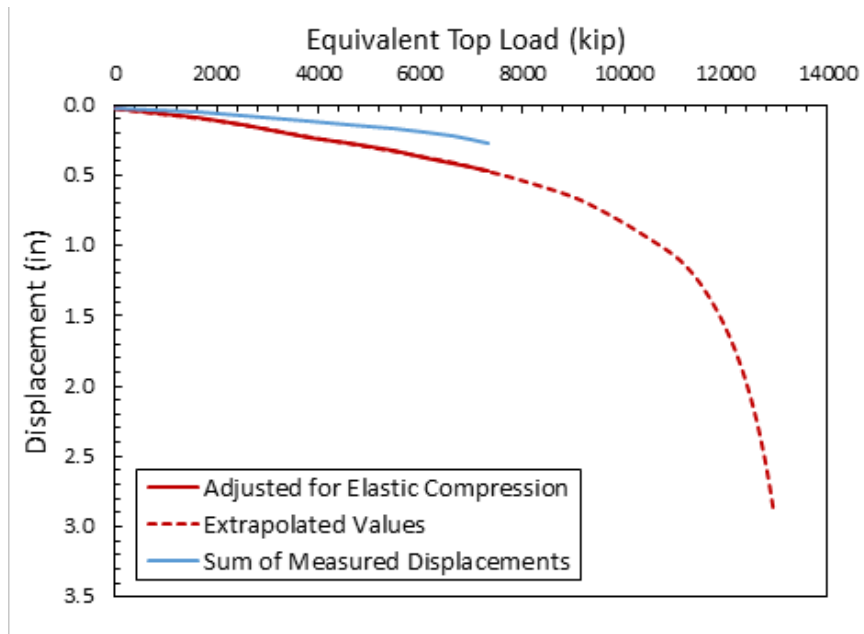


Figure D.11: Equivalent top-down load-settlement curve for data number 11

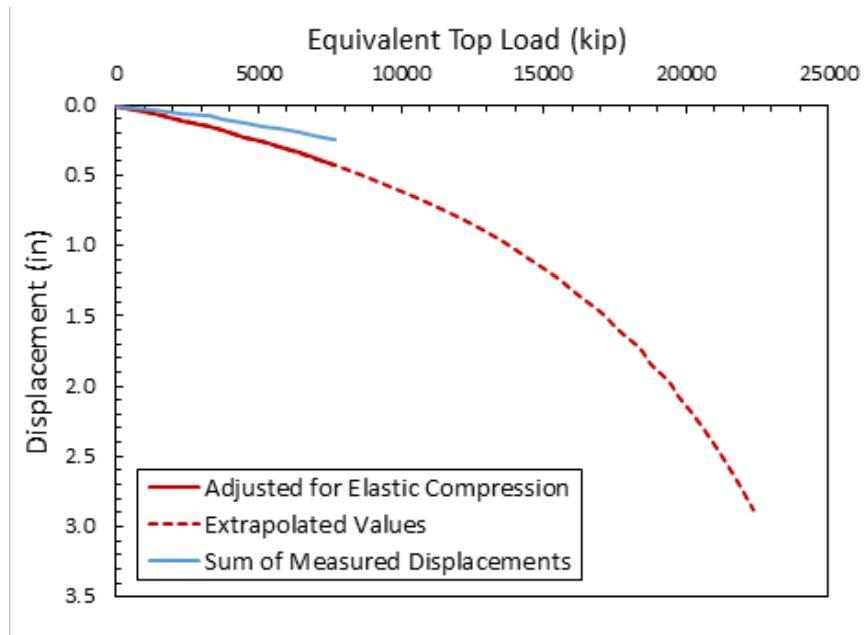


Figure D.12: Equivalent top-down load-settlement curve for data number 12

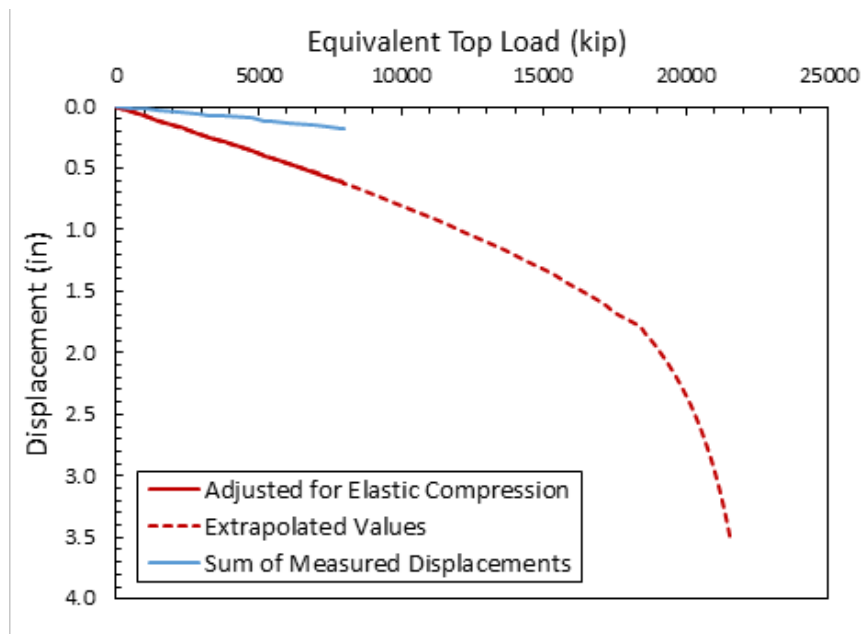


Figure D.13: Equivalent top-down load-settlement curve for data number 13

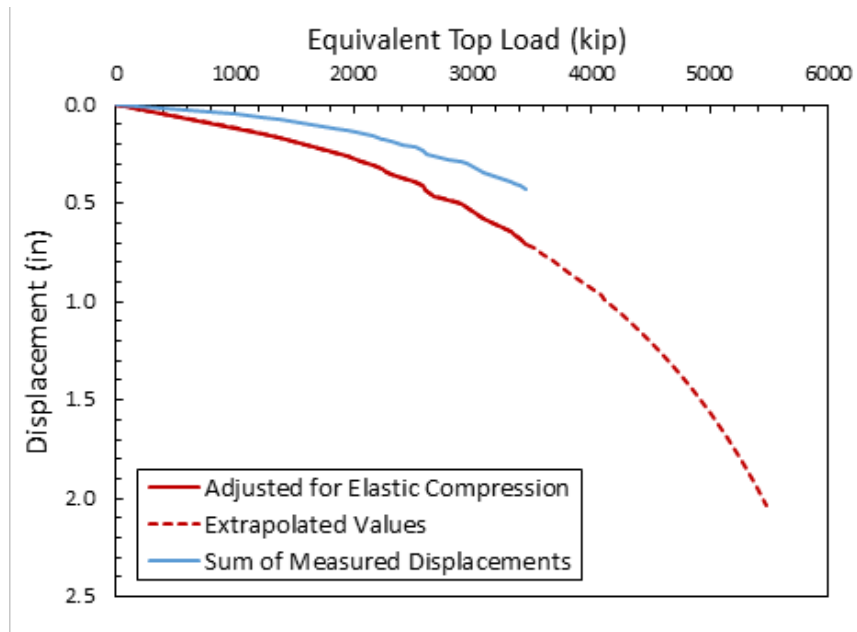


Figure D.14: Equivalent top-down load-settlement curve for data number 14

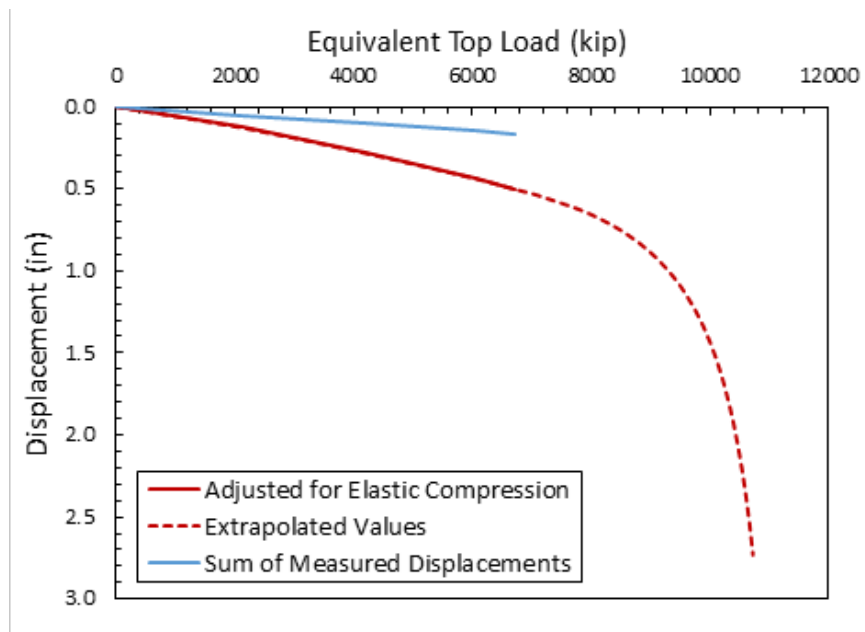


Figure D.15: Equivalent top-down load-settlement curve for data number 15

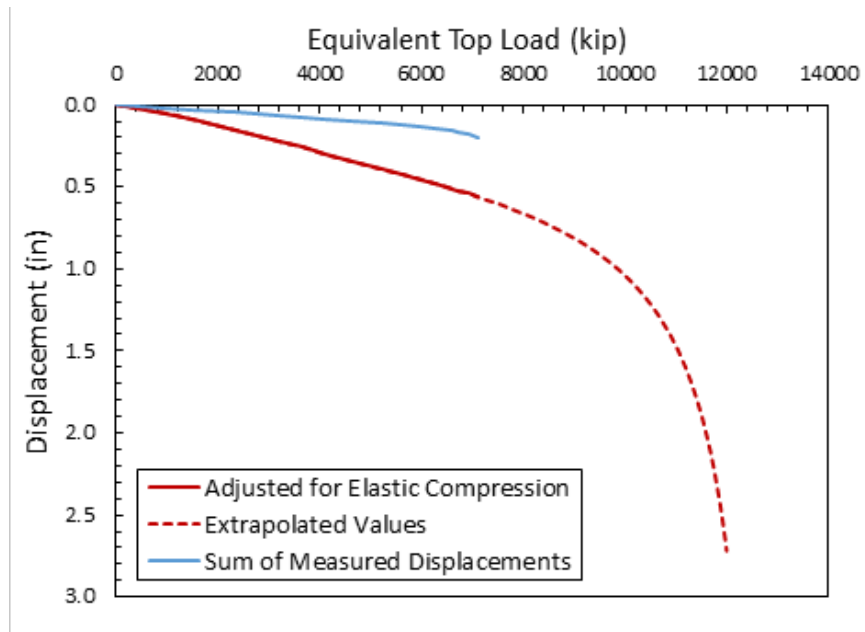


Figure D.16: Equivalent top-down load-settlement curve for data number 16

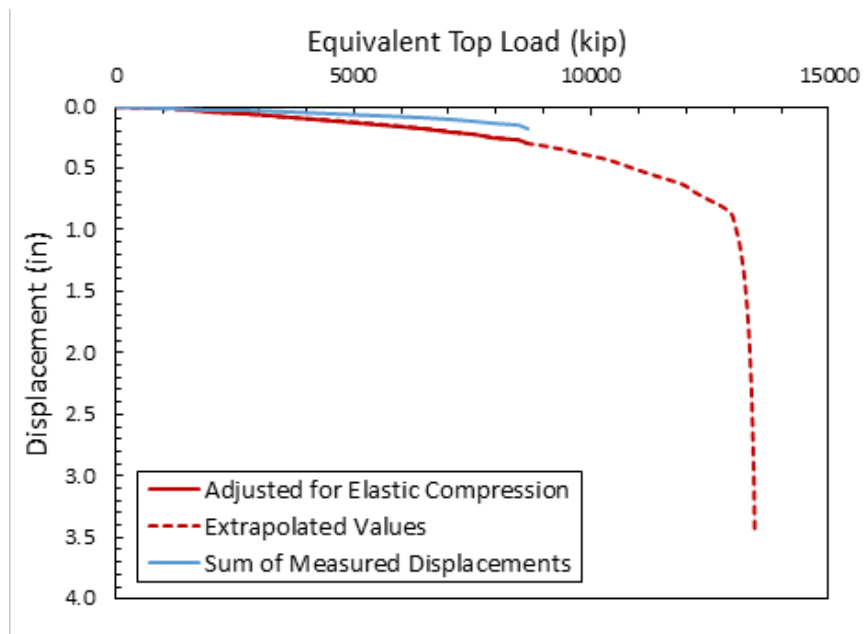


Figure D.17: Equivalent top-down load-settlement curve for data number 17

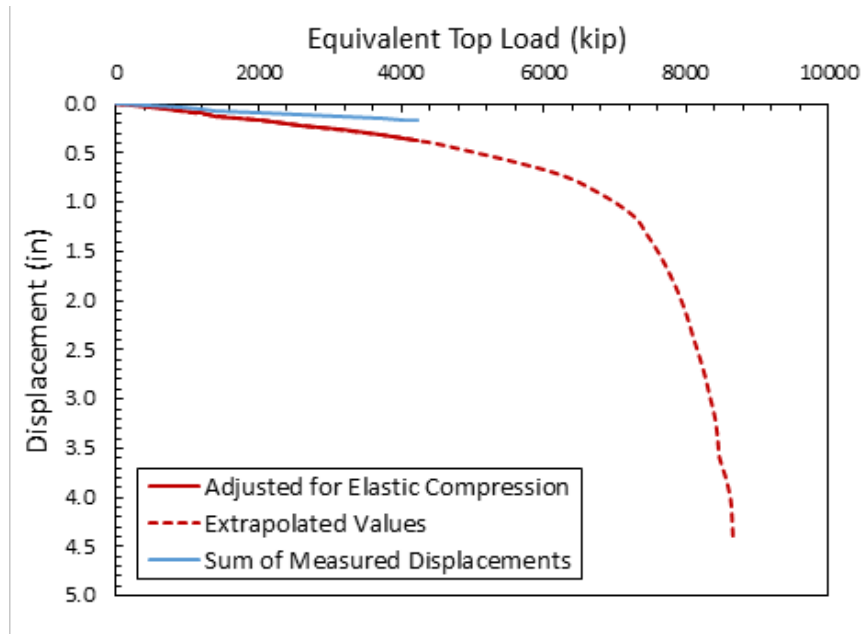


Figure D.18: Equivalent top-down load-settlement curve for data number 18

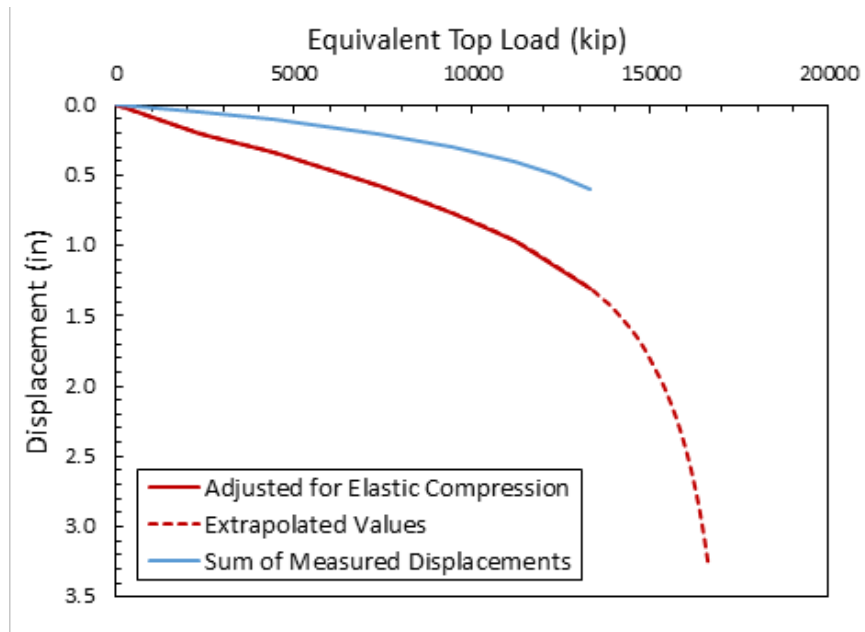


Figure D.19: Equivalent top-down load-settlement curve for data number 19

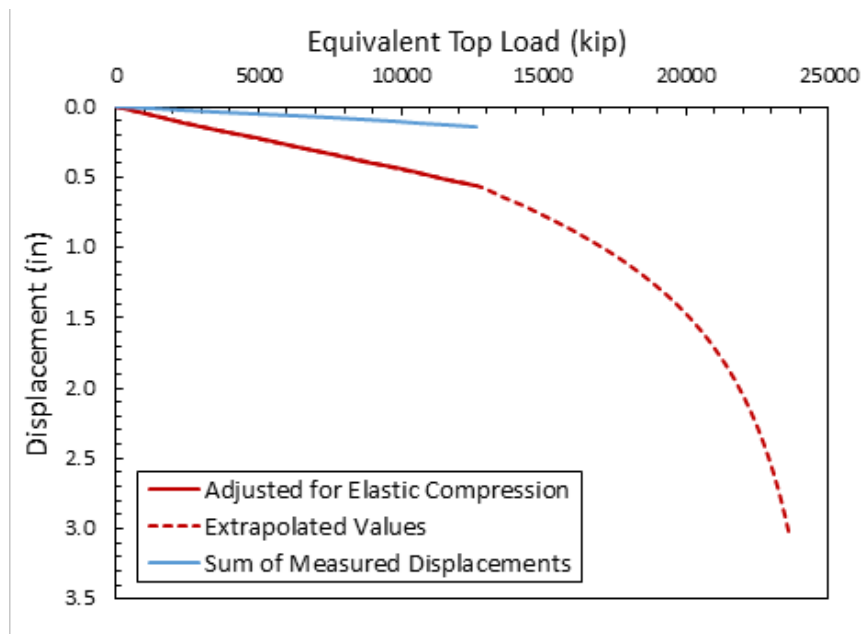


Figure D.20: Equivalent top-down load-settlement curve for data number 20

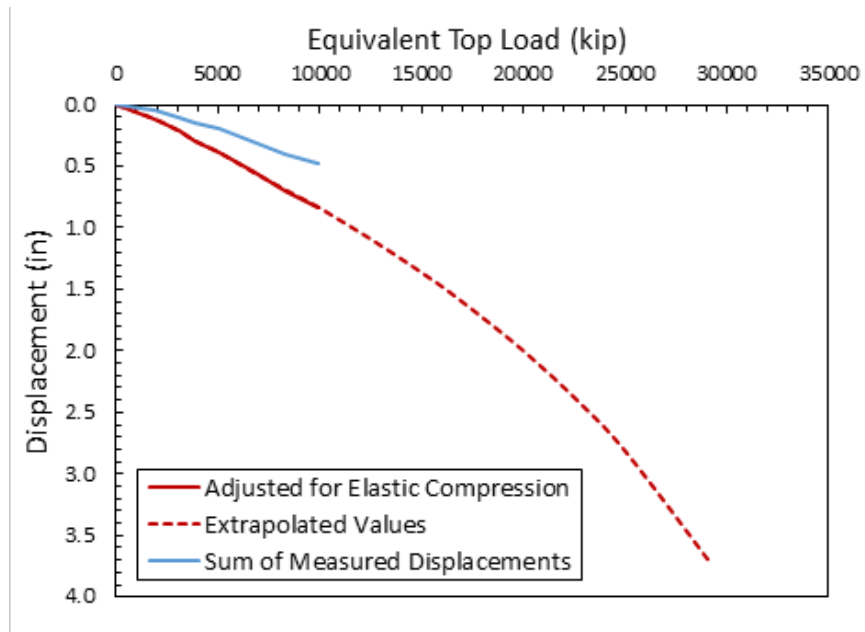


Figure D.21: Equivalent top-down load-settlement curve for data number 21

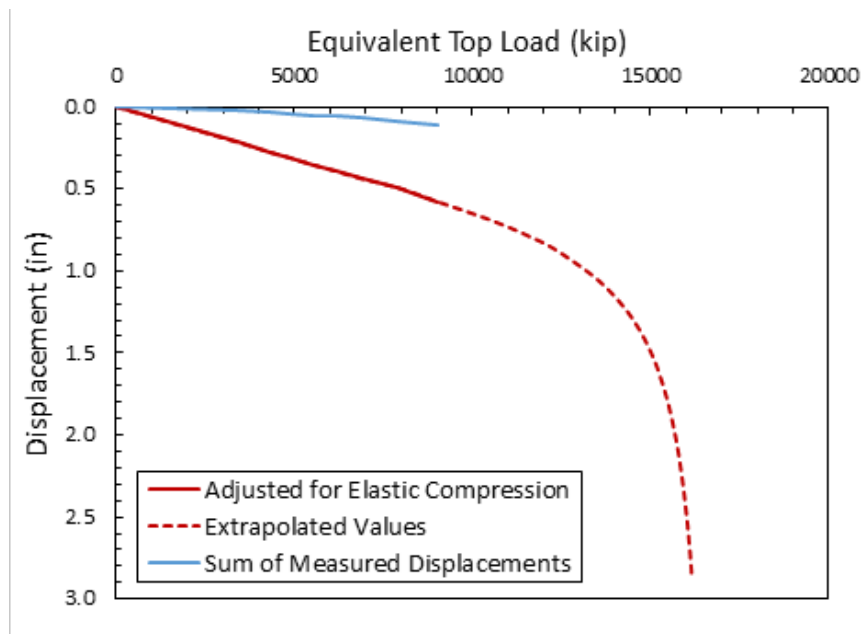


Figure D.22: Equivalent top-down load-settlement curve for data number 22

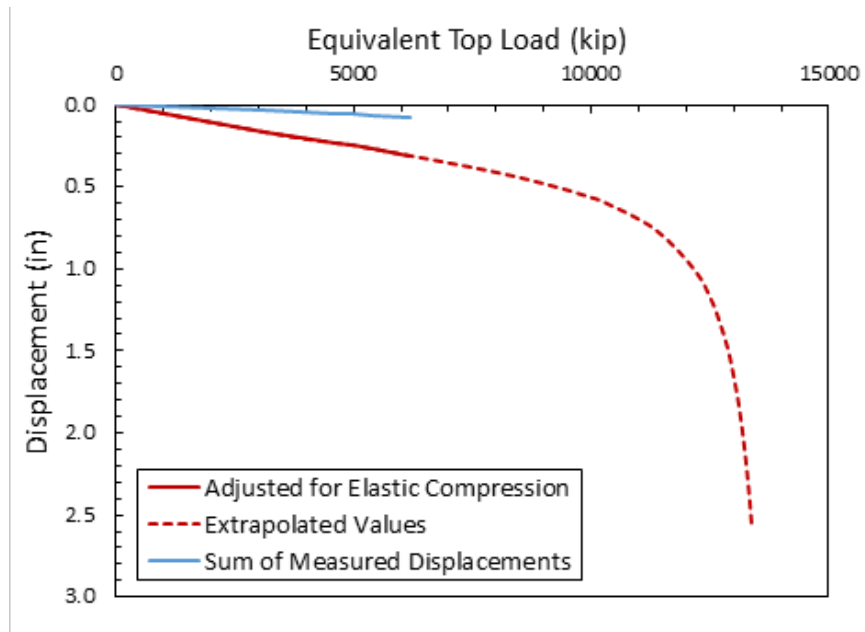


Figure D.23: Equivalent top-down load-settlement curve for data number 23

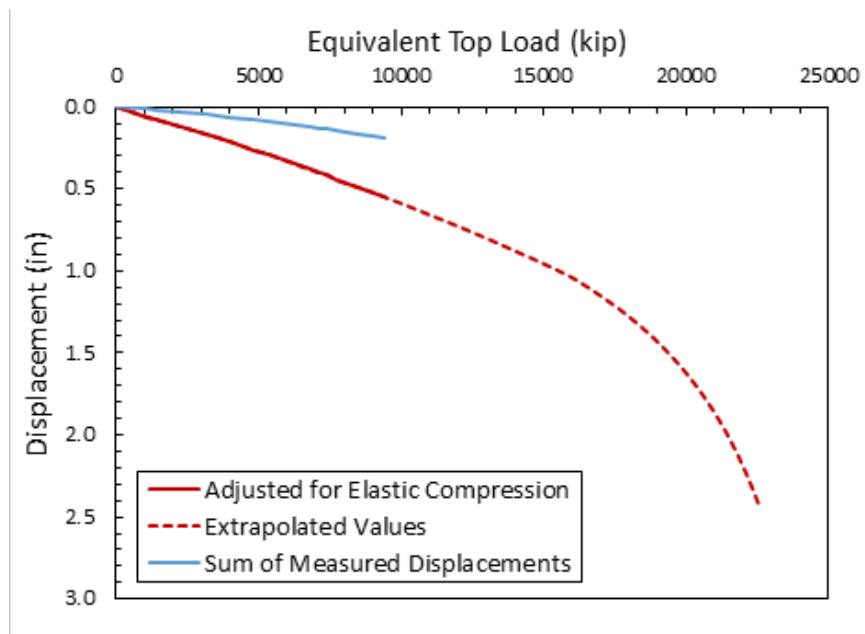


Figure D.24: Equivalent top-down load-settlement curve for data number 24

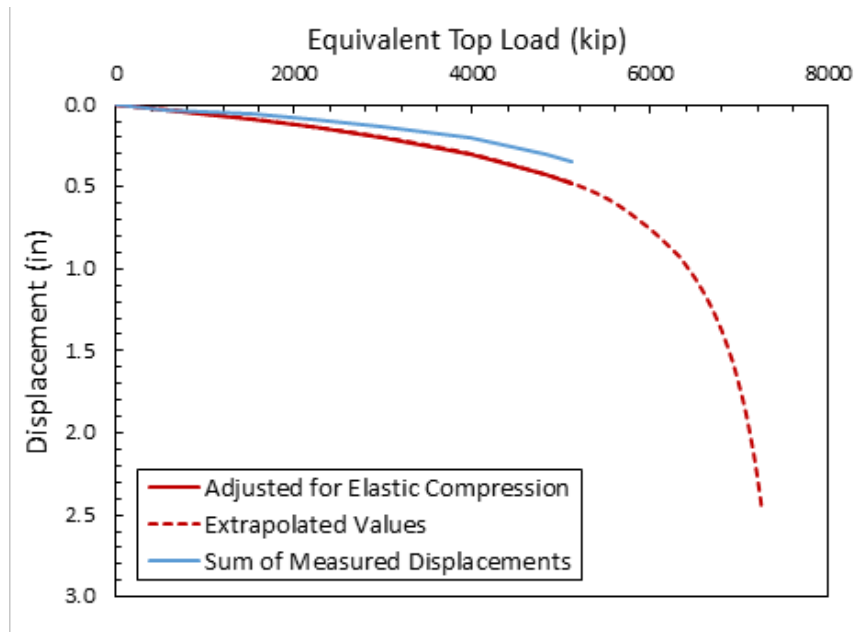


Figure D.25: Equivalent top-down load-settlement curve for data number 25

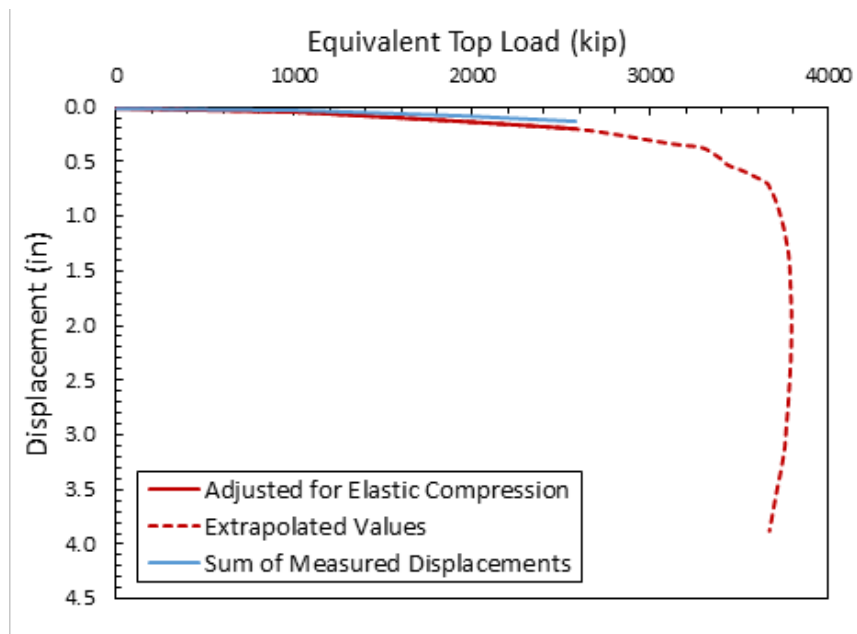


Figure D.26: Equivalent top-down load-settlement curve for data number 26

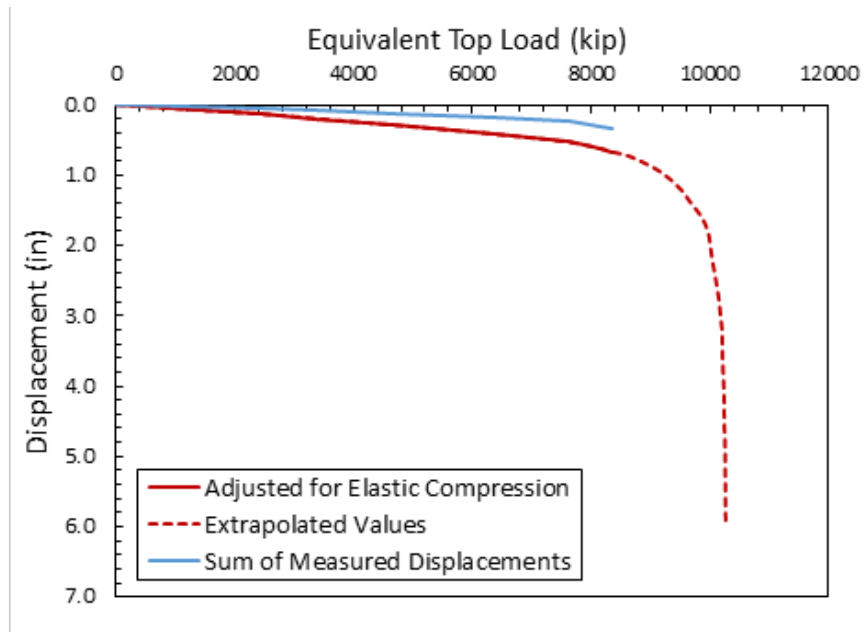


Figure D.27: Equivalent top-down load-settlement curve for data number 27

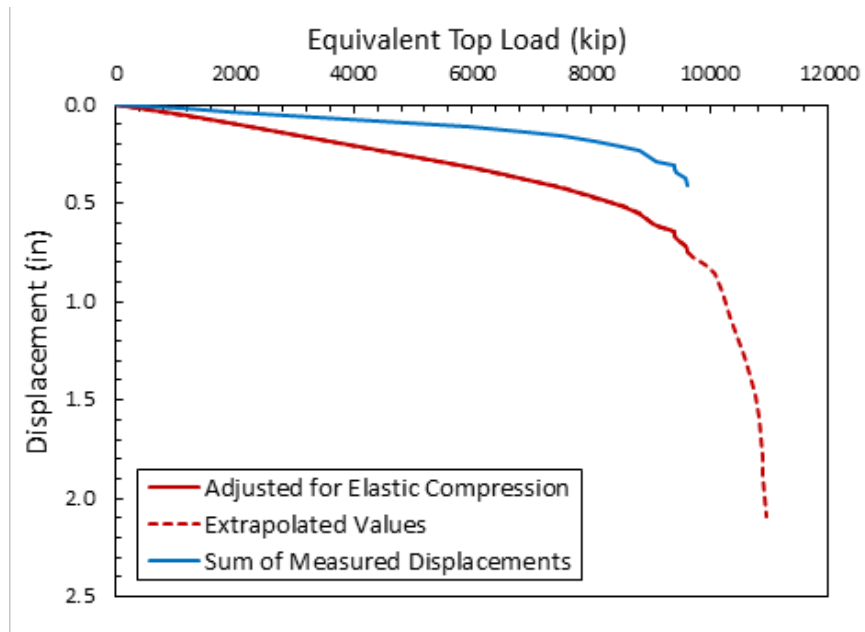


Figure D.28: Equivalent top-down load-settlement curve for data number 28

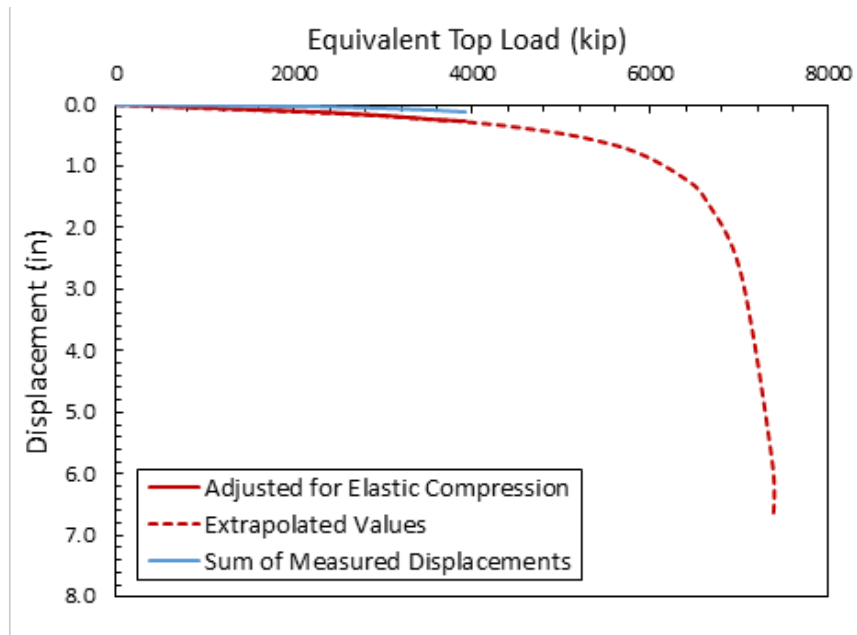


Figure D.29: Equivalent top-down load-settlement curve for data number 29

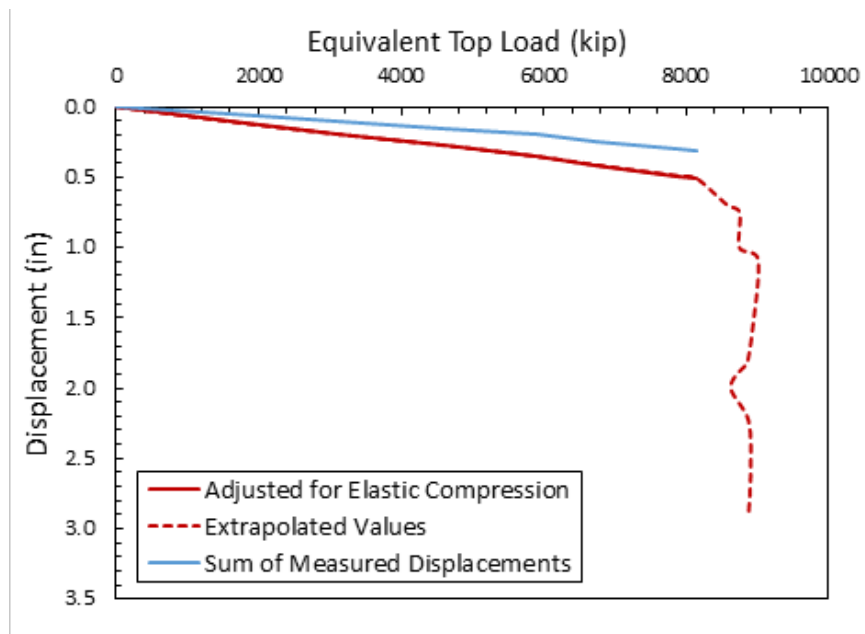


Figure D.30: Equivalent top-down load-settlement curve for data number 30

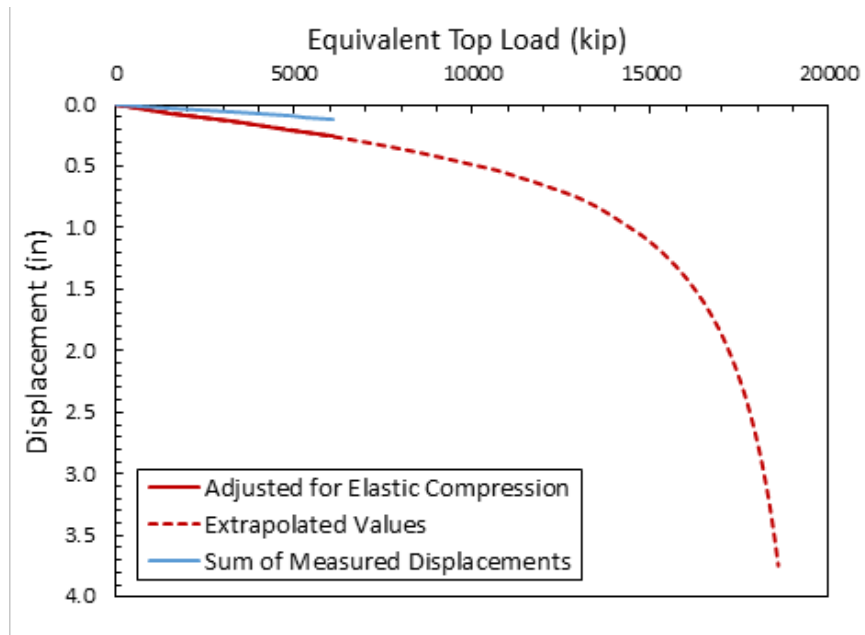


Figure D.31: Equivalent top-down load-settlement curve for data number 31

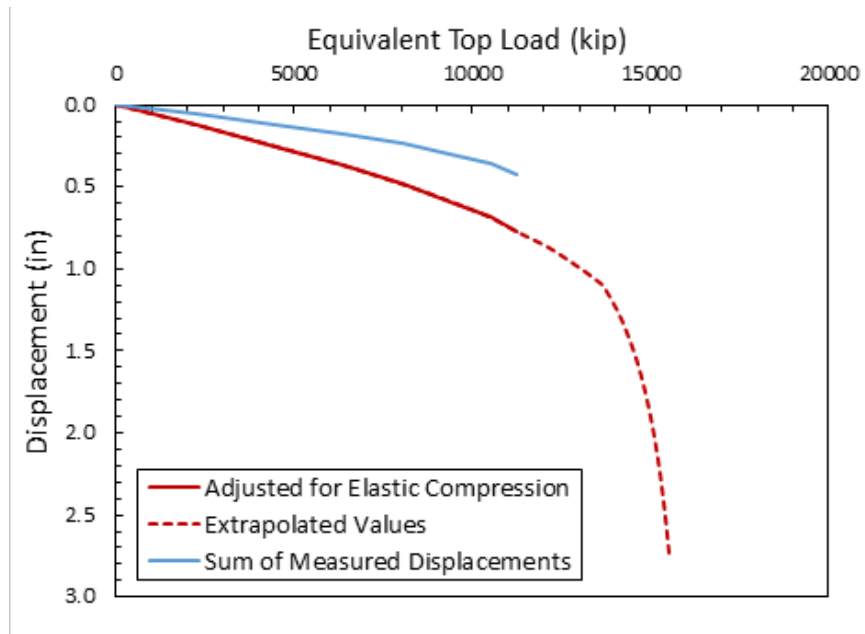


Figure D.32: Equivalent top-down load-settlement curve for data number 32

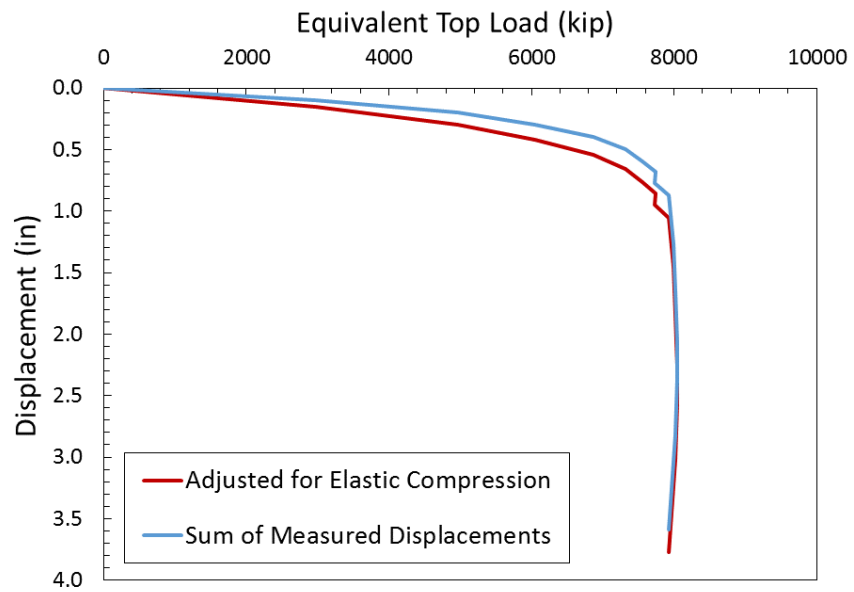


Figure D.33: Equivalent top-down load-settlement curve for data number 33

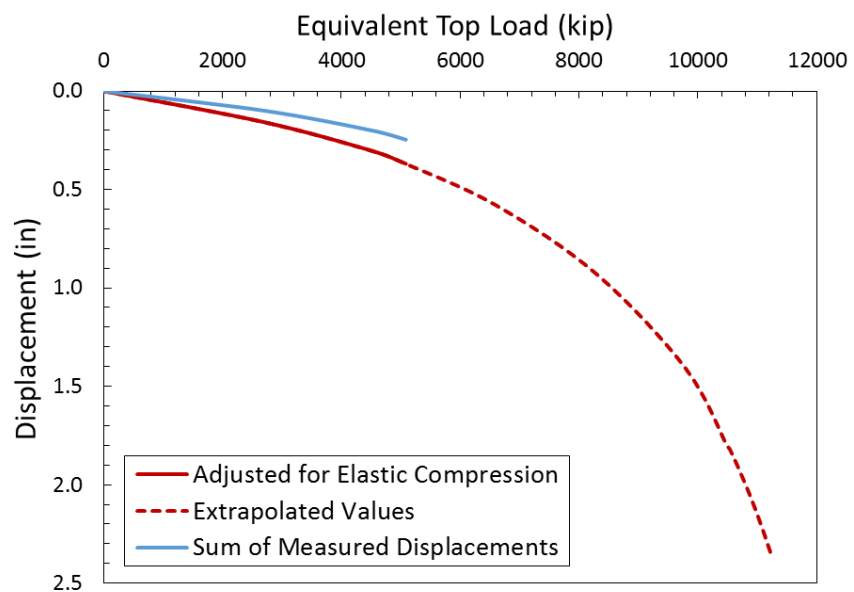


Figure D.34: Equivalent top-down load-settlement curve for data number 34

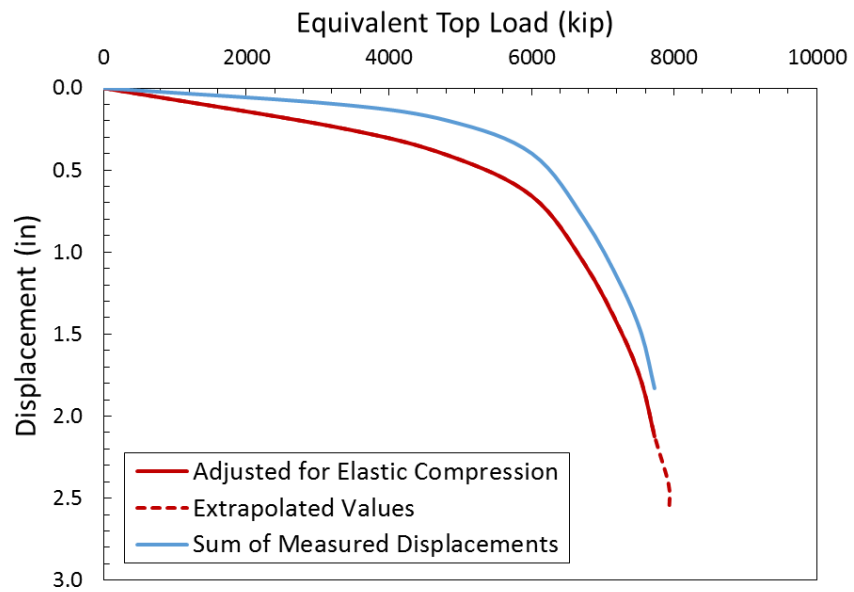


Figure D.35: Equivalent top-down load-settlement curve for data number 35

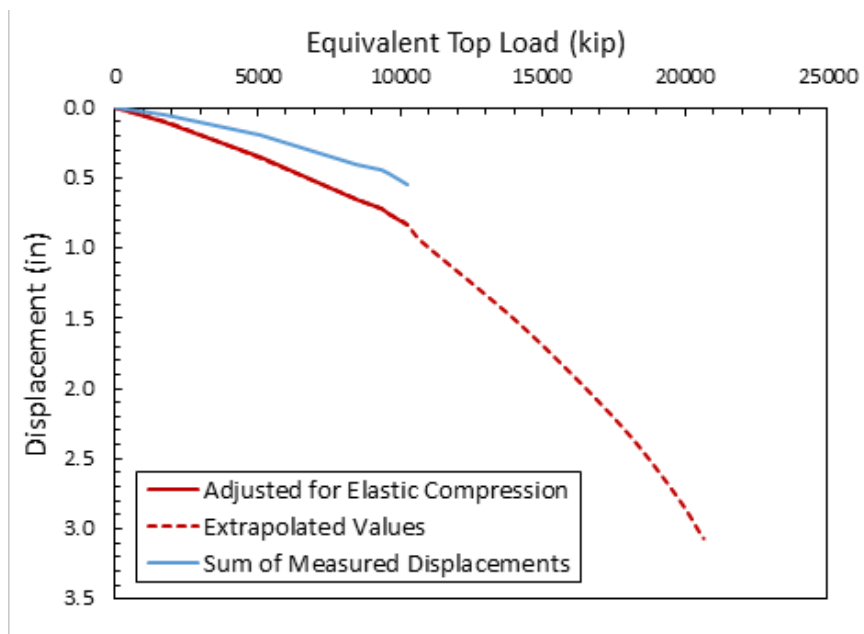


Figure D.36: Equivalent top-down load-settlement curve for data number 36

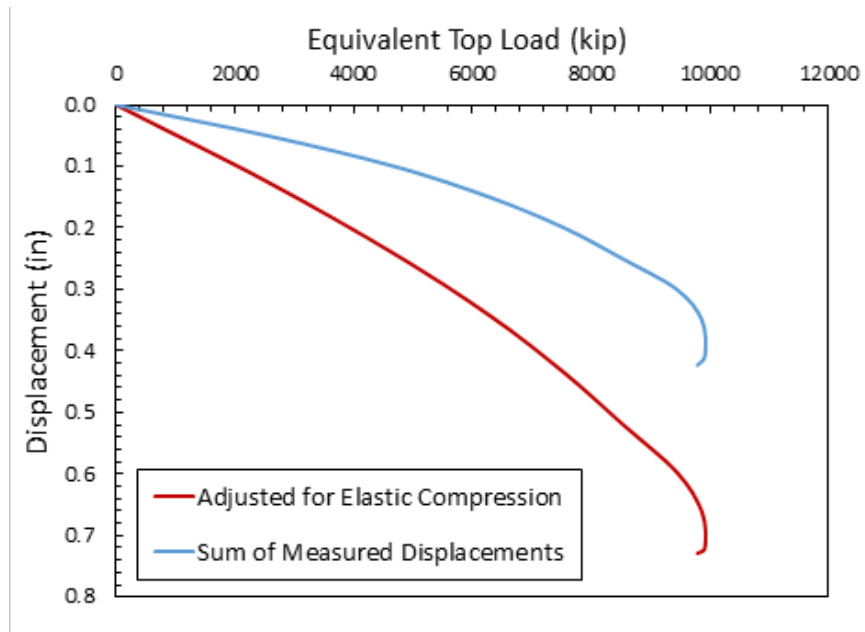


Figure D.37: Equivalent top-down load-settlement curve for data number 37

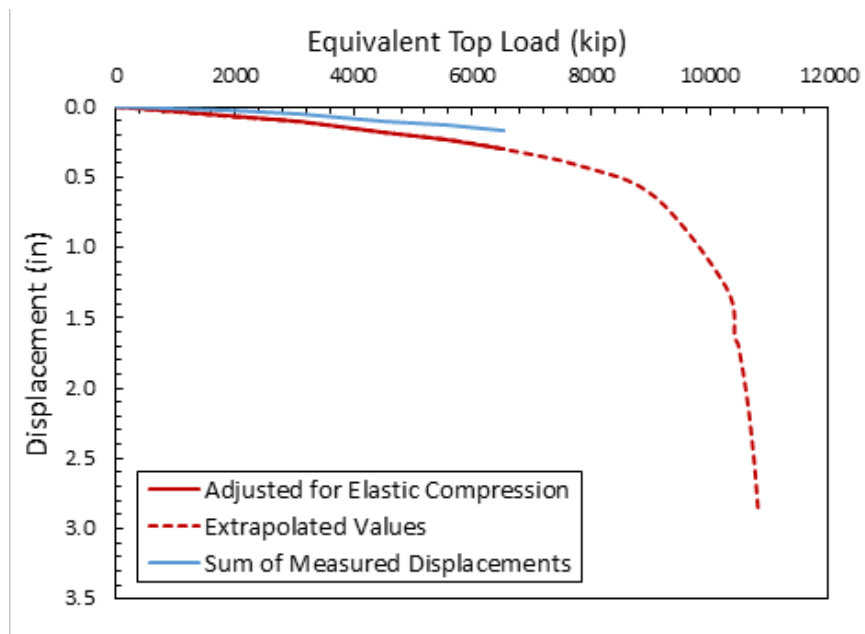


Figure D.38: Equivalent top-down load-settlement curve for data number 38

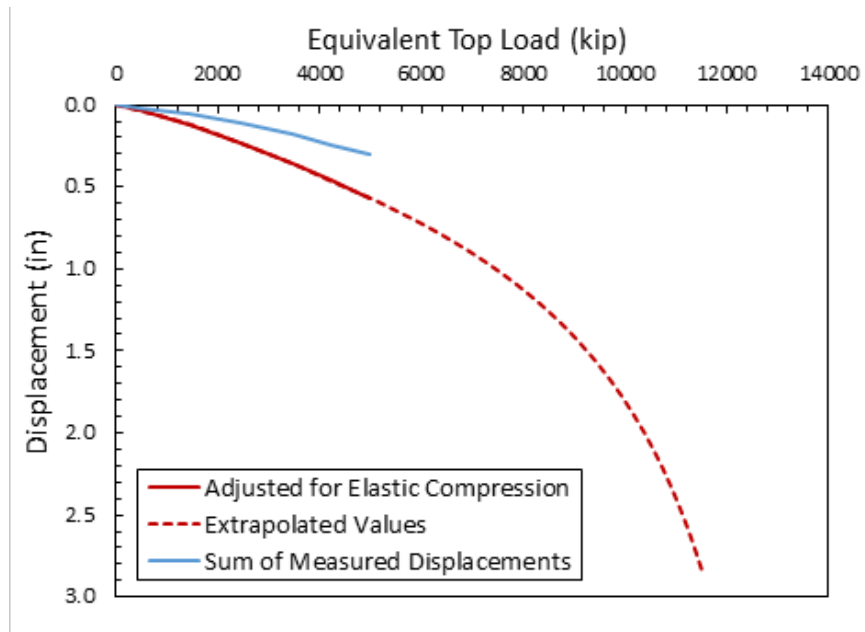


Figure D.39: Equivalent top-down load-settlement curve for data number 39

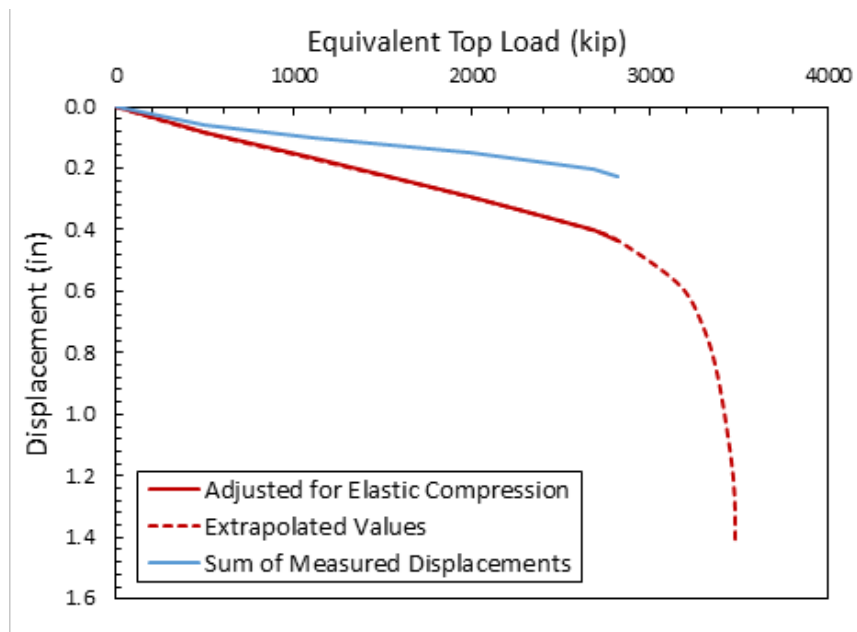


Figure D.40: Equivalent top-down load-settlement curve for data number 40

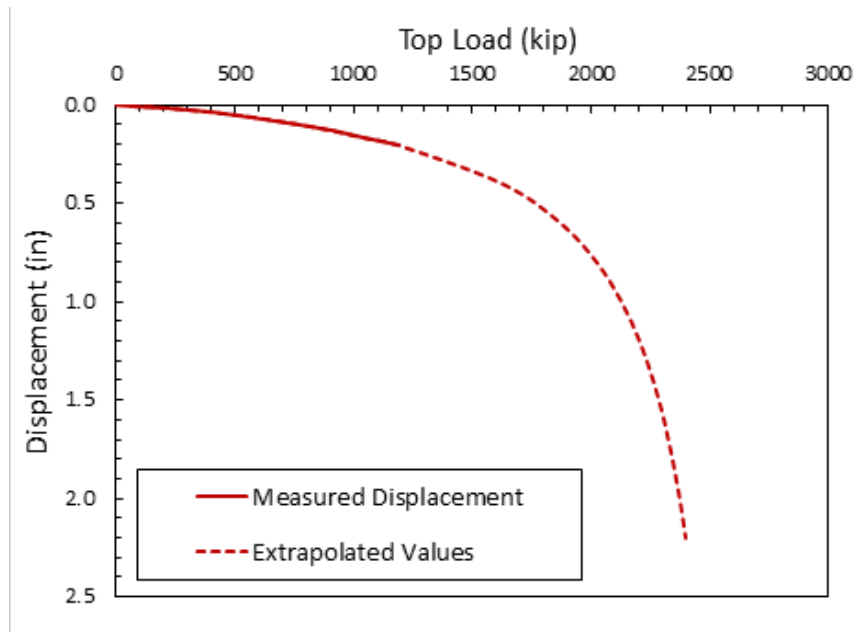


Figure D.41: Measured load-settlement curve for data number 41

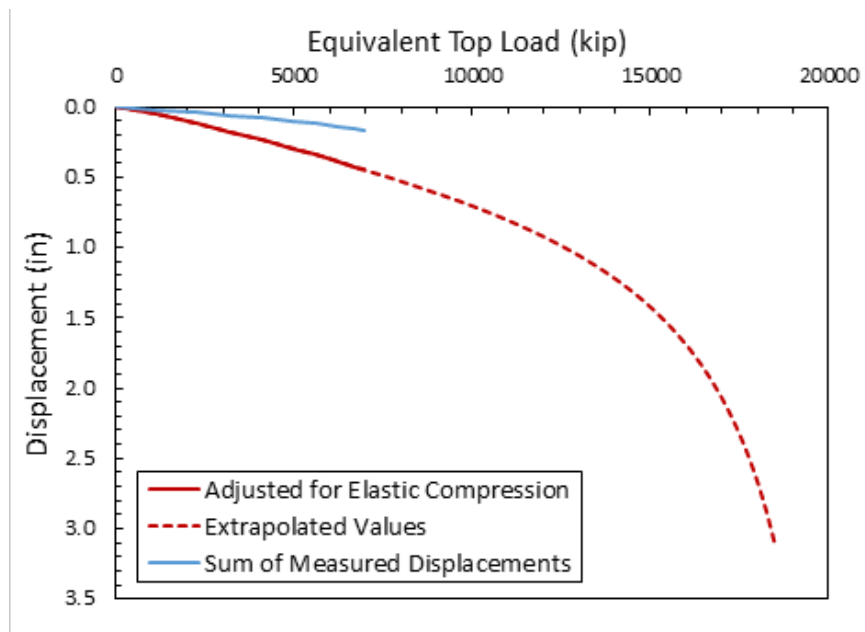


Figure D.42: Equivalent top-down load-settlement curve for data number 42

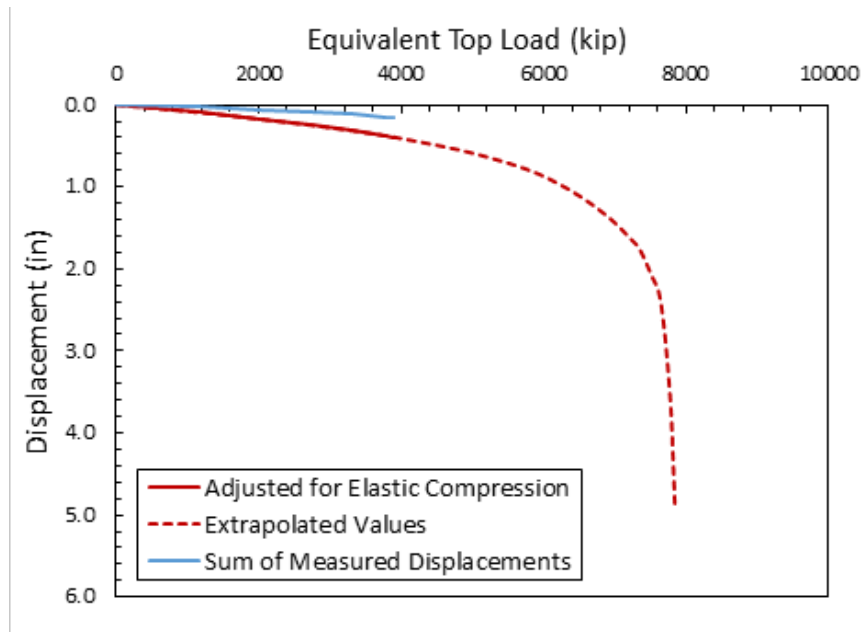


Figure D.43: Equivalent top-down load-settlement curve for data number 43

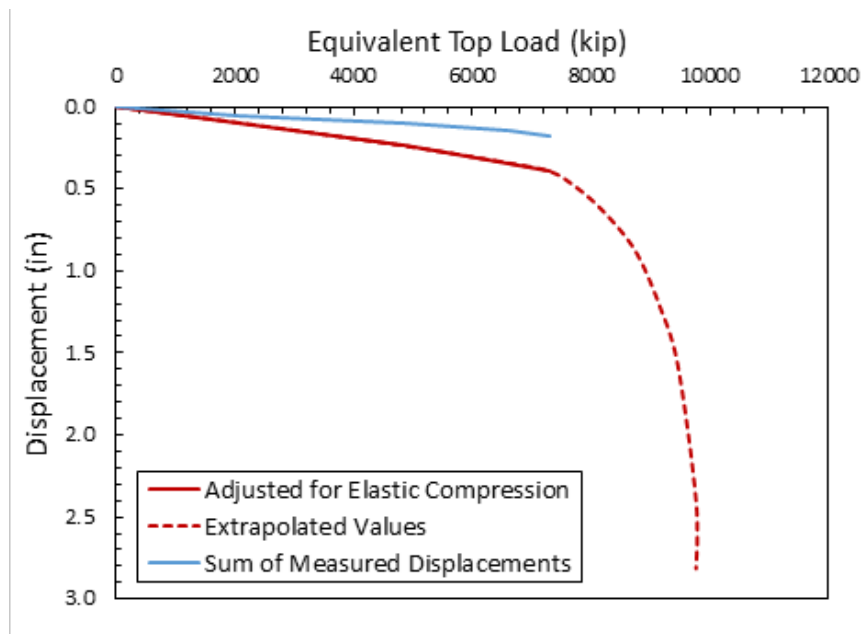


Figure D.44: Equivalent top-down load-settlement curve for data number 44

Appendix E

Recommended Procedure for Analysis of Axially Loaded Drilled Shafts in Las Vegas

1. Carry out a detailed site investigation.
 - Only fully-cemented material (i.e. determined from core samples) which reaches refusal during SPT may be classified as caliche.
 - Unconfined compression tests must be performed on samples collected from all caliche layers to determine the unconfined compressive strengths, q_u .
 - Any material which is not strongly cemented is to be treated the same as the parent material in design.
2. Determine the nominal resistances of all non-cemented material according to [AASHTO \(2014\)](#) design guidelines.
3. Side resistance in caliche is determined using Equation [E.1](#).
4. Base resistance in caliche is computed according to [AASHTO \(2014\)](#) design guidelines for rock.
5. The factored resistance is evaluated using a total resistance factor of 0.66. This is applied to the sum of all individual nominal side resistances and nominal base resistance.

$$\frac{f_{SN}}{p_a} = 0.85 \sqrt{\frac{q_u}{p_a}} \leq 15.8 \quad (\text{E.1})$$

where

f_{SN} = Unit side resistance in caliche

p_a = Atmospheric pressure

q_u = Unconfined compressive strength of caliche

Notes:

- If the q_u of caliche cannot be determined for a given layer, a value no greater than $q_u = 100$ ksf (or $f_{SN} = 12.4$ ksf) may be assumed. This is to account for the exceptionally high variation in caliche strength.
- The upper limit for caliche q_u determined from lab testing is 729 ksf.
- The site investigation should ensure that any caliche layers into which a shaft is tipped are at least as thick as 2 shaft diameters.
- It is highly recommended that measures be taken to verify the lateral extent of cemented layers before relying on their strength in design.

Appendix F

Example: Recommended LRFD Procedure for a Drilled Shaft in Las Vegas

The following example covers the recommended implementation of LRFD with M4 for a drilled shaft in Las Vegas with relatively high data quality scores (GI score = 4, load test score = 4) and a measured resistance of 3682 kip. The test shaft characteristics are taken from data number 26 (see Table 2.2) which is associated with the Trendwest Resorts (owned by Cendent). The shaft diameter (B) is 4.0 ft and its embedded length (L) extends from the ground surface to a depth of 90.5 ft. Table F.1 describes the stratigraphy along the embedded length of the shaft.

For the sake of this example, it will be assumed that laboratory testing has validated a caliche $q_u = 625$ ksf. In reality, however, no such information was available for this data point.

Table F.1: Assumed stratigraphy and material properties for data number 26 (water table depth = 28 ft).

Bottom Layer Depth (ft)	Soil Type	B (ft)	γ (pcf)	ϕ°	N_{SPT}	s_u (psf)
5	Cohesive	4	111	-	15	2828
6.5	Cohesive	4	111	-	50	8582
8	Caliche	4	140	40	-	-
10	Cohesionless (SM)	4	100	40	20	-
12.5	Cohesive	4	104	-	8	977
16	Cohesive ^{PCM}	4	111	-	50	6993
17	Caliche	4	140	40	-	-
20	Cohesive	4	111	-	50	6097
25	Cohesive	4	111	-	24	3319
28	Cohesive	4	102	-	6	767
30	Cohesive	4	120	-	6	741
35	Cohesionless (SM)	4	116	39	14	-
40	Cohesive	4	125	-	9	1148
45	Cohesive	4	118	-	7	859
55	Cohesive	4	114	-	11	1286
60	Cohesive	4	117	-	22	2463
65	Cohesive	4	124	-	10	1087
70	Cohesive	4	121	-	8	845
75	Cohesive	4	119	-	7	720
77	Cohesive	4	131	-	27	2726
85.5	Cohesionless (SM)	4	123	42	38	-
90.5	Cohesive	4	131	-	21	1995

Note: PCM = moderately cemented material

The total nominal resistance, R_N , is calculated according to Equations F.1 and F.2.

$$R_{SNi} = f_{SNi} \pi B \Delta z_i \quad (\text{F.1})$$

$$R_N = R_{BN} + \sum R_{SNi} \quad (\text{F.2})$$

where

f_{SNi} = nominal unit side resistance of an individual soil layer

Δz_i = individual layer thickness

R_N = total nominal axial resistance

R_{BN} = nominal base resistance

R_{SNi} = nominal side resistance of an individual soil layer

Thus, the nominal side resistances are as follows:

- Layers 1 and 2 - Cohesionless (SM) → β Method ([AASHTO, 2014](#), Section 10.8.3.5.2b)

Depth < 5 ft → neglect R_{SN1} ; $R_{SN2} = 72.8$ kip

- Layer 3 - Caliche → proposed approach (Equation 3.1)

$q_u = 625$ ksf → $R_{SN3} = 575.5$ kip

- Layer 4 - Cohesionless (SM) → β Method ([AASHTO, 2014](#), Section 10.8.3.5.2b)

$R_{SN4} = 33.7$ kip

- Layer 5 - Cohesive → α Method ([AASHTO, 2014](#), Section 10.8.3.5.1b)

$R_{SN5} = 16.9$ kip

- Layer 6 - Partially cemented clay

Treat as parent (cohesive) ([AASHTO, 2014](#), Section 10.8.3.5.1b) → $R_{SN6} = 263.89$ kip

- Layer 7 - Caliche → proposed approach (Equation 3.1)

$q_u = 625$ ksf → $R_{SN7} = 383.7$ kip

- Layers 8 through 11 - Cohesive → α Method ([AASHTO, 2014](#), Section 10.8.3.5.1b)

$R_{SN8} = 103.4$ kip, $R_{SN9} = 113.3$ kip, $R_{SN10} = 15.9$ kip, $R_{SN11} = 10.2$ kip

- Layer 12 - Cohesionless (SM) $\rightarrow \beta$ Method (AASHTO, 2014, Section 10.8.3.5.2b)

$$R_{SN12} = 140.2 \text{ kip}$$

- Layers 13 through 20 - Cohesive $\rightarrow \alpha$ Method (AASHTO, 2014, Section 10.8.3.5.1b)

$$R_{SN13} = 39.7 \text{ kip}, R_{SN14} = 29.7 \text{ kip}, R_{SN15} = 88.9 \text{ kip}, R_{SN16} = 85.1 \text{ kip}, R_{SN17} = 37.6 \text{ kip}, R_{SN18} = 29.2 \text{ kip}, R_{SN19} = 24.9 \text{ kip}, R_{SN20} = 37.7 \text{ kip}$$

- Layer 21 - Cohesionless (SM) $\rightarrow \beta$ Method (AASHTO, 2014, Section 10.8.3.5.2b)

$$R_{SN21} = 518.5 \text{ kip}$$

- Layer 22 - Cohesive $\rightarrow \alpha$ Method (AASHTO, 2014, Section 10.8.3.5.1b)

$$R_{SN22} = 68.9 \text{ kip}$$

Following the methodology presented in Chapter 3, the nominal base resistance, R_{BN} , is computed according to AASHTO (2014) for the cohesive soil. In this case, the mean undrained strength over a depth $2B$ below the base of the shaft is 1330 psf which leads to an estimated $R_{BN} = 139.2$ kip.

Next, summing R_{SNi} for layers 1 through 22 and R_{BN} yields a total nominal resistance $R_N = 2828.6$ kip. The factored axial resistance, R_R is then calculated using a total resistance factor of 0.66 according to Equation F.3 as follows:

$$R_R = \phi_{RT} R_N = 0.66(2828.6) = \mathbf{1866.9 \text{ kip}} \quad (\text{F.3})$$



Nevada Department of Transportation
Rudy Malfabon, P.E. Director
Ken Chambers, Research Division Chief
(775) 888-7220
kchambers@dot.state.nv.us
1263 South Stewart Street
Carson City, Nevada 89712